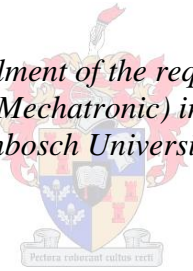


Development of an Intravenous Oxygenator

by

Wesley de Vere Elson

*Thesis presented in partial fulfilment of the requirements for the degree of
Master of Science in Engineering (Mechatronic) in the Faculty of Engineering at
Stellenbosch University*



Supervisor: Prof C Scheffer

Cr tki2014

Declaration

By submitting this thesis electronically, I declare that the entirety of the work contained therein is my own, original work, that I am the sole author thereof (save to the extent explicitly otherwise stated), that reproduction and publication thereof by Stellenbosch University will not infringe any third party rights and that I have not previously in its entirety or in part submitted it for obtaining any qualification.

Signature:.....

W. d. V. Elson

Date:

Copyright © 2016 Stellenbosch University

All rights reserved

Abstract

Patients in critical care with lung injuries need to be assisted with regards to breathing function, but current methods are not applicable for all situations. The most common method, Extracorporeal Membrane Oxygenation (ECMO) is an expensive procedure and requires trained staff to operate the equipment at all times. Lung injury may lead to the inability of the lungs to be perfused and the blood oxygenated by tracheal intubation, whereas mechanical ventilators can injure the lungs further. Especially at risk are preterm neonates, where congenital disorders or complications during birth render ECMO the only viable option. Respiratory Assist Catheters (RACs) could be used as an alternative because they do not place extra stress on the lungs, are easy to implement, cost-effective and are available for immediate use in clinical settings or in first aid situations. The development of such a device requires knowledge of possible oxygenation methods as well as the risks involved in implementing such a device. The possibility of oxygenating the blood via microbubbles by means of a RAC is promising due to the high gas transfer rates common in bubble oxygenators. It is the aim of this study to develop a prototype that could function as a RAC and to evaluate the feasibility of oxygenation by using microbubbles.

The method used to design a prototype included selection of various materials and finalization of a design to be tested. The tests selected were in vivo tests and ex vivo tests using animal models to investigate the dissolution times of the microbubbles, as well as the physiological effects of an intravenously placed device. Measurements of oxygen saturation of the blood in arterial blood (SaO_2), venous blood (SvO_2) and pulmonary pressure allowed the oxygen transfer rates and risks involved to be evaluated, and also gave an indication regarding the formation dynamics of microbubbles in the blood. An in vitro test was also

performed with the aim of determining the rate of dissolving of oxygen, and hence to give an indication regarding microbubble dissolution times. Mathematical simulations based on the dissolution rate of oxygen in venous blood confirmed the abovementioned results.

The tests and simulations were analysed in order to evaluate the feasibility of intravenously oxygenating the blood using microbubbles. Approximate bubble dissolution times were an indicator of the feasibility of the concept and showed that very large bubble dissolution times renders intravenous bubble oxygenation unfeasible. These large dissolution times also lessen the possibility of implementing bubble oxygenation in an intravenous device.

Uittreksel

Pasiënte wat a.g.v. longbeserings in hoë-sorg behandel word het hulp nodig om asem te haal, maar bestaande metodes werk nie in alle omstandighede nie. Die mees algemene metode is ekstrakorporeale membraan suurstofverbinding (Extracorporeal Membrane Oxygenation (ECMO)), maar hierdie metode is duur en het voltyds opgeleide personeel nodig om dit te beheer. Longbeserings kan lei tot die onvermoë van die longe om bloed te ontvang en ook dat die bloed suurstof kry d.m.v. trageale intubasie. Meganiese ventilators kan die longe verder beskadig. Vroeggebore babas word blootgestel aan risiko's veral waar oorerflike afwykings/steurnisse aanwesig is of komplikasies tydens geboorte en dus die EMCO die enigste lewensvatbare opsie maak. Kateters wat asemhaling aanhelp (Respiratory Assist Catheters (RACs)) kan as alternatief gebruik word aangesien dit nie ekstra spanning op die longe plaas nie, maklik is om te implementeer, koste-effektief is en beskikbaar is vir onmiddellike gebruik in kliniese omstandighede of in noodhulpsituasies. Die ontwikkeling van hierdie tipe toestel vereis kennis van moontlike suurstofverbindingsmetodes en ook die risiko's verbonde aan die implementering van die toestel. Die moontlikheid om die bloed van suurstof te voorsien d.m.v. mikroborrels deur die RAC lyk belowend a.g.v. die hoë gasoordrag-koers wat algemeen is by borrel suurstofverbinders. Hierdie studie het ten doel om 'n prototipe te ontwikkel wat kan dien as 'n RAC en ook om die lewensvatbaarheid van suurstofverbinding met mikroborrels te bepaal.

Die metode wat gebruik is om die prototipe te ontwerp sluit in die kies van verskeie materiale en die finalisering van die ontwerp wat getoets moet word. Die geselekteerde in vivo en ex vivo toetse is afgeneem deur gebruik te maak van dier-modelle om sodoende ondersoek in te stel na die oplossing van die mikroborrels en ook die fisiologiese gevolge van die toestel wat binne die aar

geplaas is. Metings van die suurstofversadiging van bloed in slagaarbloed (SaO_2), aarbloed (SvO_2) en pulmonêre druk het toegelaat dat die koers en risiko's verbonde aan suurstofoordrag geëvalueer word. Hierdie metings gee ook 'n aanduiding van die vormingsdinamika van die mikroborrels in die bloed. 'n In vitro toets is gedoen met die doel om die koers te bepaal van die oplossing van suurstof, en dus 'n aanduiding te gee van die tyd verbonde aan die oplossing van die mikroborrels. Wiskundige simulaties gebaseer op die oplossingskoers van suurstof in are het die bogenoemde toetse bevestig.

Die toetse en simulaties is geanaliseer om die lewensvatbaarheid te bepaal om suurstof binne-aars te verskaf deur mikroborrels. Geskatte tye waarteen die borrels oplos is as aanduiding gebruik vir die lewensvatbaarheid van die konsep en ook die moontlike inwerkingstelling van die binne-aarse toestel.

Dedication

A person could not ask for better parents.

Acknowledgements

The author acknowledges certain people and organisations for their assistance, without whom this project would not have been the same. The author is indebted to Prof Cornie Scheffer for his guidance and valuable insight during this project, as well as Prof Fourie and Prof Coetzee for their hands-on guidance and willingness for research. Recognition is also given to Mr Cobus Zietsman who gave practical insight into the development and testing of the flow meter, and Dr Daniel Muller and the team at Tygerberg Campus for their patience, who spent much time in helping the author with testing. The help of Prof Nice Sauer and Dr. Kiran Dellimore is also appreciated with regards to the mathematical model.

On a more personal note, the author would like to thank his fellow BERG members who have been a source of support and an endless source of ideas, as well as Wayne and Iain for their friendship.

Contents

Declaration	i
Abstract.....	ii
Uittreksel	iv
Dedication.....	vi
Acknowledgements	vii
Contents	viii
List of Figures.....	xi
List of Tables.....	xiv
Nomenclature	xv
Definitions	xvii
1 Introduction	1
1.1 Background	1
1.2 Motivation.....	2
1.3 Objectives.....	3
1.4 Scope.....	5
2 Literature Review	7
2.1 Introduction.....	7
2.2 Anatomy and Physiology	7
2.3 Quantifying Oxygenation.....	10
2.4 Current State of the Art.....	13
2.5 Membrane Oxygenators.....	15

2.5.1 Extracorporeal	17
2.5.2 Intravenous	20
2.6 Bubble Oxygenators - Extracorporeal.....	22
2.7 Concerns Regarding Microbubbles in the Blood	23
2.8 Bubble Dynamics.....	25
2.8.1 Force Balance	25
2.8.2 Effect of Material Properties	26
2.8.3 Effects of Fluid Properties	28
2.9 Summary of Chapter	29
3 Design.....	30
3.1 Performance Requirements	30
3.2 Initial Concept.....	32
3.3 Geometry and Mechanics of Operation	34
3.3.1 Conceptual Operation	34
3.3.2 Cross-sectional Area.....	37
3.3.3 Material Selection.....	39
3.4 Final Design Decision and Prototype.....	43
3.5 Biocompatibility Assessment.....	45
4 Testing of Concept	48
4.1 Introduction.....	48
4.2 In Vivo	49
4.3 Ex Vivo	53
4.4 In Vitro.....	57
4.5 Flow Meter.....	58
4.5.1 Selection Criteria	58

4.5.2 Construction and Calibration.....	59
4.6 Chapter Summary	62
5 Modelling Oxygen Diffusion	64
5.1 Introduction.....	64
5.2 Diffusion Model.....	65
5.2.1 Limitations and Focus	65
5.2.2 Proposed Solution.....	67
5.2.3 Derivation of Solution	68
5.3 Discussion	77
5.4 Chapter Summary	81
6 Conclusion.....	83
Appendix A Conceptual Designs.....	85
Appendix B Material Screening	89
Appendix C Fluid Properties	91
Appendix D Biocompatibility.....	93
Appendix E Flow Meter Calculations	94
Appendix F Mathematical Model	96
7 References	100

List of Figures

Figure 2-1: Pulmonary alveolus: alveoli and capillaries in the lungs (Encyclopaedia Britannica 2011).....	8
Figure 2-2: Partial pressures of gas within the lungs, blood and body tissue (Edwards Life Sciences 2002)	9
Figure 2-3: Oxyhaemoglobin dissociation curve (Edwards Life Sciences 2002) .	12
Figure 2-4: Types of oxygenators	14
Figure 2-5: Hollow fibres (Wickramasinghe & Han 2005).....	16
Figure 2-6: Schematic drawing of a standard ECMO circuit (Frenckner & Radell 2008)17	
Figure 2-7: Image of the Novalung (Artificial Lungs 2010)	19
Figure 2-8: Drawing of the Hattler Catheter device as positioned in the vena cava (Hattler <i>et al.</i> 2002).....	20
Figure 2-9: Photograph of the IVOX device (Mortensen 1992).....	21
Figure 2-10: Bubble formation stages: (a) Good wettability, (b) Poor wettability (Gnyloskurenko <i>et al.</i> 2003)	25
Figure 2-11: Force balance of a bubble during the critical growth period	26
Figure 2-12: Graph of bubble surface-to-volume ratio vs. water contact angle (Yasuda & Lin 2003)	28
Figure 3-1: Diagram of original concept	32
Figure 3-2: Cross-section of the deployment of the oxygenator	33
Figure 3-3: Venturi effect generates small oxygen bubbles in the liquid pathways (Sung Sam Kim & Schubert 2007)	35

Figure 3-4: Combination of many liquid pathways to form the device to be inserted (Sung Sam Kim & Schubert 2007)	35
Figure 3-5: Initial concept with the mixing chamber	36
Figure 3-6: Samples for simple tests.....	41
Figure 3-7: (a) Hydrophobic and (b) hydrophilic material	41
Figure 3-8: Example of a heat sealed prototype	45
Figure 4-1: Layout of a Swan Ganz catheter (Author n.d.)	50
Figure 4-2: Insertion into femoral vein.....	51
Figure 4-3: Swanz-Ganz catheter in position	51
Figure 4-4: Device after being removed from the porcine test subject – clotted layer can be seen alongside the device	52
Figure 4-5: Ex vivo test circuit	53
Figure 4-6: Device is inflated before oxygenation takes place.....	54
Figure 4-7: Bubbles seen emanating from weaknesses in the material	54
Figure 4-8: Initial formation of bubbles	55
Figure 4-9: Collection of bubbles at the surface.....	56
Figure 4-10: Formation of oxygen foam.....	56
Figure 4-11: Tearing of material during in vitro tests	57
Figure 4-12: Calibration laboratory arrangement	60
Figure 4-13: Flow meter being used during testing.....	62
Figure 5-1: Partial Pressure curve vs. distance from the bubble interface	69
Figure 5-2: Flow diagram for implementation of code.....	76
Figure 5-3: Radius-time relations for a bubble surrounded by multiple bubbles (Fischer <i>et al.</i> 2009).....	78
Figure 5-4: Bubble dissolution times ($R = 100 \mu\text{m}$, $D = 1.8 \times 10^{-11} \text{ m}^2/\text{s}$).....	79

Figure 5-5: Saturation vs. radial coordinate for $\Delta = 500 \mu\text{m}$ ($R = 100 \mu\text{m}$, $D = 1.8 \times 10^{-11} \text{ m}^2/\text{s}$)	80
Figure A-1: (a) & (b) An example of open and closed implementations of cross-sectional concept 4.....	87
Figure A-2: (a) & (b) Another example of open and closed implementations of cross-sectional concept 4	88
Figure B-1: Bubble formation from a submerged orifice	89
Figure D-1: ISO decision tree (ISO 2002).....	93

List of Tables

Table 3-1: Design Specifications	31
Table 3-2: Cross-sectional concepts	37
Table A-1: Conceptual RAC designs.....	85
Table B-1: Sample material properties	89
Table C-1: Fluid Properties.....	91
Table E-1: Flow meter design calculations.....	94
Table E-2: Flow meter calibration readings and calculations.....	94

Nomenclature

$A-aDO_2$	Alveolar-arterial oxygenation gradient
$CaCO_2$	Arterial carbon dioxide content
c	Haemoglobin binding capacity
C_d	Mass fraction of dissolved oxygen in the blood
CO	Cardiac Output
CvO_2	Venous oxygen content
D	Diffusion constant
Hb	Haemoglobin
HbO_2	Haemoglobin-bound oxygen
p	Pressure
Q	Fluid flow rate
P_{50}	A parameter of Hill's equation
PaO_2	Arterial partial pressure of oxygen
PO_2	Partial pressure of oxygen
PvO_2	Venous partial pressure of oxygen
SaO_2	Arterial oxygen saturation
SO_2	Oxygen saturation
SvO_2	Venous oxygen saturation
VO_2	Oxygen consumption by the tissue

α	Solubility of oxygen
Δ	Distance between two bubble centres
λ	Slope of saturation curve
μ	Viscosity
ρ	Density
ρ_b	Density of blood
ρ_{STP}	Density of oxygen under standard conditions
σ	Surface tension

Definitions

<i>Acidosis</i>	Increased acidity of the blood
<i>Blood/Device interaction</i>	The interaction between a device and the whole blood or part of the blood which results in an effect on the blood, downstream organs or on the device itself (ISO 2002)
<i>Bubble point pressure</i>	The pressure required to form a gas bubble through a small orifice for a specific fluid, gas and pore size
<i>Embolectomy catheter</i>	A catheter used to surgically remove emboli in the blood circulation system.
<i>Embolism</i>	The act of clogging of an arterial capillary due to an embolus
<i>Embolus</i>	Any object that can obstruct an arterial capillary
<i>Erythrocyte</i>	Red blood cell
<i>Extracorporeal</i>	A process or machine which is placed or occurs outside of the body
<i>Ex vivo</i>	Describes the test setup that allows blood to be shunted from a human subject or test animal outside the body (ISO 2002)
<i>Haemolysis</i>	The release of haemoglobin from ruptured red blood cells

<i>Heparin</i>	A widely used injectable anticoagulant
<i>Hydrophilic</i>	Surfaces that have a strong affinity for water
<i>Hydrophobic</i>	Surfaces that lack an affinity for water
<i>Hypoxemia</i>	Decreased partial pressure of oxygen in arterial blood, could lead to hypoxia
<i>Hypoxia</i>	When the body or tissue does not receive an adequate oxygen supply
<i>Intravenous</i>	Within the veins
<i>In vitro</i>	Outside of a living system, usually within a test tube or petri dish
<i>In vivo</i>	Within a living organism
<i>MAS</i>	Meconium Aspiration Syndrome is a condition where the new-born breathes in a mixture of meconium and amniotic fluid into the lungs during birth
<i>Myopia</i>	A refractive defect of the eye (near-sightedness)
<i>Necrosis</i>	Cell death, death of body tissue
<i>Oxygenation Index</i>	The ration of oxygen being delivered to the lungs to the amount diffusing into the blood
<i>Perfusion</i>	The act of injecting a fluid into a blood vessel in order to reach the organs or tissue.
<i>PPHN</i>	Persistent Pulmonary Hypertension of the New-born is characterised by high pressure in the lung

	capillaries, allowing blood to be directed away from the lungs
<i>Preterm neonate</i>	A child born before full term, and younger than 28 days
<i>Pulmonary</i>	Pertaining to or affecting the lungs
<i>RAC</i>	A Respiratory Assist Catheter is an intravenous device that assist with oxygenation of the blood
<i>RDS</i>	Respiratory Distress Syndrome is characterised by the underdevelopment of the lungs, mostly seen by the collapse of alveoli due to insufficient surfactant production
<i>ROP</i>	In extreme cases Retinopathy of Prematurity can lead to blindness due to oxygen toxicity or hypoxia, of which preterm neonates are especially at risk.
<i>Shunt</i>	May be an anatomical or physiological occurrence where fluid is moved through the lungs to the other without being oxygenated
<i>Thrombosis</i>	A mixture composed of red blood cells, fibrin, platelets and other cellular elements
<i>Tracheal intubation</i>	Placement of a tube into the trachea for purposes of ventilation, airway maintenance or administering anaesthesia

1 Introduction

1.1 Background

Historically, the research and development of medical devices has had the main aim of assisting people in need of medical care. Medical devices are often technically complex and are highly regulated, and therefore require a lot of resources to be produced and maintained. Today, other constraints are being placed on medical devices due to economic and logistical contextual moulds, such as the cost of medical devices, training of the persons operating the devices and a high degree of safety required for the patient. Therefore innovative solutions are needed to address these unique problems faced. This is done with the hope that such devices will be able to achieve the aim of providing medical care in previously unexplored applications. In clinical situations, most medical devices are used to facilitate the medical team in providing the best possible medical care.

In most surgical procedures and critical care wards, oxygen delivery to the patient is of utmost importance. Without adequate oxygen delivery necrosis can occur, nullifying other attempts at life support. Conventional oxygen delivery devices are well-established and have been researched to a large degree. They have ranged from Screen-type oxygenators, to Bubble as well as Membrane oxygenators. Membrane oxygenators have been implemented to oxygenate the blood while it is still inside the body, or pumping the blood outside the body and oxygenating it before returning the blood to the patient. Extracorporeal Membrane Oxygenators (ECMO) are widely used in clinical settings, and are regarded as the norm for oxygenating human blood due to the increased safety and reliability compared to previous oxygenators. ECMO devices do however remain costly, are large or immobile (not allowing ambulatory use), and require an appreciable preparation

time before use. Iwahashi *et al.* (2004) stated that a small non-pulsatile oxygenator is needed which is available for immediate use by the surgeon in the operating theatre or in first aid situations.

1.2 Motivation

A person in a critical care situation relies on the skills of the people attending to them, as well as the efficacy of the medical devices being used when they are being attended to. Supplying oxygen to such a person may be hampered due to the limited availability of a breathing support device, as can happen during a sporting accident. However, the supply of oxygen is often limited due to a physiological phenomenon. This may be due to a mechanical blockage such as when a swimmer drowns and has fluid in their lungs or an obstacle to tracheal intubation, such as a tracheal tumour. Other scenarios include damage to the fragile alveoli due to hot or toxic gases being drawn into lungs, or due to other effects that obstruct oxygenation, of which neonates are particularly susceptible. Specific cases are the occurrence of disorders almost exclusive to preterm neonates, such as Meconium Aspiration Syndrome (MAS), Respiratory Distress Syndrome (RDS) and Persistent Pulmonary Hypertension of the Newborn (PPHN) (Carey & Colby 2009). PPHN is characterised by high pulmonary vascular resistance, resulting in the shunting of pulmonary blood to the systemic circulation. In effect, the blood is not fed into the pulmonary bed in the lungs, but passes via an extrapulmonary pathway without being oxygenated, and causes systemic arterial hypoxemia (Steinhorn 2011). Mortality rates can be as high as 30 % (O'Rourke *et al.* 1989), and necessitates that the patient's blood be oxygenated apart from the lungs (Thakkar *et al.* 2001).

A method of providing breathing support independent of the lungs using respiratory devices or artificial lungs in place of mechanical ventilators, has tremendous clinical potential which as of yet has not been realized (Kaar *et al.* 2007). Conventional mechanical ventilation could damage the lungs even further

by positive airway pressure (Schubert *et al.* 2003), and does not address the case of inability of the lungs to be perfused. Modern artificial systems such as membrane oxygenators indirectly expose the blood to oxygen by use of a membrane, thereby allowing the partial pressure of oxygen in the blood to increase due to passive diffusion. These oxygenators have limitations on efficacy and ease of implementation. Clotting does occur on the membrane surface, reducing the rate of diffusion, and the patient needs to be monitored by a trained specialist at all times (Conrad *et al.* 1994; Frenckner & Radell 2008). Consequently a device that can oxygenate the blood independent of the lungs, that is simple to use and mobile enough to use outside of the clinical setting, could be very beneficial. If such a device sufficiently oxygenates the blood, it may allow addressing cases which mechanical ventilation cannot (such as MAS and PPHN). If the device is inexpensive and simple to use, it can find application in areas outside the hospital and clinics or in areas where ECMOs cannot be afforded. This may allow the treatment of cases that are currently not addressed and allow a larger proportion of patients that require blood oxygenation to be assisted.

1.3 Objectives

The concept of intravenously oxygenating the blood through microbubbles originated from research conducted by Prof Pieter R. Fourie (Private Paediatrician and Biomedical Engineer) and Prof Andre R. Coetzee (Executive Head, Anaesthesiology and Critical Care, Faculty of Health Sciences, Stellenbosch University). This research has led to the initiation of a project with the Biomedical Engineering Research Group (BERG) at Stellenbosch University. The present work relates to investigating the concept of oxygenating the blood through microbubbles, as well as all developmental aspects in producing an intravenous oxygenator.

There are many concerns regarding the introduction of microbubbles into the blood, but it is required to know whether the blood in a human can be oxygenated

using microbubbles, and to what degree oxygen transfer can take place. The concerns are mainly due to the risk of bubbles causing embolisms, reducing the blood flow to certain tissues which can lead to necrosis. It is thus necessary to make the bubbles smaller than a certain threshold to ensure dissolution before reaching the capillaries of the lungs and the brain. If the blood is oxygenated by the presence of microbubbles in the blood, it is beneficial towards the development of an oxygenator to determine the rate at which oxygenation can take place, and how this compares to the basal requirements of an adult (roughly 250 ml O₂/min). The factors influencing oxygen transfer are to be identified as well as how these relate to the design of the device.

Previous research has shown large difficulty in producing a prototype that is easy to implement, as large amounts of bleeding have occurred with other intravenous devices (Conrad *et al.* 1994; Snyder *et al.* 2006). In light of this, and the unknown oxygen transfer rate by the introduction of bubbles into the bloodstream, it is necessary to investigate the feasibility of a device that can be inserted intravenously, and determine the constraints on the size and the shape there might be on the design of such a device. These objectives can be summarised into a few research questions:

- Can the blood be sufficiently oxygenated by microbubbles?
- Do the bubbles cause damage to the patient?
- What effects can be observed?
- Can a device be made that is the appropriate size for intravenous purposes?
- Can such a device be inserted safely?
- What is the approximate bubble dissolution time?

The outcome of this thesis will be to have a better understanding of whether it is possible to intravenously oxygenate the blood using microbubbles. To have a better indication if the objectives have been achieved, the specific requirements

need to be determined for the design of the device. Size constraints on the prototype to be inserted into the femoral vein or the jugular vein so that bleeding is minimised are to be investigated. The ultimate measure of success within the context of this thesis would be if animal studies show that an animal's oxygen requirements can be supplied by the oxygenator, and that the animal can be sustained such that SaO_2 levels are acceptable.

1.4 Scope

In order to achieve the objectives as laid out previously, an understanding is necessary of how oxygen normally enters the blood, and how the rate of oxygenation can be quantified. In order to obtain a better understanding of the problem, this has been included together with an overview of previous research involving blood oxygenators in Chapter 2. How the oxygenators introduce oxygen into the blood stream is mentioned, and some advantages and disadvantages of such devices are highlighted. Concerns regarding the introduction of bubbles into the blood are discussed, to what degree these are important for the oxygenation of blood by microbubbles and why they may be more or less prominent for this study. Expected dissolution times are investigated and the implications to an intravenous bubble oxygenator are discussed. The factors affecting the formation of bubbles in the blood are also discussed in Chapter 2.

The outline gained by the literature review in Chapter 2 gives the context for which the intravenous oxygenator is to be designed, and allows the design specifications to be articulated more accurately. The discussion regarding the design of the device in Chapter 3 includes the mechanism of operation, as well as the geometry of some concepts and their respective advantages and disadvantages. The selection of materials and production of a prototype is also included herein, explaining the thought process followed in working towards a prototype that can be tested with animals. The classification of an intravenous device regarding

biocompatibility is also considered, indicating steps required to assess the biocompatibility if the device is to be introduced into the medical market.

To address many of the objectives laid out previously, a large part of this thesis revolved around the testing of prototypes by using animal models, both intravenous as well as extracorporeal (Chapter 4). The testing would give a broader indication of the efficacy of oxygenating the blood using microbubbles, as well as indicate the dangers of large bubbles. To assess the rate of oxygen delivery a flow meter was made and calibrated to be used during the animal tests. Chapter 5 shows the mathematical model developed to validate the findings in the animal tests. Conclusions and recommendations are presented in Chapter 6.

2 Literature Review

2.1 Introduction

Successful development and testing of an intravenous device requires a thorough understanding of the factors that influence oxygenation in human beings. A keen grasp of current methods allows the motivation of the project to be understood in greater depth, and also allows knowledge to be gained with respect to hindrances faced with previous devices. In this chapter an outline is given of the oxygen transfer that occurs in the lungs and how it can be quantified, which allows the factors influencing oxygen transfer to the blood to be investigated. Hindrances to oxygenation are then mentioned, as well as the current state of the art in terms of oxygenation, and some advantages and disadvantages of current systems that have sought to address problems in oxygenation. Concerns regarding the intravenous introduction of bubbles into the bloodstream are discussed, as well as the dynamics involved in the formation of bubbles from a submerged orifice.

2.2 Anatomy and Physiology

In the human body oxygenation of blood occurs in the lungs. The blood acts as a carrier in transporting oxygen (O_2) at a rate of roughly 1000 ml per minute to various parts of the body, as well as carbon dioxide (CO_2) from the tissue back to the lungs to be exhaled at a rate of 200 ml per minute. Oxygen consumption (VO_2) by the tissue is around 230 ml per minute and is affected by factors such as stress and exercise (Edwards Life Sciences 2002). The amount of oxygen delivered to the cells is a product of the amount of oxygen contained in the arterial blood (oxygen content) and the blood flow (cardiac output) that delivers the oxygen to the cells.

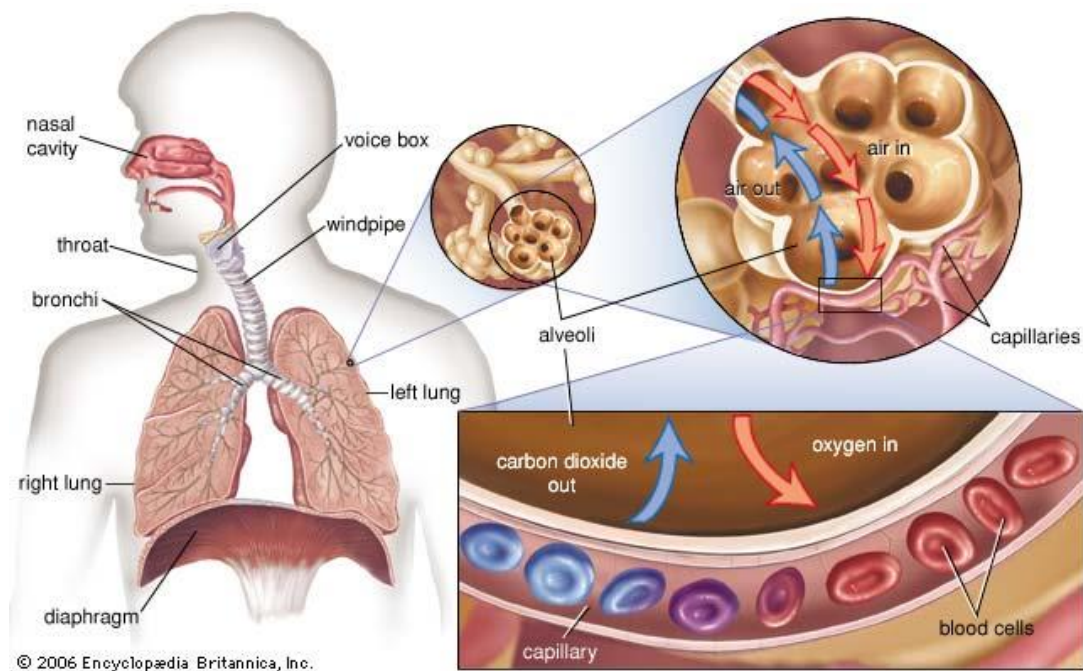


Figure 2-1: Pulmonary alveolus: alveoli and capillaries in the lungs (Encyclopædia Britannica 2011)

The human lung consists of millions of air sacks (alveoli) as seen in Figure 2-1, which combined creates a large surface area estimated at about 70 m^2 to allow for maximum oxygenation. Diffusion of gases takes place across the thin alveolar capillary wall, which is about $1 \mu\text{m}$ thick, and creates a barrier between the liquid (blood) and gas phases. In this way, the red blood cells are exposed to a source of oxygen and a place to release carbon dioxide (Stamatialis *et al.* 2008). The blood flowing through the capillaries in the lungs are oxygenated by the influx of oxygen due to the concentration gradient between the oxygen in the blood and the oxygen in the alveoli. Oxygen movement is from regions of high partial pressure to regions of low partial pressure, as seen in Figure 2-2 below.

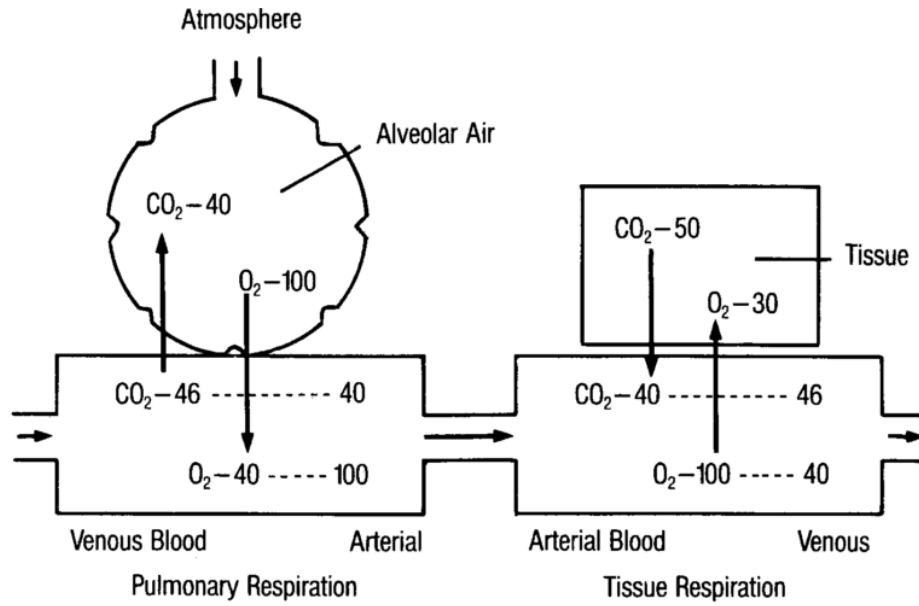


Figure 2-2: Partial pressures of gas within the lungs, blood and body tissue (Edwards Life Sciences 2002)

The driving force for oxygen is about 13 times that of carbon dioxide, but the lung membrane is over 20 times more permeable to carbon dioxide than oxygen (Stamatialis *et al.* 2008). The mass diffusion is governed by Fick's law of diffusion with constant diffusivity (Fischer *et al.* 2009). Fick's first law is stated as:

$$J = -D \times \frac{\partial \phi}{\partial x} \quad (1)$$

where J is the mass flux of oxygen;

D is the diffusivity;

$\partial \phi$ is the rate of change in concentration; and

∂x is the rate of change of the diffusion distance.

Equation (1) shows how the flux is dependent on the change of concentration with respect to distance. Introducing the above equation with the conservation of mass it leads to Fick's second Law as seen in equation (2), and indicates the rate of change of the concentration of the solute in the solvent due to diffusion.

$$\frac{\partial \varphi}{\partial t} = D \times \frac{\partial^2 \varphi}{\partial x^2} \quad (2)$$

where the symbols have the same meaning as before, and t is time. Oxygen uptake is a complex process, and the haemoglobin molecule consists of four *heme* groups to which oxygen molecules can attach. Most of the oxygen is either chemically bound to haemoglobin (98.5%) which is governed by the Hill equation, or dissolved in the blood plasma (1.5%) (Fischer *et al.* 2009). The chemical binding occurs quickly, and is also reversible, which allows the oxygen to be bound to the red blood cells in the lungs, and released in the tissues with ease. The oxygenated blood is transported to tissue via arterial pathways, and returns via venous pathways.

The plasma of oxygenated (arterial) blood usually contains 0.3/100 ml, and when exposed to tissue fluid which contains 0.13 ml per 100 ml of blood, diffusion occurs to achieve equilibrium. Because of the high concentration of oxygen bound to haemoglobin within the red blood cell, 100 ml of blood can supply 5 ml of oxygen to the tissue (Iwahashi *et al.* 2004).

The carbon dioxide that is then produced due to the metabolic process diffuses into the blood, and bonds to the haemoglobin, diffuses into the plasma or is resident in the plasma in the form of bicarbonate (70 %). Carbonic anhydrase acts as a catalyst to hydrate the carbon dioxide to form bicarbonate. This is then transported back to the lungs to be exhaled and fresh air to be inhaled. In the case of lung trauma or physiological reasons as described in Section 1.2, the blood is not perfused to supply the needs of the patient and some or all of the blood is shunted.

2.3 Quantifying Oxygenation

Perfusion is defined as the passage of fluid through blood vessels or tissue, or more specifically the movement of blood to supply oxygen to tissues or organs and remove carbon dioxide. Quantifying the perfusion allows one to understand the effects of different factors, and to know the efficacy of the attempt at oxygenation.

Physiological factors such as oxygen saturation (SO_2), cardiac output (CO) and Haemoglobin concentration (Hb) allow the oxygen delivery and consumption to be evaluated.

SO_2 is the measurement of how much oxygen is bound to the available haemoglobin, of which the saturation of oxygen in arterial blood (SaO_2) is typically 98 %. SvO_2 is referred to as the saturation of oxygen in mixed venous blood, due to the fact that the value is best measured inside the right atrium and is the average value of the blood returning from various tissues. Typical values are 75 %, but can be in the 60-80 % range (Edwards Life Sciences 2002). SO_2 is expressed as a ratio of the amount of haemoglobin that has oxygen bound to it per total amount of haemoglobin available in the blood (Edwards Life Sciences 2002), and can be expressed as:

$$SO_2 = \frac{HbO_2}{Hb + HbO_2} \times 100 \quad (3)$$

where HbO_2 is the haemoglobin-bound oxygen; and

Hb is the amount of haemoglobin in the blood (typically 15 g/100 ml blood).

The saturation of blood is dependent largely on the partial pressure (PO_2) of oxygen in the blood, although SO_2 is not a linear function of PO_2 . This relationship can best be described by the oxyhaemoglobin dissociation curve which relates PO_2 to SO_2 , as seen in Figure 2-3.

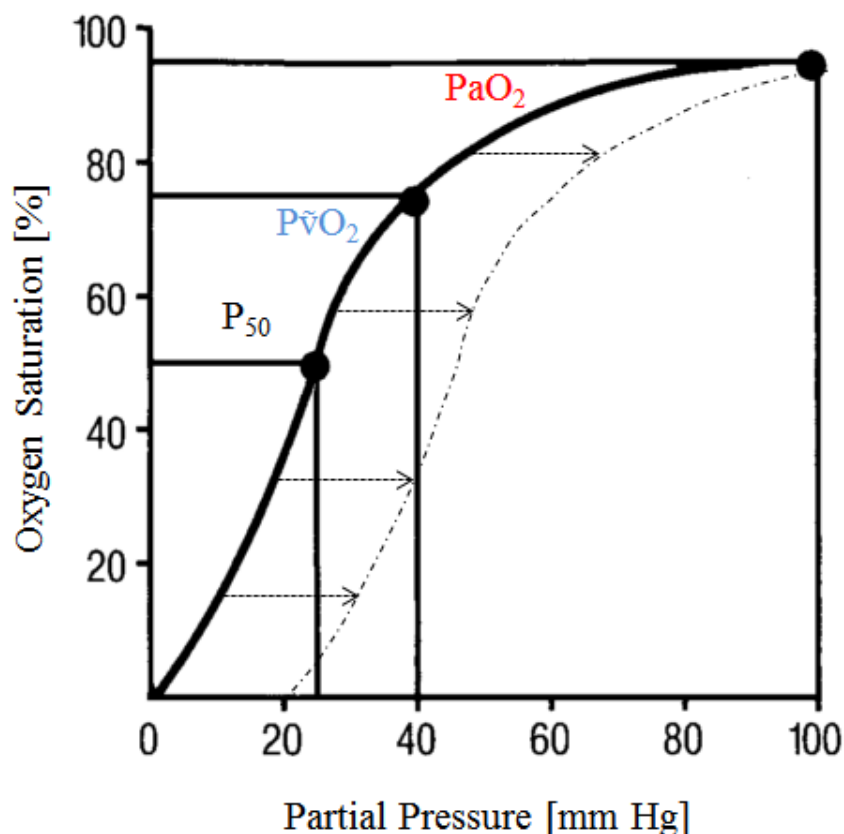


Figure 2-3: Oxyhaemoglobin dissociation curve (Edwards Life Sciences 2002)

This curve can be separated into two regions describing different conditions. The central region describes the conditions found in mixed venous blood ($P_{\bar{v}O_2}$), whereas the upper right region describes the arterial blood conditions (P_{aO_2}). As can be seen for venous blood conditions, a small change in the PO_2 in venous blood will have a large effect on the SvO_2 . For arterial blood, however, a large change in the PO_2 will have a small effect on the SO_2 , where the blood reaches fully saturated conditions. The affinity of Hb for oxygen is affected by several factors, one of which is the pH of blood. An increase in hydrogen ion concentration, for example due to respiratory acidosis (a build-up of carbon dioxide in the blood) causes a *decrease* in haemoglobin-oxygen affinity, shifting the oxy-haemoglobin curve to the *right* (Edwards Life Sciences 2002; Stamatialis *et al.* 2008). A higher PO_2 is then needed to cause the same value of SO_2 (Edwards Life Sciences 2002).

In order to provide an adequate amount of oxygen to the patient the oxygen requirements need to be known. This can be determined from equation (4) which describes the venous oxygen content of the blood (CvO_2). The CvO_2 is the amount of oxygen contained per 100 ml of blood and is the sum of the amount bound to the haemoglobin as well as the amount dissolved in plasma (Edwards Life Sciences 2002). The uptake of oxygen by the blood is balanced with the consumption of oxygen by the tissues through metabolic processes.

$$CvO_2 = (1.38 \times Hb \times SvO_2) + (0.0031 \times PvO_2) \quad (4)$$

where 1.38 is the amount of oxygen (in ml) that can be bound by 1 g of haemoglobin, and 0.0031 indicates the solubility of oxygen in the blood plasma. The amount of oxygen that the tissue consumes (VO_2) is difficult to measure directly; instead the best indicator is the amount of oxygen that is extracted from the blood by the tissue. This is calculated based in the saturation values in the arterial and venous blood as shown in equation (5)

$$VO_2 = CO \times Hb \times 1.38 \times (SaO_2 - SvO_2) \quad (5)$$

where CO is the Cardiac Output.

2.4 Current State of the Art

Traditionally oxygenators have been used as life support devices in operating theatres, thus specific requirements regarding the needs of the patient in critical conditions have led to the designs in use today. Mechanical ventilators have been known to cause damage to lungs by over pressurising the lung tissue (barotrauma) as well as over distending the lungs (volutrauma) (Kaar *et al.* 2007). In view of this, many different designs and approaches have been employed in the past few decades in the pursuit of an artificial oxygenator (Iwahashi *et al.* 2004) and (Haworth 2003).

In this pursuit, both in the form of an extracorporeal device (external) or intravenous device (internal), the objective is to mimic the human lung. It is not possible to exactly replicate the thin alveolar wall that exists in the lung, but methods have been employed that at least perform the action of adequately oxygenating the blood. Of the different methods employed, they can be classified depending on the type of interface formed between the oxygen source and the blood.

Since the 1950's the methods that have been implemented ranged from bubble to screen/film oxygenators, and finally the implementation of hollow fibre membranes (Iwahashi *et al.* 2004; Haworth 2003), but have mostly been limited to membrane and bubble oxygenators (Stamatialis *et al.* 2008; Liddicoat *et al.* 1974; Leonard 2003). Membrane blood oxygenators are viewed to be safer (Hakoshima *et al.* 1989; Masters 1989), and are therefore more widely used (Liddicoat *et al.* 1974). The work done in the field of oxygenators can be separated into classes, depicted in Figure 2-4. The types that are noteworthy will be discussed in the sections that follow.

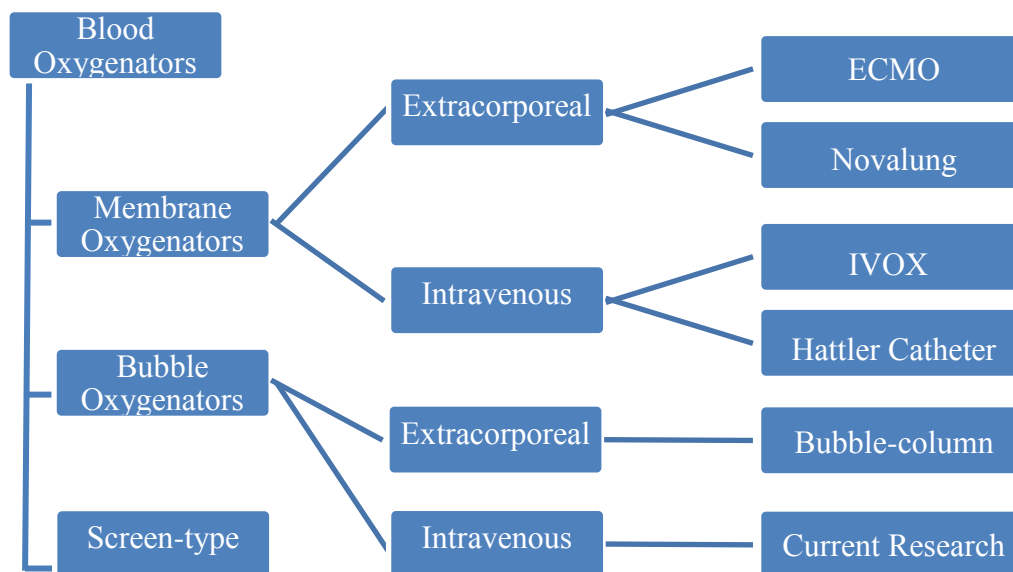


Figure 2-4: Types of oxygenators

The most common type has been the Extracorporeal Membrane Oxygenators (ECMO), which is discussed in more detail in Section 2.5.1. In all cases of

oxygenator designs, efficient oxygen transfer is limited by the blood film between the oxygen exchange surface and deoxygenated red blood cells. Effective mixing can minimise the thickness of this layer, reducing the distance that the gas needs to diffuse (Iwahashi *et al.* 2004). Efficacy of an oxygenator is determined by the following criteria (Stamatialis *et al.* 2008):

- The device must be able to oxygenate up to 5 l/min of venous blood to 95-100 % haemoglobin saturation.
- Carbon dioxide removal such that normal levels are attained (see Figure 2-2), reducing the risk of removing too little (acidosis) or too much (alkalosis) carbon dioxide.
- Have a small blood priming volume.
- Not unnecessarily damage the blood, and avoid haemolysis and protein denaturation.
- Be easy and safe to use by the person administering oxygenation, as well as sterile.

2.5 Membrane Oxygenators

Membrane oxygenators are characterised by the oxygenation taking place due to passive diffusion across the membrane material. The diffusion is limited by the membrane thickness, porosity to certain mediums, and is determined by the concentration gradient per unit area of the membrane. In the human body, membranes are manufactured from organic materials, but there is no limit to the nature of the barrier for use in various industries, as metal, plastic or even ceramic membranes can be produced (Yasuda & Lin 2003). Microporous membranes have dominated the market for use in oxygenators, often in the form of hydrophobic hollow fibres which offer increased surface area (Leonard 2003; Eash *et al.* 2004). The hollow fibres are mostly grouped as bundles, or form a cross-flow mesh as seen in Figure 2-5.

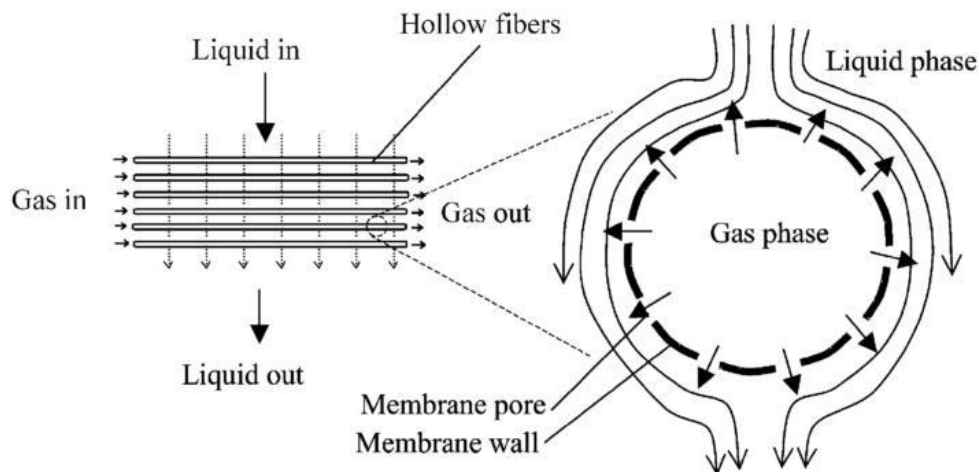


Figure 2-5: Hollow fibres (Wickramasinghe & Han 2005)

The membrane acts as a barrier, separating the gas and liquid phases and prevents the blood from coming into direct contact with the oxygen. The blood plasma that is in contact with the membrane can have high concentrations of oxygen due to the diffusion into the fluid, which implies that the efficiency can be limited due to the lack of gradient across the membrane (Leonard 2003; Iwahashi *et al.* 2004). For this reason high blood flow rates need to be maintained in order to facilitate the mixing of the blood, and hence increase mass transport of oxygen into the blood as well as carbon dioxide removal. This increases mechanical agitation of both oxygenated as well as unoxygenated red blood cells, and can cause mechanical stress and damage (Yasuda & Lin 2003; Hakoshima *et al.* 1989). The interface created by the membrane implies that haemolysis levels are generally lower than with other oxygenators (Iwahashi *et al.* 2004). The blood is also exposed to a larger foreign matter surface area, especially increasing the need for biocompatible coatings of the hollow fibres if long term blood oxygenation is required.

2.5.1 Extracorporeal

2.5.1.1 Extracorporeal Membrane Oxygenators

Extracorporeal Membrane Oxygenators often work on the principle that blood is drained from a major vein, after which the oxygenated blood is returned to a major artery (veno-arterial ECMO), or a major vein (veno-venous ECMO). When the patient is a small child it is placed close to the aortic arch as these vessels are generally the largest extra thoracic objects. The femoral artery is often used in older children (Frenckner & Radell 2008).

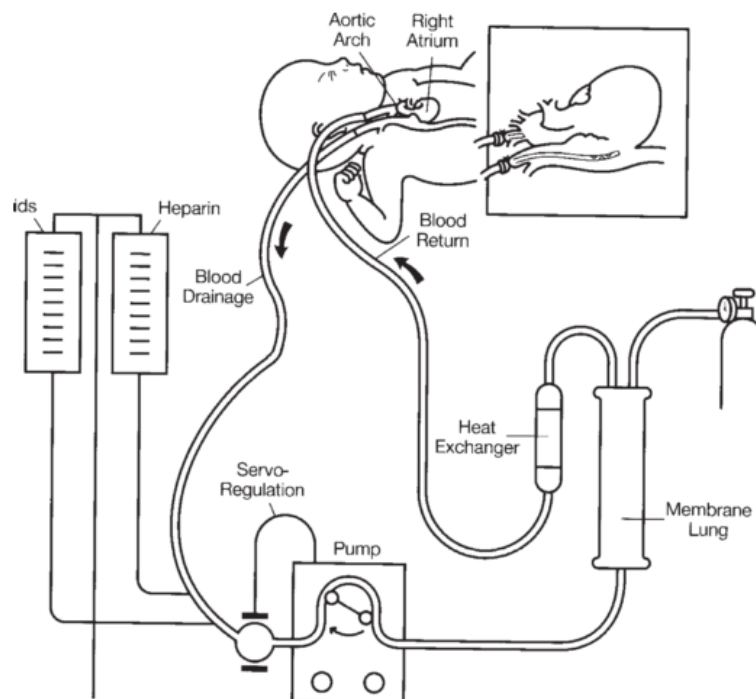


Figure 2-6: Schematic drawing of a standard ECMO circuit (Frenckner & Radell 2008)

After the blood is withdrawn from the patient, it is drained to a collapsible bladder. Heparin and other fluids are then added to the blood before the blood is pumped through the oxygenator and heat exchanger. The addition of substances to the blood, as well as the complexity of machinery, requires that trained personnel need to be

present at all times (Conrad *et al.* 1994; Frenckner & Radell 2008). In the research done by Frenckner and Radell (2008), it was noted that as many as 21500 neonates have been treated with ECMO, with an overall survival to discharge of 76 % (Petrou *et al.* 2006). The survival success of patients is often predicted by observing common indicators such as $A-aDO_2$, PO_2 as well as the Oxygenation Index (OI). The OI is a function of the Mean Airway Pressure (MAP), inspired oxygen concentration and PaO_2 , where an OI value higher than 40 has been shown to predict a mortality rate exceeding 80 % (Frenckner & Radell 2008).

One of the major disadvantages of ECMO's is the high initial cost, as well as the high continuous running costs. In an interview with Murdoch Thomson (a perfusion technologist at Tygerberg Hospital), some light was shed on the typical considerations when using an ECMO. In South African terms, initial costs of the heart-lung bypass machines are a few million Rand, while tubing sets and calibration expendables cost over R 7 000 per patient (Thomson 2011). Lead times before oxygenation can take place are roughly one hour, where the majority of the time is spent anaesthetising the patient and preparing the chest cavity for the insertion and removal points for the blood. After this has been completed the preparation of the oxygenator can take place, which usually takes 12-20 minutes. Systemic heparinisation is initiated to prevent the blood from clotting, but can cause uncontrolled internal bleeding. Tubing and oxygenator kits which have been heparinised are available, but the cost of such kits is more than double that of normal kits, and essentially halves the amount of patients that can be treated due to available funds. The high cost is a large disadvantage in countries where resources are limited.

In a large study done by Petrou *et al.* (2006) it was found that the average health service costs of neonates in the first seven years of treatment were roughly £ 30 000 (R 450 000), almost three times that of treatment via conventional methods. The policies implemented in this study showed a decrease in death and severe disability (36.6 % of 93 cases) when using ECMO compared with conventional methods (58.7 % of 92 cases), but patients spent on average almost double the amount of time

in hospital when ECMO was implemented. Although these figures are overwhelmingly in favour of the use of ECMO for neonates, the situation is not so certain for adult patients, and is highly dependent on the specific disease or syndrome being treated (Crow *et al.* 2009). Recently, survival rates of adult patients have been shown to have improved, with a particular case showing survival rates for severe Acute Respiratory Distress Syndrome (ARDS) to be as high as 52 %. Although the cost and risk to the patient have been extensively analysed, ECMO devices remain complex and expensive machines (Kim *et al.* 2006; Thomson 2011).

2.5.1.2 Novalung

Strictly speaking, the Novalung is a paracorporeal artificial lung, using the heart to pump the blood through the membrane oxygenation section, and hence places extra strain on the heart. This is a concern for cases where neonates are being treated, or where the patient is already in a critical condition. The oxygenator has been implemented in parallel, where the blood is shunted from the pulmonary artery to the left atrium, but this increases the risk of thrombosis and oxygen emboli. It has also been implemented in series as seen in Figure 2-7.

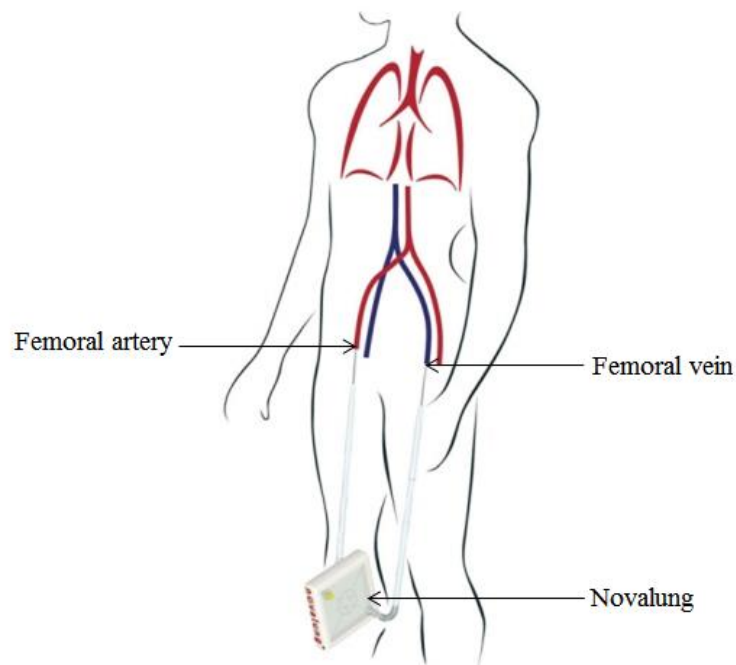


Figure 2-7: Image of the Novalung (Artificial Lungs 2010)

Although this is less risky than the parallel case, there is an increase in the strain placed on the heart. Gas transfers can be improved if larger than the current 1.3 m² membrane surface areas are used (Camboni *et al.* 2009). This device is one of the first commercially available devices that is ready for ambulatory use, although the elevation of the device above the patient is important, as a negative pressure can cause the formation of bubbles (Schmid *et al.* 2008).

2.5.2 Intravenous

Intravenous oxygenators have been used as complementary methods of supplying oxygen in conjunction with mechanical systems. These devices incur similar physiological interactions compared to the extracorporeal devices, although the insertion of a relatively large device intravenously is more complex. Also, the risk of gaseous emboli or detachment of a thrombus is increased because the device now sits entirely within the body, which is the case with the Hattler Catheter as shown in Figure 2-8. Consideration needs to be given to the following:

- The presence of bubbles or foam in the blood stream.
- Lacerations, tears or cuts in the arteries during insertion and operation.
- Obstruction of the blood returning to the heart due to occupation of the vena cava.

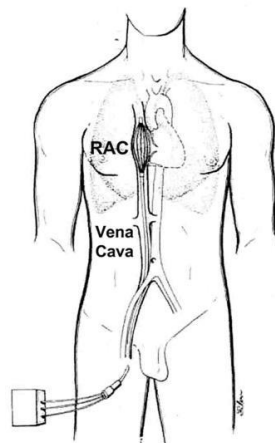


Figure 2-8: Drawing of the Hattler Catheter device as positioned in the vena cava
(Hattler *et al.* 2002)

2.5.2.1 IVOX

The IVOX device is inserted similar to the Hattler Catheter. It consists of crimped hollow fibres that are curled up into a compact bundle before it is inserted into the venae cava (as seen in Figure 2-9). This gas inlet is connected to a 100 % oxygen supply at atmospheric pressure, and the gas outlet line is connected to a vacuum pump.

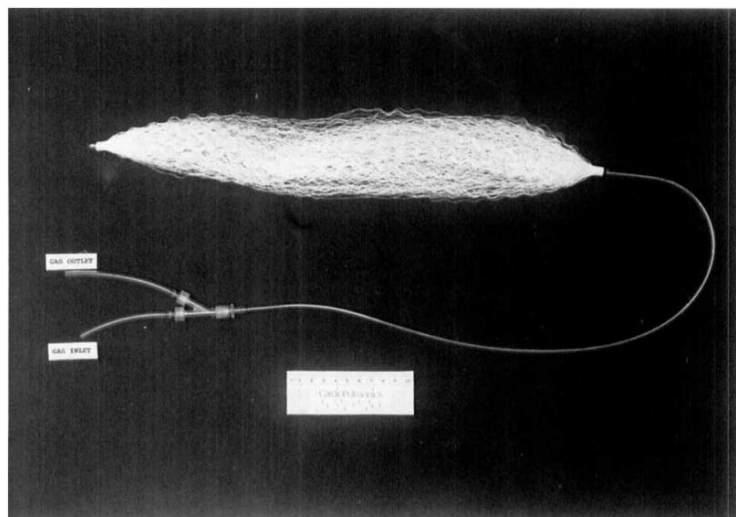


Figure 2-9: Photograph of the IVOX device (Mortensen 1992)

The summary of the clinically relevant findings by Conrad *et al.* (1994) show favourable results concerning the support given through implementation of intravenous oxygenation methods, but maximum oxygen transfer rates were found to be 70 ml/min. Although this represents only about 30 % of the total requirements of an adult, the PO_2 levels were increased above the critical 60 mmHg mark within the first eight hours of implementation (Conrad *et al.* 1994). One of the biggest problems faced with the IVOX is bleeding at the insertion site due to insertion and removal. In the above-mentioned study, blood loss due to IVOX implantation averaged 376 ml and IVOX removal averaged 175 ml per patient. In one particular study, implantations resulted in blood loss in excess of 500 ml in 15.9 % of the 164 reported cases. Most of the clinical trial investigators were pleased with the IVOX device, but

suggested that the device should transfer more gas, be easier to implant and to remove and be able to be utilised without the need of systemic coagulation.

2.5.2.2 Hattler Catheter

The aim of the research done by Eash *et al.* (2005) was to develop a RAC that could provide sufficient gas exchange such that ventilator support could be minimised, named the Hattler Catheter. What makes this device different from the IVOX is that a pulsating balloon assists in the movement of blood across the gas exchange membranes (Snyder *et al.* 2006). The device is positioned similar to the IVOX. Placement of the device next to the right atrium has the advantage of the gas exchange fibres coming into contact with blood entering the right atrium from the upper half of the body as well, showing notable improvements of carbon dioxide exchange. The pulsating balloon allows for the blood to be exposed to a larger membrane surface area, and therefore increases the mass transfer (Snyder *et al.* 2006). Due to the increased mass transfer capabilities, surface areas of 0.17 m² have been achieved, but the pulsating balloon has been shown to increase mass transfer in the length where the balloon operates. Target transfer rates of 75-85 ml/min were not reached with early designs, but design changes were made to increase fluid velocities past the hollow fibres (Eash *et al.* 2005). This would have the effect of increasing mechanical agitation of the blood, and thus cause a larger amount of haemolysis.

2.6 Bubble Oxygenators - Extracorporeal

Between 1950 and 1980 the most commonly used oxygenator was the disposable bubble oxygenator. It was popular due to its low cost and ease of implementation (Iwahashi *et al.* 2004) as well as good heat and mass transfer rates (Kazakis *et al.* 2008b). Many third-world countries are advocating the return to older methods such as bubble oxygenation due to their simplicity, and that the oxygenators can be manufactured easily (Leonard 2003). The production of bubbles in oxygenators can be produced in several ways, producing complex multiphase flows through which

oxygen is introduced and carbon dioxide is removed (Kazakis *et al.* 2008b). Oxygen bubbles can be produced through orifices in a plate or formation through a nozzle, but unintended formation can occur in membrane oxygenators by cavitation and boiling (Corchero *et al.* 2006). The most common type of bubble oxygenators consist of a vertical column of blood in which the gas bubbles are directly introduced, where buoyancy forces cause high bubble speeds. Thus large amounts of turbulence causes the saturated boundary layer to be minimised (Yang *et al.* 1971b). This increases red blood cell contact and causes the bubbles to dissolve faster, making the process very simple, yet efficient (Iwahashi *et al.* 2004).

The main drawbacks regarding bubble oxygenators are red blood cell mechanical damage, as well as contact with a new foreign surface and the need to remove bubbles before re-entering the patient. The production of bubbles causes the blood to continually be exposed to new surfaces, unlike the stationary interface as found in membrane oxygenators (Leonard 2003). Antifoam is used to remove the froth that forms due to the bubbling action (Litwak 2002), but has been shown to have negative consequences, such as possible carcinogenicity (Thomson 2011) and an emboli from the antifoam itself (Cassie *et al.* 1960).

2.7 Concerns Regarding Microbubbles in the Blood

Although the introduction of microbubbles into the bloodstream may be intentional such as the formation of microbubbles for ultrasound imaging, it may also be introduced unintentionally by mechanical heart valves (Fischer *et al.* 2009). The introduction of microbubbles into the blood is a major concern as they are known to have negative effects. Microbubbles cause haemolysis and denature proteins in the blood due to the mechanical action of the microbubbles on the blood cells, but can also be a factor leading to tissue damage. Further investigation shows why these concerns are applicable to an intravenous oxygenator, and what physiological effects can be expected.

Physical forces such as shear stresses are thought to play a major role in haemolysis. Damage of red blood cells can be due to solid surface interaction, damage at the gas/blood interface, cell/cell interaction and viscous heating (Leverett *et al.* 1972). Significant haemolysis can take place in the gas/blood region, but it is considered that high shear stress levels causes damage, which is due to the shear stress acting directly on the cells (Leverett *et al.* 1972). Regarding the physical size of the bubbles, they must be small enough so that they dissolve quickly, not obstruct blood flow, and not coalesce with other bubbles upon formation (Schubert *et al.* 2003). It is the relatively high surface tension of the blood-air interface that causes bubbles to be trapped in small vessels, and causes mechanical obstruction of the blood flow (Misra & Gadhinglajkar 2009; van Blankenstein *et al.* 1997). Bubble entrapment has been characterised by three factors: blood pressure, diameter of the vessels in which the bubbles are trapped, and surface tension of the gas-bubble interface (van Blankenstein *et al.* 1997). This implies that small capillaries as found in the brain and lungs are especially susceptible to the entrainment of microbubbles.

Another concern is that of the introduction of pure oxygen into the blood stream, as it is generally considered to be toxic. Oxygen toxicity is dependent on exposure time and oxygen concentration, but can be aggravated by high levels of carbon dioxide, stress and fatigue. It manifests as Central Nervous System toxicity – known as the Bert effect – which includes progressive but reversible myopia and delayed cataract formation (Patel *et al.* 2003). It can also cause pulmonary damage in which case it is known as the Lorraine effect. Retinopathy of Prematurity is one of the largest causes of blindness during childhood, and is mostly due to uncontrolled administration of high concentrations of oxygen (Patel *et al.* 2003). Premature and weak neonates are at higher risk and are more prone to develop chronic lung diseases due to oxygen toxicity (Patel *et al.* 2003). Pure oxygen (100 %) can be tolerated at sea level pressure for 24-48 hours, but thereafter tissue damage will occur (Patel *et al.* 2003). Thus there is a possibility that the advantages of short-term implementation of an intravenous bubble oxygenator may outweigh the risks such as haemolysis and oxygen toxicity.

2.8 Bubble Dynamics

2.8.1 Force Balance

The formation of bubbles in multiphase flows is dependent on different factors of the phases, where a force balance indicates the effects of different properties. The formation of bubbles from a pore can be classified into four stages: nucleation period, under-critical growth, critical growth and necking (Gnyloskurenko *et al.* 2003). When necking is complete, the bubble detaches, and becomes free of the surface effects found along the membrane surface. The different stages can be seen in Figure 2-10, showing the effects on bubble formation of a surface with good wettability, compared to one with poor wettability. It can already be seen what effects wettability has on bubble formation.

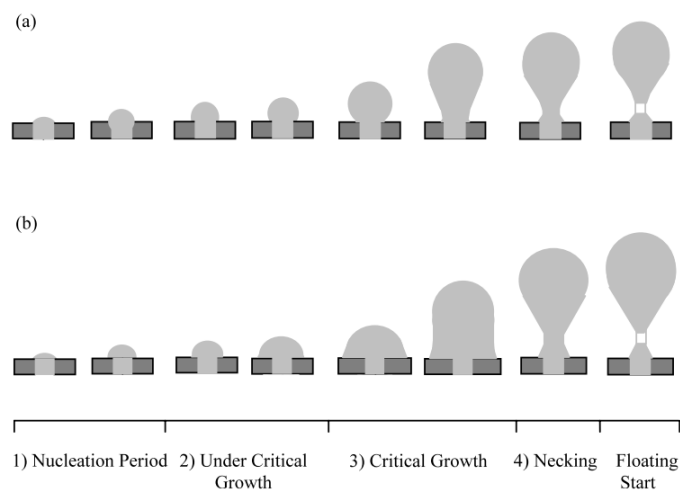


Figure 2-10: Bubble formation stages: (a) Good wettability, (b) Poor wettability
(Gnyloskurenko *et al.* 2003)

Investigating the forces acting on the bubble reveals that forces act either to detach the bubbles, or to resist detachment. Detachment forces on the bubble are gas momentum, gas pressure force and tangential viscous drag, while retardation forces are the parallel viscous drag working in the axial direction of the pore, inertial force of the liquid and surface tension forces (Kazakis *et al.* 2008b), (Nahra & Kamotani

1998), (Krishnan 1994). Buoyancy may act to detach the bubble or to retard its detachment, depending on the orientation of the device. Figure 2-11 depicts the forces and the line of action.

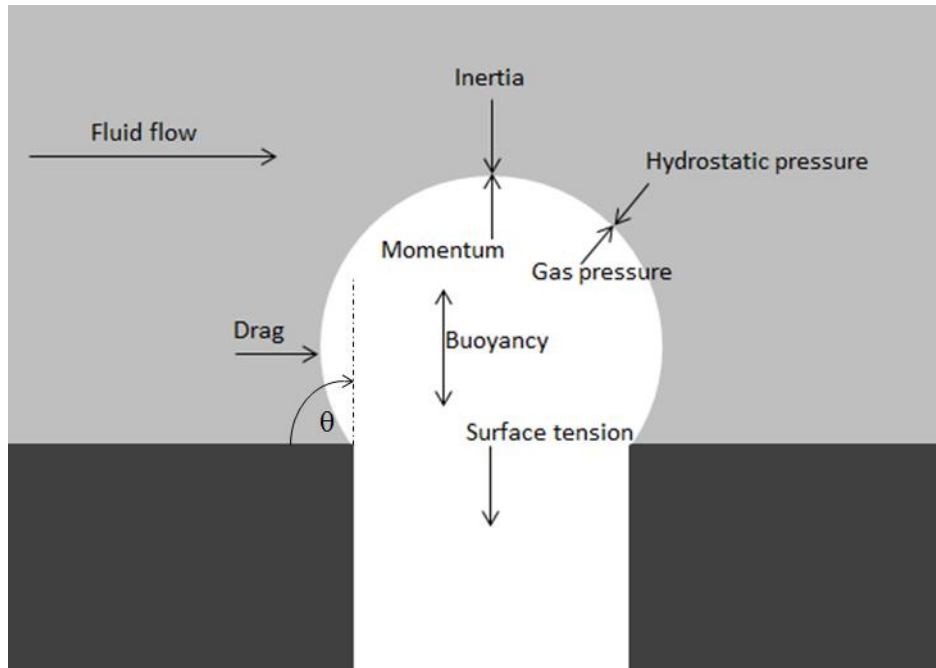


Figure 2-11: Force balance of a bubble during the critical growth period

2.8.2 Effect of Material Properties

For bubble formation to occur from a submerged orifice the capillary pressure needs to be overcome. The pressure is inversely proportional to the capillary diameter, which is known as the bubble point pressure, and gives an indication of the pore sizes of the material. After this pressure is overcome and a bubble starts to form, the bubble grows to such a point that it detaches from the pore. The capillary pressure is given by (Kazakis *et al.* 2008b):

$$\Delta p = \frac{2 \times \sigma_L}{r_p} \quad (6)$$

where σ_L is the surface tension;

r_p is the pore radius; and

Δp is the capillary pressure.

Apart from haemocompatibility, the material properties affect the bubble production based on wettability, as well as pore size (Gnyloskurenko *et al.* 2003). Smaller pores form more numerous, smaller bubbles (Kazakis *et al.* 2008b). There are two distinct regions that exist, as seen in Figure 2-11, that of the gas/liquid (blood) where the bubble is formed and one of the membrane/liquid where there are no pores. The first is dominated by viscosity and surface tension effects, whereas the second is dominated by surface tension and polarity of the liquid and polymer surface. The bubble that is formed at the pore does not extend its base further than the pore edges when a hydrophilic (good wettability) material is used (Corchero *et al.* 2006; Martin *et al.* 2006), as seen in Figure 2-10, but reaches final size when other forces such as buoyancy or drag cause the bubble to detach.

The material properties affect the bubble size based on the fact that surfaces with higher energy are *more hydrophilic*, and are therefore characterised by smaller water contact angles (in the $0 < \theta < \pi/2$ range). In effect, the surface is electrically polarised which allows polar fluids such as water (and therefore also blood) to form hydrogen bonds with the surface. Research shows that for very hydrophilic surfaces below the $\theta = \pi/4$ cross-over angle (see Figure 2-11), bubble size is a function of the size of the orifice only, and not the contact angle (Yasuda & Lin 2003; Gnyloskurenko *et al.* 2003) as illustrated in Figure 2-12. This implies that if a material is chosen with high wettability, i.e. small contact angle, that the pore size can be minimised which will minimise the bubble volume, and hence increase the surface-to-volume ratio of the bubble introduced into the blood. The surface-to-volume ratio is an indication of the size of the bubbles, where a larger ratio is advantageous for bubbles in the blood as this implies a larger surface area for oxygen transfer.

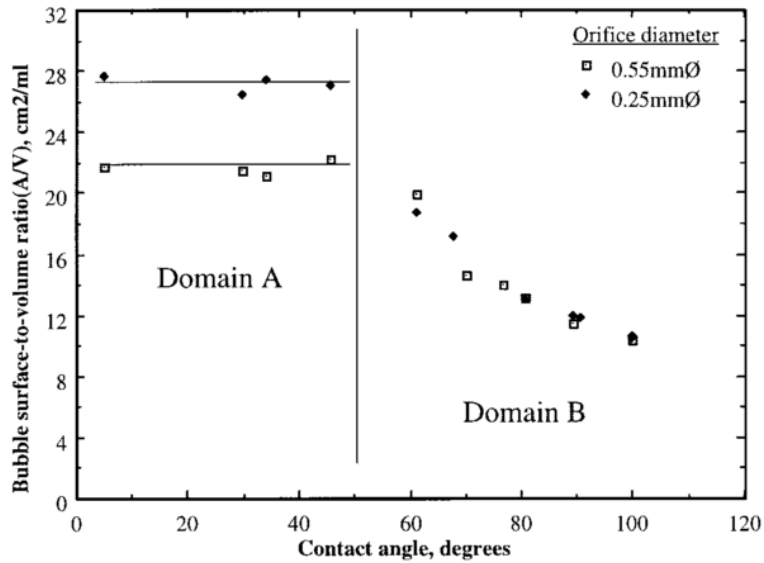


Figure 2-12: Graph of bubble surface-to-volume ratio vs. water contact angle
(Yasuda & Lin 2003)

For larger contact angles ($0 < \pi/2 < \pi$), the surface is hydrophobic, and has low surface energy (Yasuda & Lin 2003). In this range, bubbles size is independent of the pore size, but is rather dependent on the surface energy of the submerged surface. On a very hydrophobic surface the base of the bubble can be up to 10 times the diameter of the orifice (Yasuda & Lin 2003). Surfaces which exhibit lower contact angles allow the bubble size to be determined by the pore size, allowing bubble sizes to be minimised.

2.8.3 Effects of Fluid Properties

The liquid that the bubbles is being formed into plays a large role in terms of bubble formation and bubble movement. During growth and detachment phases, the bubbles may coalesce with other bubbles emanating from neighbouring formation sites to form a larger bubble (Kazakis *et al.* 2008a). The low surface tension of the blood may hinder coalescence of bubbles, as the thin film between neighbouring connected bubbles is not drawn away completely (Kazakis *et al.* 2008a; Tse *et al.* 1998). Tan *et al.* state that coalescence is minimised because viscous drag and buoyancy forces have the effect of removing the bubbles from the formation site, reducing the chance

of coalescence (Tan *et al.* 2000). The drifting action is more pronounced when the bubbles are produced in a high viscosity fluid, as buoyancy forces are negated by drag forces. Higher liquid viscosity increases drag, and coupled with the normal flow of the blood with respect to the gas flow assists to detach the bubbles from the pores. Kazakis *et al.* noted that smaller bubbles were formed in fluids with higher viscosity (Kazakis *et al.* 2008b). This is attributed to more pores being activated due to the normal direction force on already forming bubbles for the same gas flow rate, which also means that the mean bubble size is reduced, and more numerous bubbles are produced (Kazakis *et al.* 2008b).

2.9 Summary of Chapter

The amount of oxygen dissolution in the blood and oxygen supply rates to the tissue can be quantified by observing the blood saturation equations as described in equation (4) and (5). The SO_2 of the blood is a function of PO_2 as seen in the oxyhaemoglobin curve (Figure 2-3), which indicates that a small change in PO_2 in venous blood can cause a large change in the SvO_2 . Although oxygenation devices have been in development for the past 60 years, there are still shortcomings with regards to increasing the PO_2 in the blood of the patient, such as extra harm to the lungs, the incidence of blood trauma as well as high costs of some of the devices. The short-term implementation of an intravenous bubble oxygenator may however prove useful when considering the impracticality of larger ECMO devices, or the reduced oxygen transfer of respiratory assist devices such as the IVOX, Hattler Catheter or Novalung. The risks regarding the introduction of microbubbles into the blood have been highlighted, and it is noted that long-term bubble oxygenation is more dangerous to the patient than when membrane oxygenators are used. To minimise the risk presented by the bubbles, the bubble sizes need to be minimised, and in effect increasing the surface-to-volume ratio and hence oxygen transfer rates. The factors that influence bubble formation were investigated, and it was found that hydrophilic membranes are advantageous for the production of smaller bubbles from a submerged orifice as the bubble sizes are controlled by the pore sizes only.

3 Design

3.1 Performance Requirements

A method of oxygenating the blood is desired that can temporarily replace the function of the lungs. This method must be safe, effective and easy to implement. A few ideas were drawn up and discussed with Prof Coetzee to obtain clarification regarding the implementation of such devices, as well as possible insertion techniques for a catheter-like design. Thereafter, a more general design was decided upon, which would allow the concept to be proven. Emphasis was placed on two main factors in order to achieve the objectives laid out in Section 1.3 regarding the design of the device. Firstly, the selection of a material is considered that can be used to produce microbubbles within the blood. The microbubbles preferably need to be less than 300 μm to ensure adequate dissolution; it is however uncertain exactly what size bubbles are too large. Further testing will give an indication regarding bubble sizes, and what physiological effects can be seen that will be an indication of damage caused by the bubbles.

Secondly, the size and geometry of the design is determined by the size of the femoral vein (where the device is inserted) as well as the vena cava (where the device is placed). The final implementation of the device needs to be such that bleeding is minimised while still being easy to implement. These requirements, as well as other requirements outlined by Prof Fourie were used to construct a list of specifications given in Table 3-1.

Table 3-1: Design Specifications

Parameter	Limits	Reason
Device Outer Diameter	6 mm (18Fr)	Minimise bleeding
Insertion and Removal Method	Via standard catheterisation procedures	Equipment exists and procedures are safe and well established
Oxygen Delivery	75-125 ml/min	Represents 30-50 % of adult basal requirements
Bubble Size	Less than 300 μm	Initial estimate on minimum bubble size required for dissolution of bubbles before reaching the lungs
Internal Pressure	High pressures - dependent on material pore size	Material must under no circumstances rupture or tear as this would cause death of the patient
Material Properties	Hydrophilic, less than 5 μm pore sizes	Smaller bubbles are produced from smaller pores and a hydrophilic surface
Oxygenation Assistance Time	Less than 30 minutes	The device is not intended for long term usage, but rather for short term intervention or assistance as a means of first aid
Biocompatibility	Haemocompatible	Possibly a compatible coating on the device surface, but duration of oxygenation must be taken into account

3.2 Initial Concept

The safety and ease of use of such a device is mostly attributed to its physical geometry and surface properties of such a device. In an email from Prof Fourie (2010), some criteria were outlined that the oxygenator needed to fulfil, and consideration was given to the design to fulfil these criteria. Intravenous oxygenators already exist that are inserted and operated similar to that of regular catheters. The concept of a RAC has several advantages, mostly concerning insertion and removal of the device, as well as ease of producing a prototype. Catheterisation of venous areas is a common procedure, and thus the testing of such a device could easily be implemented. The device must be easy to insert and to remove, and cause little bleeding to the patient, as these were issues faced with other RACs. It also should be sturdy and reliable, i.e. provide a constant, known amount of oxygen to the patient to supply 30-50 % of the patient's oxygen requirements. The basic shape is shown in Figure 3-1, and includes the oxygen transfer section, oxygen supply tube and the insertion nipple. Different concepts can be seen in Table A-1 in Appendix A. These range from star-shaped cross sections to tangling hollow-fibres, but the final concept that was chosen is depicted in Figure 3-1. The oxygenation section could be up to 300 mm in length due to the length of vena cava, and match the diameter of the vena cava (which varies with age, but is roughly 25 mm). One of the requirements laid down by Prof Fourie (2010) was that the cross-sectional area must not obstruct more than 50 % of the vena cava.

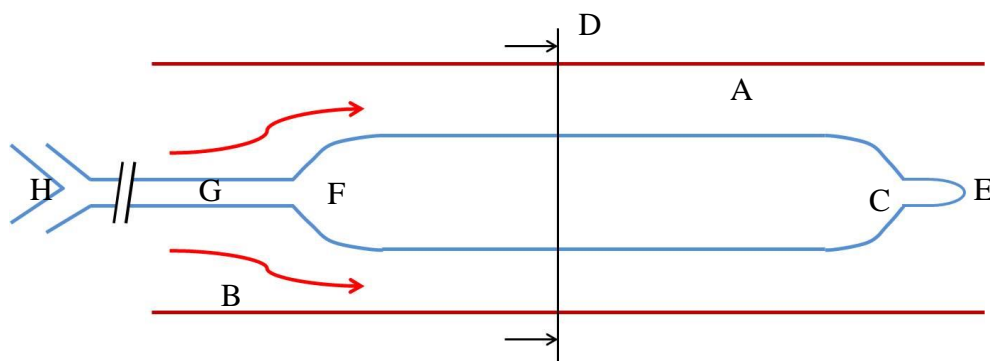


Figure 3-1: Diagram of original concept

A layout of the final concept shows that the device lies within the vein (A), while the blood (B) flows past the oxygenation section (C) where the bubbles are produced. A cross-sectional view (D) of the device being deployed can be seen in Figure 3-2. The insertion nipple (E) allows for the oxygenator to be guided into the vein without damaging the endothelium of the veins. This could typically be constructed of silicon. The other end of the device is connected to the oxygen supply tube (G) at the base of the oxygenator (F). The end of the device that is inserted first (E) and lies closest to the heart will henceforth be known as the *proximal end*, and the end furthest from the heart the *distal end*. The oxygen supply tube is connected via ports (H) to the oxygen supply tank, as well as to a pressure gauge if required.

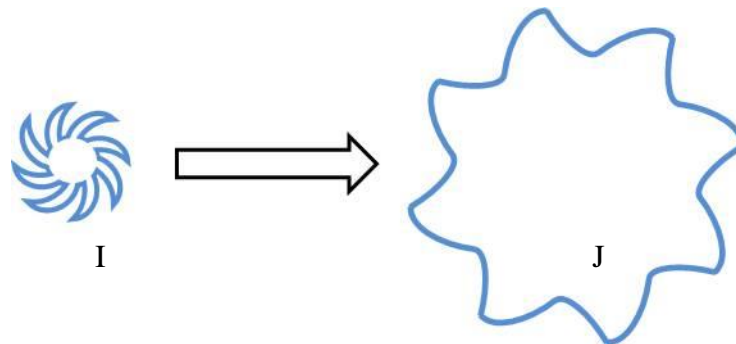


Figure 3-2: Cross-section of the deployment of the oxygenator

The deployment of a folded oxygenation section would allow a larger oxygenation section to be exposed to the blood. The folded section (I) as seen in Figure 3-2 would occupy less space than the deployed section (J), and would add extra rigidity for inserting the device into the vein. It was noted early on that producing a prototype with the shape as shown in Figure 3-2, would be difficult due to the sealing that would be necessary along the length of the tubular structure, as well as at the ends of the device. The proximal end of the oxygenation section would be sealed around the flexible nipple, and the distal end would be sealed around the oxygen supply tube. This could be achieved through a Nylon insert, but would add volume and complexity without an increase in seal quality. The supply tube could also temporarily house the guide wire if needed

and remove waste gasses if needed. Prof Coetzee suggested that the device incorporate a static pressure transducer or a blow-off valve (at H in Figure 3-1) to prevent excessive pressure developing inside the device. This was not implemented in the prototypes but could be considered for future work.

3.3 Geometry and Mechanics of Operation

3.3.1 Conceptual Operation

The initial idea for the mode of operation of the device was conceived after the design specifications of the oxygenator were considered. The operation depended on the insertion method, size constraints, as well as material properties and availability of materials. The decision to use a membrane material was made after initial research showed that polymer membranes are commonly used in oxygenators (Haworth 2003), and thus such materials are readily available from suppliers, as well as that the membranes can be coated to improve biocompatibility of blood contact devices. The method of bubble formation was investigated to obtain a better understanding regarding possible production methods of a prototype. Previous authors have looked into the production of microbubbles for introduction into the bloodstream (Schubert et al. 2003). One of the methods was by microetching silicon liquid and gas pathways, which allows the oxygen bubbles to be formed by a venturi effect when the blood flows past the constricting wall, as shown in Figure 3-3. This constricting wall creates a nozzle of high velocity against the walls to assist in formation of smaller bubbles, and also creates turbulence in the flow direction to facilitate mixing.

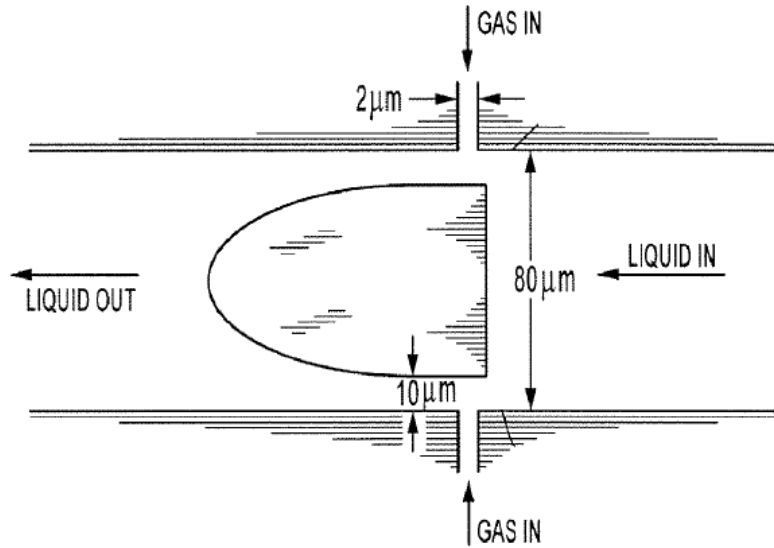


Figure 3-3: Venturi effect generates small oxygen bubbles in the liquid pathways
(Sung Sam Kim & Schubert 2007)

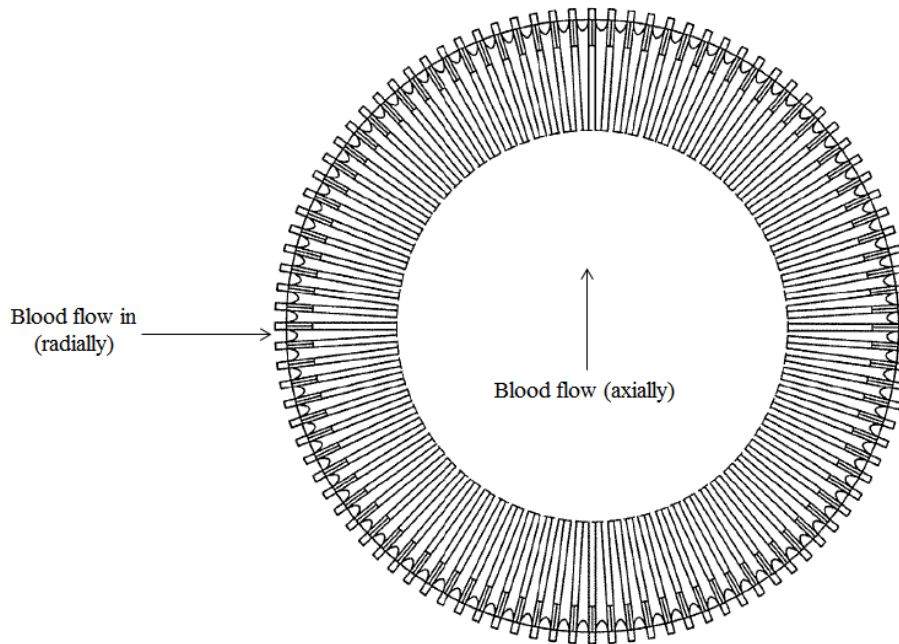


Figure 3-4: Combination of many liquid pathways to form the device to be inserted (Sung Sam Kim & Schubert 2007)

As seen in Figure 3-4, many liquid pathways are microetched in a radial manner to create a surface where fluid and gas can flow. Blood flows from the outside of

the device towards the inner section and is thus oxygenated. Previous researchers have also aimed to produce bubbles by pulsing oxygen through a fine nozzle at very high frequencies (Schubert *et al.* 2003).

Due to the risk of microbubbles damaging the tissue, consideration was given to include a defoamer section that would allow the bubbles to be broken down, removed or contained. The formation of a blood-foam facilitates oxygen transfer, but if it progresses without control can hamper gaseous transfer (Villavicencio & Warren 1962). As seen in Figure 3-5 this design would be implemented by having a mixing chamber (A) where the oxygen transfer effectively takes place and which also functions to channel the blood and thus contain the movement of bubbles to within this chamber (E). The mixing chamber is attached at the base (C) of the smaller oxygenation section (D), and the blood flow (B) is redirected to flow through the mixing chamber.

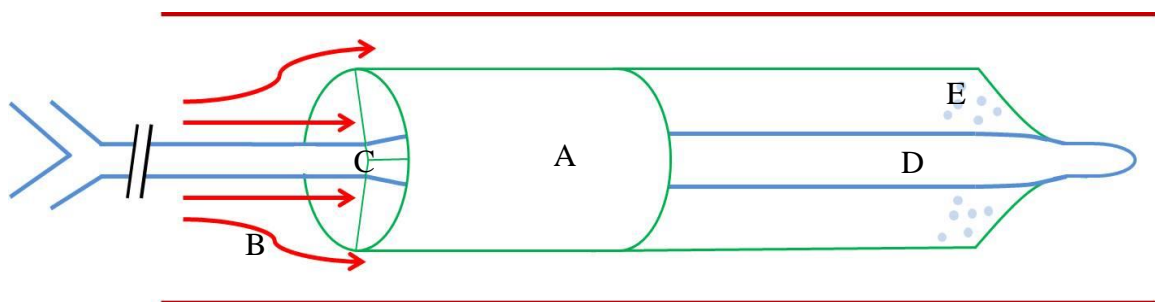


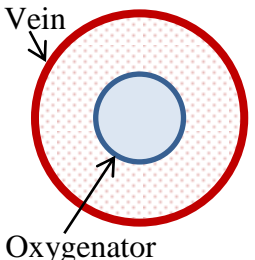
Figure 3-5: Initial concept with the mixing chamber

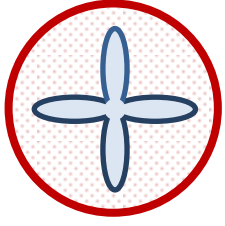
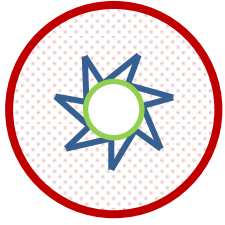
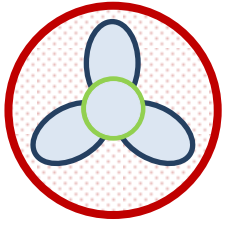
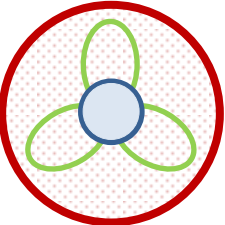
The mixing chamber can be manufactured from different materials, but would typically be of a sponge-like material or a mesh/fabric. In some cases Antifoam A (polymethylsiloxane) has been used, but has been shown to cause embolisms in the brain and kidneys (Villavicencio & Warren 1962). For the purpose of this thesis the defoamer section was not included due to the added complexity in the proof of concept tests. Additionally, animal testing would possibly reveal the extent to which small microbubbles could cause harm.

3.3.2 Cross-sectional Area

Usage of a membrane material requires that the surface properties, pore sizes and material strength fulfil the design specifications. The membrane sheets available on the market are polymers that often have the same thickness and flexibility as paper. The membrane material could possibly be folded into a shape that would optimise its exposed surface area, while decreasing its volume for easy insertion. The exposed surface area causes obstruction of flow that facilitates the mixing of the blood and oxygen bubbles. The orientation of the device within the vena cava would also have an impact, as this would determine the exposed surface area, as well flow obstruction and the facilitating of mixing and the production of smaller bubbles. A few conceptual cross-sections were considered and are classified according to the method the oxygenation section as secured to the supply tube, and consequently the amount of surface in contact with the blood. Examples are shown in Table 3-2. The advantage of cross-sections with lobes/veins is that the membrane can be folded to make the device smaller and stiffer for insertion, but upon applying a high internal pressure the device would unfurl and expose a larger area for bubble production. The concepts are described in the table (blue outlines indicate surfaces where bubbling occurs, whereas green outlines are support structures for the oxygenation surfaces).

Table 3-2: Cross-sectional concepts

Number	Shape	Description
1		This is the simplest design, but does not allow for the device to self-centre within the vein, and could possibly be unstable with respect to position within the vein.

2		<p>Four lobes increase the surface area while reducing the cross-sectional area being obstructed, but if the internal pressure is high enough the lobes will expand. The lobes can be folded for easy insertion, and can act to locate the oxygenator within the vein.</p>
3		<p>This concept is a slight adaptation of the above concept, but the lobes are attached to a central support structure to prevent the veins from expanding under higher pressures. Folding the lobes for insertion may also make the device easier to remove due to partial shape retention.</p>
4		<p>Upon high internal pressure the lobes expand and are firm enough to enable the device to centre itself within the vein while exposing the oxygenation surface to the blood flow.</p>
5		<p>This design differs from the previous one in that the blood flow is not completely external to the device, but there is a dedicated mixing chamber, noted by the green lines (as structural). The oxygenation takes place mainly between the blue and green sections, which implies that there is a reduction in surface area and thus oxygenation capability. The mixing chamber needs to be of a stiff, not necessarily porous material, but will again allow placement of the device within the vein.</p>

Some of these designs were realised by making paper models, to imitate the expected working condition of the oxygenator within the body. This was done to get a rough idea of the expansion and the rigidity of the material, which was similar in strength and thickness to paper, examples of which can be seen in

Figure A-1 and Figure A-2 in Appendix A. The paper allowed for models to be produced easily and different folding techniques to be explored (on a scale of 1:5), with the aim of finding the smallest possible folded size while not hampering unfurling of the device. This took into consideration the length of the veins (or lobes), and the outer circumference of the folded shape, which gave insight into limitations regarding material stiffness and minimum device sizes.

3.3.3 Material Selection

The selection of a membrane material to be used for the oxygenator was done in conjunction with simple tests to investigate the properties of different materials. Sample materials were obtained from a local representative of PALL Corporation, and were screened to investigate the bubbles emanating from a submerged orifice based on pore size, material type and free surface energy. Added to the concept of bubbling oxygen directly into the blood is the idea that the oxygenation area is no longer directly dependent on the *device geometry and surface area*, but now rather on the *bubble surfaces*. According to previous work done on intravenous membrane oxygenators, surface areas ranging from 0.21-0.52 m² are available in products such as the IVOX, whereas a pulsating balloon device such as the Hattler Catheter could reduce the contact area with blood to about 0.17 m² (Snyder *et al.* 2006).

Considering that the device needs to supply oxygen at the rate of 125 ml/min and that the exposed surface is known, the oxygen transfer per surface area per minute can be calculated. If the oxygenation section is 300 mm long, and the approximate insertion size allows for an exposed circumference of 25 mm (which is dependent on the concept shape and cross-sectional area), the total exposed area would be 75 cm² (7.5x10⁻³ m²). Comparing this to the approximate 70 m² surface area that the lungs occupy it can be seen that very high transfer rates must be attained to make such a device comparable to the efficiency of the lung. This can potentially be achieved by increasing the surface area to volume ratio, such that more of the oxygen is in contact with the blood. For example, a bubble of 300 µm diameter

will have a surface area of 0.283 mm^2 and a volume of 0.0141 mm^3 , or 1.41×10^{-5} ml. As depicted in Figure B-1 in Appendix B, a rough estimate when looking at some of the photos taken for glycerol tests show that roughly 400 bubbles can be formed (of $300 \text{ }\mu\text{m}$ size diameter) per second from a surface area of 20 mm^2 (or 0.2 cm^2). This yields an oxygen bubble production rate of 0.028 ml oxygen per second per square cm of the device.

Important factors that surround the bubble size and distribution, are the oxygenator geometry, operating conditions (such as blood viscosity), physical properties of the two phases and the type of bubble producing method used (Kazakis *et al.* 2008b). For the purposes of this thesis, bubbles would be produced by the application of a pressure gradient across a membrane material. A set of initial tests were performed with the aim of determining which material could possibly be used as the oxygenation section. These tests were performed in conditions that simulated the operation of the intravenous device, but were simplified to a degree to which clarification could be found without compromising reliability. Various materials of different filters were supplied by a local representative of Pall Corporation and consisted of blood transfusion filters to air filters (more details can be seen in Table B-1 in Appendix B). The specific properties of the materials have been optimized for the intended use of the filter, the properties of which include the polymer type, pore sizes (determined by the bubble point method), surface energy and material strength (which is a function of the polymer type).

The simplest test setup was to test the materials while submerged under water, to investigate the effect of the material type, pore size and surface energy on bubble production. The tests were performed under standard conditions at room temperature. Air was forced through the different materials under different pressures by use of a simple medical syringe, with the knowledge that air and oxygen have densities and viscosities similar enough for the purpose of these tests. The production of bubbles as well as the performance of the materials was

investigated. Test samples were prepared by cutting a circular material section about 15 mm in diameter and placing it over one end of 40 mm length clear tubing to create an exposed membrane surface area of roughly 15-20 mm². Heat-shrink tubing was then slipped over the clear tubing and material, and heat applied to allow the heat-shrink to grip the material onto the clear tubing. Adhesive was used to fill in the gaps and ensure that the material did not slip off under gas pressures (Figure 3-6). It was already seen that the heat applied to some of the test samples damaged some of the materials, thus some samples were prepared using adhesive only. Initially it was observed that some materials (such as polyester) were sensitive to the type of adhesive used. The difference of hydrophobic and hydrophilic materials is shown in Figure 3-7.

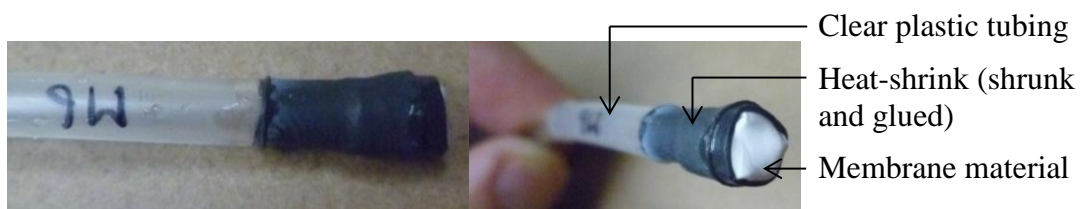


Figure 3-6: Samples for simple tests

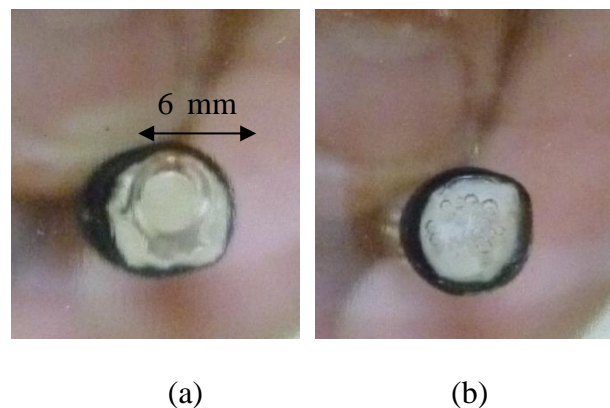


Figure 3-7: (a) Hydrophobic and (b) hydrophilic material

The samples would be manufactured by first folding the material around the clear plastic tubing, after which heat-shrink would be used to facilitate the forming of the membrane material over the opening of the tubing. The adhesive would then be used ensure that no gaps existed between the membrane material and the heat-

shrink. Another layer of heat-shrink would then be used to ensure an air tight seal. This process was followed in making all the samples used in the simple tests; care was taken to ensure that heat and mechanical damage to the samples were mitigated.

Initial observations of 11 materials (see Table B-1) indicated that smaller bubbles were produced by membranes with smaller pore sizes and would thus be better suited for the oxygenator. At higher flow rates, larger bubbles were formed at higher frequencies. Higher pressures were required to overcome capillary pressure for small pore sizes, most evident was the high pressure needed to initiate bubble formation from the material with the smallest pore, the positively charged Nylon filter with 0.2 μm pore sizes (M6 as seen in Table B-1). However, the bubbles were not as small as expected, as the slightly hydrophobic nature of the material caused coalescence of bubbles along the surface of the material. Weaknesses in the materials caused large bubbles to form at the damage sites, which would have been a cause of an enlargement of pores. This is due to the decreased amount of pressure needed to overcome capillary pressure. Some bubbles would continue to grow and coalesce until buoyancy forces caused the bubbles to detach. Materials M5 and M6 exhibited the most favourable bubble sizes, mostly due to the small pore sizes of the materials. Based on this knowledge, samples were requested from PALL Corporation to be used for further testing and the development of prototypes. Due to the long waiting periods for delivery (between 6 weeks and 4 months) only the Nylon and PES membranes were further tested.

For further analysis of the materials, a cylindrical tank was used and filled with a glycerol-water-saline mixture, with an equivalent surface tension and viscosity to that of blood (Rodriguez 2011). The glycerol mixture was based on research done by a previous student and a mixture was prepared by mass, consisting of 48 % glycerol, 52 % distilled water and 9 g salt per kg of final solution (densities can be found in Table C-1 in Appendix C. Sodium azide is often included in mixtures simulating the blood, but due to its high toxicity and difficulty of disposal

(specifically the highly reactivity with copper pipes) it was decided not to use this mixture. Approximately 11 ℓ of mixture was prepared, with a final density of $\rho = 1.125 \text{ kg/m}^3$.

The screened materials were used to make test samples using the same method as for the initial tests and the air forced through in a similar way. Different flow rates were investigated for the different materials and it was found that for smaller pore sizes the bubbles produced were smaller than with the water tests. It was also seen that bubble size was directly proportional to flow rate and dependent on the type of fluid used. The smallest bubbles that could be observed were in the 200-300 μm range.

3.4 Final Design Decision and Prototype

The final design shape was decided upon based on the fact that the concept had to be proven to work first. The design that was simplest to manufacture and that could prove the concept was thus selected. The final design that was decided upon was achievable in the sense that the manufacturing would be done by simple yet effective means. Manufacturing of a prototype was problematic due to limited expertise and information available regarding polymer sealing methods and compatibility. Different companies were approached regarding the assistance of manufacturing a prototype but none could be of assistance, either due to lack of facilities or because this research falls outside of their scope of work. It was then decided that a prototype would be produced by manually sealing the membrane onto an oxygen supply tube, and possibly incorporating the insertion nipple as discussed earlier.

Different chemical adhesives were considered to create a robust seal between the membrane and other structures of the oxygenator, but it was found that certain adhesives damaged the materials. For example, the polyethersulfone (PES) samples deteriorated when used in conjunction with superglue (cyanoacrylate

based adhesives). Also, none of the adhesives could cause the membranes to be attached to the silicon tubing that was considered for the oxygen supply tube to create a proper seal. Thus, polymer welding was considered and more specifically high frequency welding and ultrasonic welding, as well as heat sealing. High frequency welding is commonly used for polyamides such as Nylon, but due to the high cost to develop a single prototype heat sealing was considered.

An industrial heat-sealer was obtained to seal the selected material (Nylon). Good seals were achieved with Nylon, but sealing onto the silicon tubing was not possible. A PVC catheter was next considered, but efforts to heat seal onto PVC catheters resulted in the catheters being damaged. The incompatibility of a silicon insert with the Nylon membrane did not allow the insert to be used either. The seal formed on the Nylon membrane was often stronger than the material on its own, but it was difficult to be sure that the seal was of a good quality. Seemingly strong seals were not as strong as expected and would easily tear upon application of an internal pressure. Through improving the manufacturing process it was found that a medium heat on one side of the folded membrane, and then a slightly higher temperature on the other side (both held for maximum heating time and pressure), would ensure a very good bond. This process was highly dependent on learning the heating characteristics of the impulse sealer, as well as the melting characteristics of the Nylon material. Interestingly, it seemed that the already melted Nylon would have a higher resistance to the flow of heat. Upon cooling, the melted and transparent material would shrink, and distort the folded shape, which inhibited the production of sufficiently long prototypes due to the fact that distortion reduced the ease with which a double-sided seal could be achieved. For initial prototypes as shown in Figure 3-8, a cylindrical shape was produced by folding a membrane sheet in half and sealing at angles of about 60° to the axial line of the device. The distal end of the device was cut to allow the insertion of the oxygen supply line.

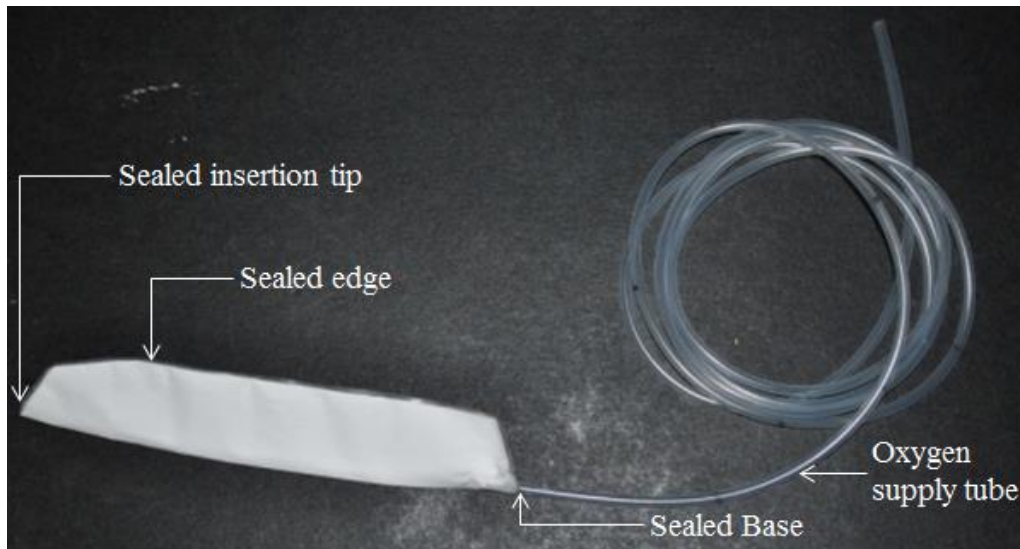


Figure 3-8: Example of a heat sealed prototype

A few of the prototypes were tested under water to inspect the quality of the seal. Some of the prototypes seemed to perform well with regards to bubble size and withstanding high internal pressures, but it was discovered only after the first animal test that the heat-sealing of the Nylon possibly damaged the material. This could be due to the opening of pores due to material shrinkage upon cooling, distorting the material near the seals. This nullified the use of a material with very small pores, and is believed to have been one of the complications with the *in vivo* animal test (Chapter 4). A batch of five adhesives were then further explored to find an adhesive that is compatible with Nylon, and this was then used to manufacture a prototype that was used in the *ex vivo* tests. The device was based on an embolectomy catheter, and proved to be of sufficient strength to withstand the internal pressures upon testing without separating.

3.5 Biocompatibility Assessment

Surface modifiers can be added to blood contacting devices to improve haemocompatibility of the devices. Improving the haemocompatibility is closely linked to the protein adsorption by the foreign material due to the fact that protein adsorption triggers the coagulation sequence. Other methods of coagulation

include platelet activation as well as the compliment system and tissue factors. Insertion and operation of the device can cause vessel trauma, which is related to the generation of a local positive charge and suggests that surfaces with negatively charged groups will exhibit good biocompatibility. Some developments do however show that biocompatibility can be achieved by using hydrophilic or non-ionic surfaces, as have been implemented in this thesis. Generally, improving biocompatibility concerns altering the surface properties that suppress or prevent blood interactions, but allows the bulk of the material which displays certain favourable properties, to be left unchanged (Mao *et al.* 2004).

For a device to be implemented in a clinical setting it often needs to comply with certain national and international standards. Although the haemocompatibility is not very important for the proof of concept tests for the purpose of this thesis, the implementation of a device within a South African context requires that it complies with certain standards. These standards require that the correct procedures for medical registration are followed which will allow the device to be available on the South African market. According to the Medicines and Related Substances Act, 1965, Act No. 101 of 1965 (2011), the intravenous oxygenator would fall under category C2 due to the penetration of the body by the device, and can be further classified as Low, Low Moderate, High Moderate or High Risk. According to the *ISO 10993-4 Biological evaluation of medical devices – Selection of tests for interactions with blood*, a decision tree can be followed to determine the tests that need to be performed to evaluate the biocompatibility of medical devices. The decision tree (shown in Figure D-1 in Appendix D) suggests that for the device being considered, ISO blood interaction tables need to be consulted.

The ISO standards classify the type of blood contacting devices as non-contact devices, external communicating devices or implant devices. A device such as a RAC would be classified as an external communicating device and similar to a catheter in design, but acts as an oxygenator. The blood/device interactions can be

assessed according to ISO 10993-4:2002(E) and based on the type of device, requires that all five categories of blood interactions should be investigated, i.e. thrombosis, coagulation, platelets, haematology and complement system (ISO 2002).

It goes without saying that, where appropriate, a device that is intended to be used *ex vivo* is to be tested *ex vivo*, and similarly with a device intended to be used *in vivo*. This includes testing the device under circumstances that simulate the clinical applications with respect to geometry, blood contact method and time, temperature and blood flow conditions. Inspection of the blood interactions with a device of defined geometry allows the ratio of test parameter to exposed surface area can be evaluated, which will give an indication of total blood/device interaction.

Animal tests were conducted with the aim of validating the design of the device, and investigating the blood interactions. A porcine model was used due to the similarities in the blood of such animals compared to that of humans, and is explored more in Chapter 4. During the *in vivo* test an anticoagulant (heparin) was not added immediately, but was added later due to the blockages that were assumed had formed in the proximal and distal ports of the Swan-Ganz catheter, around which the prototype was based. It was required that measurements could be taken of the blood to evaluate the dissolved as well as bound oxygen.

4 Testing of Concept

4.1 Introduction

Previous analysis (Chapter 3) of bubble production from a submerged orifice has given an indication regarding possible bubble sizes that can be produced, but these tests are limited to information gained regarding a device placed within the body (in vivo). For this thesis, using an animal model would yield a better understanding of the concept as the physiological environment is the same as would be found in a human patient. Before animal models could be used to investigate concepts, an application was sent in for review by the Research Ethics Committee: Animal Care and Use, under the title '*Evaluating the effects of intravenous oxygenation on blood-gas parameters and lung pathology*'. Approval of such a proposal allows sentient animals to be used for research, teaching and testing. This takes into consideration the moral philosophy of non-human animal tests, which includes the humane treatment of animals such that the best interest of the animals is a priority. Appropriate persons were responsible for the various aspects of the animal tests. This included the provision and proper removal of the animals (according to standard methods implemented by the Animal house Manager at the Faculty of Health Sciences) as well as the actual testing procedures as commonly practised.

A testing protocol for the respective tests was established, which included the preparation of the animal model all the way through to final observations. The in vivo and ex vivo tests were performed in a similar manner, but the in vitro tests will be dealt with separately, the details of which are explained in the respective sections. The first step in the protocol was preparation of the animal model, which

included anaesthetising the animal ensuring that the animal was properly monitored and ventilated. This was done by the team at Tygerberg Campus of Stellenbosch University where the testing took place. For the preparation of the ex vivo tests specifically, a circuit was set up prior to testing using standard medical expendables. Observations were then made regarding the condition of the animal in terms of physiological factors such as heart rate, SO_2 and body temperature. The device was then placed inside the animal for the in vivo tests, and inside the extracorporeal circuit for the ex vivo tests. For the in vivo tests, the condition of the animal was again observed and noted, to investigate whether any physiological changes could be seen. The placement of the device within the ex vivo circuit was much easier than in vivo circuit due to the size of the catheters used in the respective tests.

The supply of oxygen was then initiated, while the flow rate of oxygen was very closely monitored and correlated with the physiological effects as seen in the animal in the in vivo test, as well as correlated with the formation of bubbles in the ex vivo test. The flow rate was then increased systematically and physiological effects and bubble formation monitored. Finally, after testing had been completed, the animals were euthanized and the devices were removed.

4.2 In Vivo

The in vivo tests were done using a porcine model to investigate the performance of the oxygenator under controlled conditions. This simulates the conditions of implementation in a human due to the similarities in the physiology between porcine animals and humans. This would give information regarding the rate of dissolution of the bubbles, as well as the physiological effect this would have on a biological specimen. The first prototype consisted of 5 μm pore size Nylon membrane attached to silicon tubing, but due to the size and insufficient sealing of the membrane to the silicon tubing, the prototype was not used. A second prototype was based on a Swan-Ganz catheter which allowed for blood samples to

be taken distal and proximal of the device. The balloon (see Figure 4-1) was removed with the aim of supplying oxygen via the Balloon Port, to inflate the oxygenator and provide oxygen to the animal during testing.

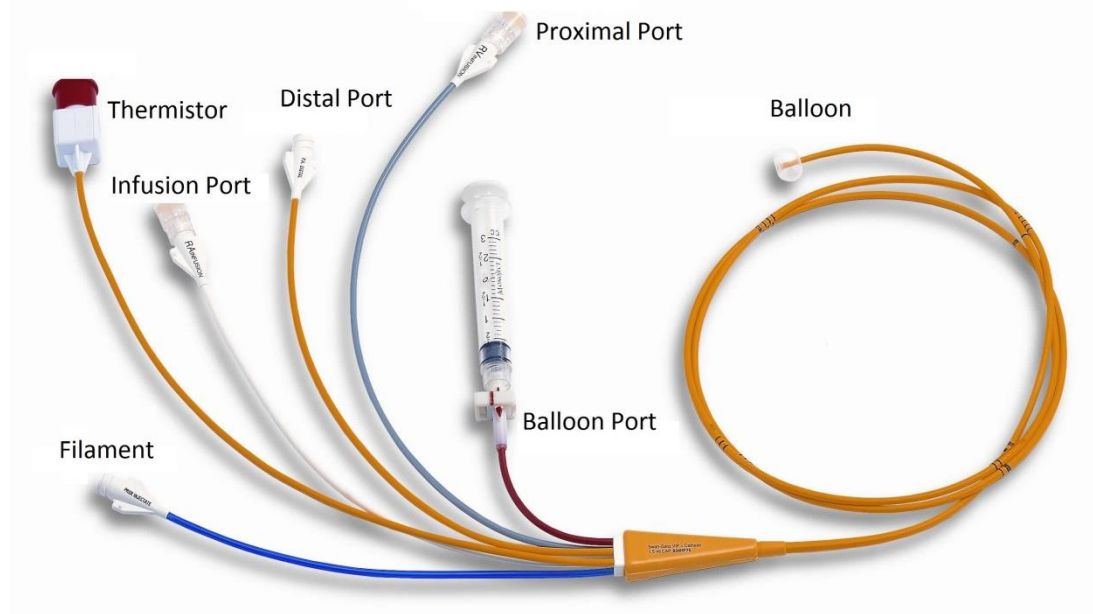


Figure 4-1: Layout of a Swan Ganz catheter (Author n.d.)

The oxygenation section of the device was made of a gas permeable Nylon membrane, and was heat sealed to ensure the device was mechanically safe. This was a possible cause of a weakness in the material which led to the production of large bubbles and the damage of the lungs in the *in vivo* test. Further testing was performed on a porcine model and the device was placed within the vena cava by insertion via the femoral vein (Figure 4-2 and Figure 4-3) prior to testing being performed by two other researchers. For this test, the insertion method was not via standard cannulation methods, as the prototype was too large. The device was inserted into the porcine model for approximately an hour before oxygenation was initiated by using the intravenous device.

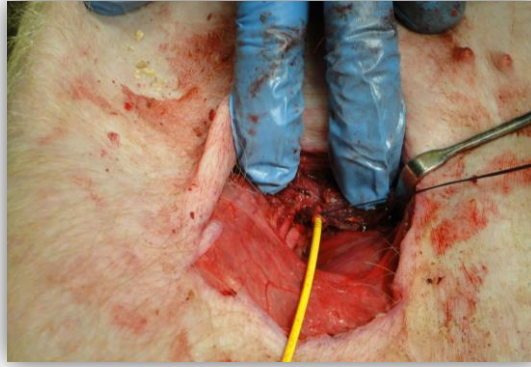


Figure 4-2: Insertion into femoral vein



Figure 4-3: Swanz-Ganz catheter in position

Operation of the ventilating machine was continued to allow for ventilation and perfusion of the animal during operation. The Swanz-Ganz catheter allowed blood samples to be taken directly after the device to investigate the possible increase in SvO_2 and if there was a change in this value. There would be no need to discontinue the use of the ventilating machine, because if oxygenation due to the intravenous oxygenator was not sufficient, continuous ventilation would provide the animal's oxygen needs. Oxygen flow was initiated to the device and the pulmonary pressure was closely monitored, as this would be the first sign of damage to the lungs due to an embolus. The initial pulmonary pressure was 28/17 mmHg, but after 5 minutes of initiation of oxygen the pulmonary pressure was seen to increase to 45/32 mmHg, indicating damage to the lungs of the

animal. It could also be seen that the SaO_2 (arterial oxygen saturation) decreased indicating that there was not only an insufficient amount of oxygen uptake due to the intravenous oxygenator, but also that the ventilating machine could no longer provide the necessary oxygenation. This indicated possible emboli in the lung capillaries. The design and implementation of the device was not successful, because the porcine test subject could not be supported by the oxygenation device alone, neither could the intravenous oxygenator be implemented as a Respiratory Assist Catheter.

At the time of oxygenation however, it was found that the proximal port was blocked when attempts at measuring the SvO_2 were made. Heparin was subsequently added through the distal port in an attempt to physically clear the blockage. The blockage could have been due to a blood clot, and the release thereof could have been one of the reasons for the damage to the lungs – the addition of heparin would have reduced any further clotting. Upon removal of the device, it was observed that clotting had occurred and that a layer approximately 1 mm thick had formed on the outside of the device (Figure 4-4).



Figure 4-4: Device after being removed from the porcine test subject – clotted layer can be seen alongside the device

Upon closer inspection it could be seen that the membrane material had been wetted to a degree that there was some plasma leakage through the membrane. A hydrophilic material had been used such that smaller bubbles could be formed, but it was unsure whether or not the large pores ($\approx 5 \mu\text{m}$ in diameter) were small enough to ensure that small enough bubbles could be produced.

4.3 Ex Vivo

Due to the inconclusive result of the in vivo test regarding bubble formation and the reason for the damage to the lungs, an external bypass circuit was set up for the next test using clear tubing as depicted in Figure 4-5. This circuit could allow more accurate inspection of bubble formation and transport, as well as dissolution times. This also lessened the complexity of the animal testing because attention could be given solely to the interaction of the device within the blood circuit and the size of bubbles emanating from the device. Initially, a saline solution was used to inspect the formation of bubbles, after which blood was used.

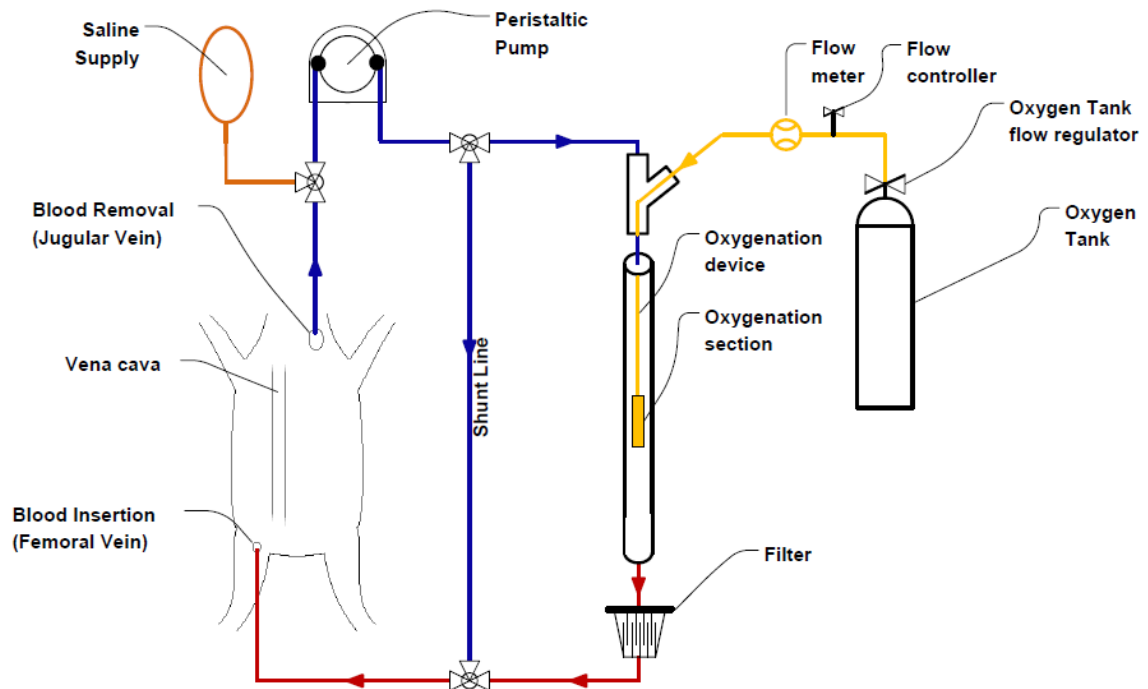


Figure 4-5: Ex vivo test circuit

In the saline solution, oxygen was fed into the oxygenator to inspect the soundness of the seal. During this it was already seen that there were weaknesses in the material (Figure 4-7).



Figure 4-6: Device is inflated before oxygenation takes place

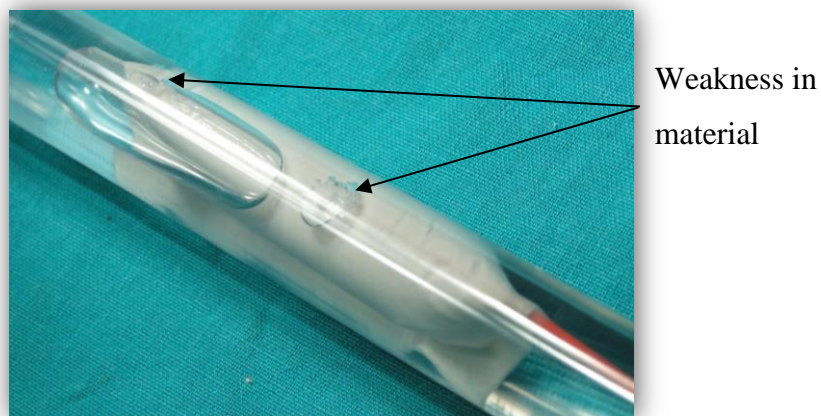


Figure 4-7: Bubbles seen emanating from weaknesses in the material

It could clearly be seen that a positive pressure inside the device was required to overcome capillary pressure and to initiate the production of bubbles from the membrane material. For the ex vivo tests the heat sealing of the membrane was replaced by usage of an epoxy to seal the membrane and attach it to the embolectomy catheter. A weakness on the surface of the material, possibly caused

during manufacturing of the device or caused during insertion, offered less resistance than the pores, and a cloud of large bubbles emanated from the weakness. There were also some complications with the bypass circuit where the blood was removed from the animal through the jugular vein, as it could be seen that the fluid feed rate (determined by the peristaltic pump) was too high and the cannula sucked air. Also, one of the T-connectors leaked, causing air to be pulled into the blood circuit and making removal of the bubbles a constant concern. A filter was placed in the circuit before the fluid was sent back into the animal to prevent gaseous emboli.

It was decided that testing would continue, and the device was inserted into the saline solution. The blood was then fed into the bypass circuit and the saline was pumped back into the storage container. This exposed the oxygenator to the deoxygenated blood. Samples were taken distal and proximal of the device with the blood flow rate initially at roughly 60 ml/min. The oxygen control valve was adjusted to allow pressure to build up inside the device and inflate it, and eventually to overcome capillary pressures in the pores and allow bubbles to form. At roughly 40 ml/min oxygen, a large amount of bubbles could be seen, which collected at the topmost surface of the tubing due to buoyancy forces. These did not immediately coalesce, which indicated that if smaller bubbles could be produced they will become entrained in the fluid because buoyancy forces are dominated by viscous drag (successive pictures can be seen in Figure 4-8 to Figure 4-10). Higher blood flow rates could possibly carry smaller bubbles away from the formation zone and facilitate blood mixing, and hence oxygen transfer.

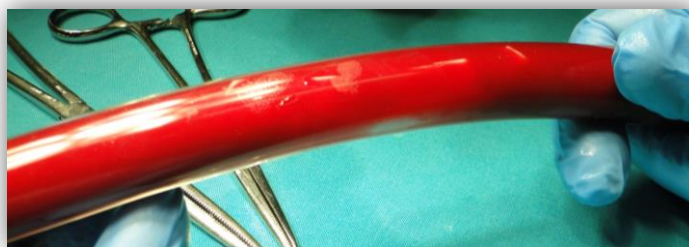


Figure 4-8: Initial formation of bubbles



Figure 4-9: Collection of bubbles at the surface



Figure 4-10: Formation of oxygen foam

As the bubbles were seen to form, the oxygen flow was increased to inspect the bubble dynamics within the blood. It was found that at higher gas flow rates, a larger amount of bubbles were formed, and that bubbles coalesced to form larger bubbles, and eventually brittle oxygen foam which was hard to remove. It is expected that the coalescence factor in this case was the increased bubble contact time. The brittle foam could be caused due to the oxygen drying out the blood at the interface, and so creating a harder interface. Oxygen uptake was minimal, due to the bubbles being too large and that the exposed surface was too small, but could also have been due to the leak in the circuit allowing the blood to become almost completely saturated before reaching the oxygenator. This would prevent any oxygen to dissolve in the blood.

4.4 In Vitro

Due to the difficulties encountered in the ex vivo test, a circuit was considered that did not depend on the animal model. The test circuit was similar in type to the one seen in Figure 4-5, but without the animal model. A saline solution was used to investigate the increase in partial pressure of the oxygen in the fluid. Again a peristaltic pump was used to feed the fluid through the circuit, and knowing the length of the tube the dissolving rate of the oxygen in the fluid could be calculated. Based on this, knowing the area of the oxygenation section, transfer rates per area could be calculated. Samples were taken of the saline fluid before and after the device and analysed for the amount of oxygen contained in the solution. This would give an indication of the rate of dissolving of oxygen in the saline solution. As expected, high pressures were required to overcome capillary pressures in materials with small pore sizes. Figure 4-11 shows an example of a sample that ruptured before capillary pressure was overcome.



Figure 4-11: Tearing of material during in vitro tests

Analysis of the samples taken before and after the device then showed no increase in partial pressure of the oxygen, and in fact that the partial pressure of oxygen after the oxygenation section was lower than before the device. This is contrary to what was expected, especially since pure oxygen was introduced into the saline

mixture. Such deviations are attributed to the samples being taken incorrectly, and that the timing between samples were taken was not correlated accurately. This would give an apparent reduction in the partial pressure of oxygen as seen in this test. Also, slow dissolving rates of oxygen in the saline mixture could cause residual concentrations in the sample port from which the samples were taken, giving incorrect readings. Due to these tests not being implemented to a degree of accuracy well enough to ensure appreciable readings, these results cannot be trusted and did not yield any conclusive information.

4.5 Flow Meter

4.5.1 Selection Criteria

Accurate measurements of oxygen flow rate to the oxygenator were necessary in order to evaluate the formation of bubbles for specific flow rates and supply pressures. The low flow rates being fed to the oxygenator made the selection of a flow meter difficult, as common flow meters used in hospital settings (of the rotameter/variable area type) are generally unable to measure such low flow rates. Common oxygenators such as ECMOs are often supplied with high flow rates of oxygen, and thus do not show a quantifiable indication of flow for flow rates below 500 ml/min. Industrial flow meters that measure such low flows are available, but are expensive and have a limited accuracy.

For the experiments a flow meter was required and would be manufactured to measure the expected flow rates of the oxygen supply to the oxygenator, with increments of no more than 10 ml/min and maximum flow rate of 400 ml/min. It was decided to use a pressure drop flow meter. According to the Hagen–Poiseuille equation, the pressure drop across the length of a tube is directly proportional to the flow rate inside that flow tube, and inversely proportional to the fourth power of the tube diameter:

$$Q = \frac{\Delta p \times \pi \times D^4}{128 \times \mu \times L} \quad (7)$$

where Q is the flow rate;

L is the pressure drop length of the tube;

D is the tube inner diameter; and

μ is the gas viscosity.

The Hagen–Poiseuille equation makes the assumption that the flow is laminar, viscous and incompressible. Although the assumption of incompressible flow is not entirely correct and that the flow is usually expressed relative to the output pressure, the small pressure drop and isothermal conditions, as well as the assumption of ideal gas behaviour were expected to yield appreciable accuracy at low flow rates. The flow tube was selected to ensure that the Reynolds number was below 2300 and laminar flow is achieved (a value of $Re = 230$ was calculated), validating the use of the Hagen–Poiseuille equation. The pipe selected had to be large enough to ensure that the expected flow rate, and hence velocity of the oxygen, resulted in laminar flow, but had to be small enough to ensure that a large enough pressure drop could be achieved. The pressure drop is a function of the tube diameter, and had to be small enough to yield an adequate resolution. The calculations of flow rates and pressure drop, as well as tube diameter can be seen in Table E-1 in Appendix E.

4.5.2 Construction and Calibration

The pressure difference along the length of the tube was measured using a Freescale MPXV5004 differential pressure transducer, which outputs an analogue signal which is proportional to the differential pressure. The value was sampled using the 10-bit A/D converter on board an Arduino Duemilanove microcontroller board. This gave a resolution of roughly 5 Pa, which meant that the smallest flow that could be measured was 8.7 ml/min. The Atmega 168

microprocessor on board the Arduino was programmed for data conversion, correct for a DC bias value and to interface with a personal computer for data display. The analogue value read from the sensor was multiplied by conversion factors to obtain the actual pressure difference, which was then multiplied by a factor dependent on the gas being measured (K_{relation}) to find the flow rate of the gas being measured. The value was streamed to the serial (USB) port of a PC, and displayed on a simple form which was written in Visual C#.

In order for the measurements to be validated, the flow meter had to be calibrated. This was done by measuring the amount of water flowing out of an enclosed tank with another opening attached to the flow meter, as shown in Figure 4-12 below.

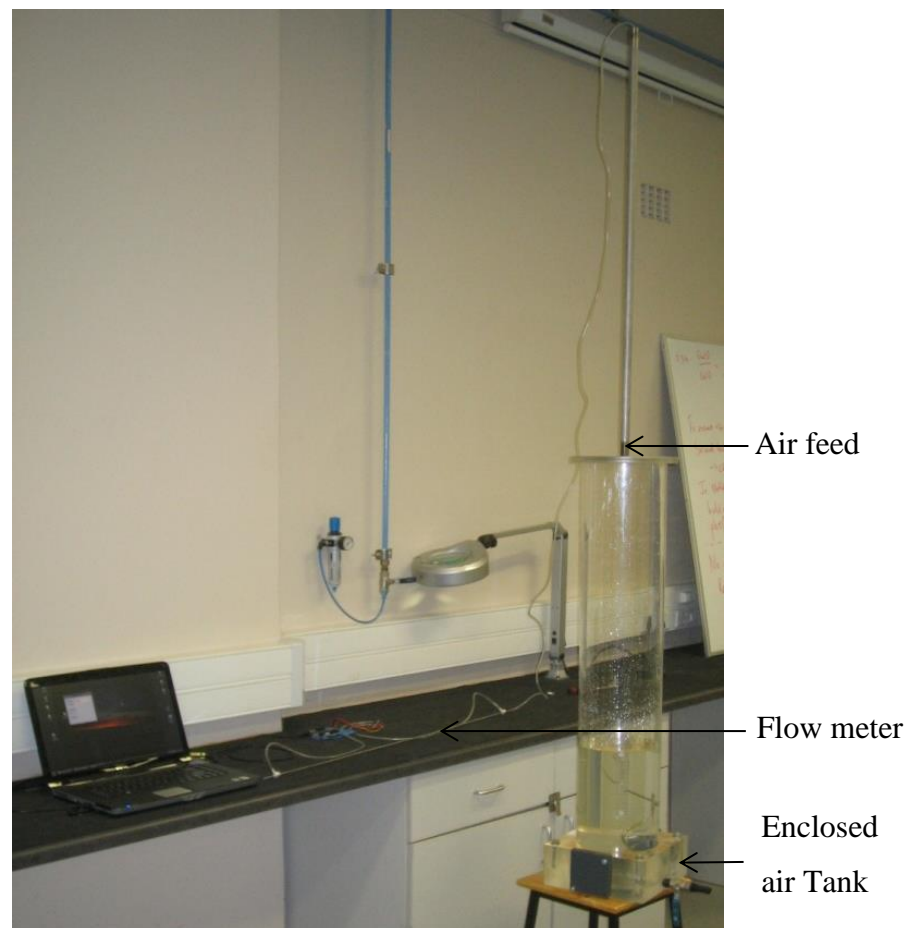


Figure 4-12: Calibration laboratory arrangement

The volume of water flowing out over a certain period of time would be measured, which would correlate to the amount of air drawn into the enclosed chamber through the air feed, which is attached to the flow meter. The peak air flow rate would be observed (the capacitance of the air would cause this value to be reached after a small amount of time), and this correlated to the actual amount of water calculated. The average ratio of the actual flow against the calculated flow was calculated for the first batch to determine a calibration factor (stored as *Calibrate*), which was then multiplied by the measured flow rate to obtain the actual calibrated flow rate. *Calibrate* was calculated to be 1.153 based on initial estimates, which shows a 15 % deviation in the actual flow rate measured for a given pressure drop. This is attributed to inaccuracies regarding the diameter of the flow tube used which would have a large effect due to the relation of the flow rate to the diameter of the tube. Two more batches of calibration tests were performed; the result of which are documented in Table E-2 Appendix E. It was found that the measured values were within 2 % of the actual values after the multiplication factor was included, which falls within an acceptable range. The flow meter was implemented in the initial animal tests along with a modified rotameter as seen in Figure 4-13 below, where the rotameter was used mainly to detect whether or not very small flows existed if the pressure drop flow meter did not work.

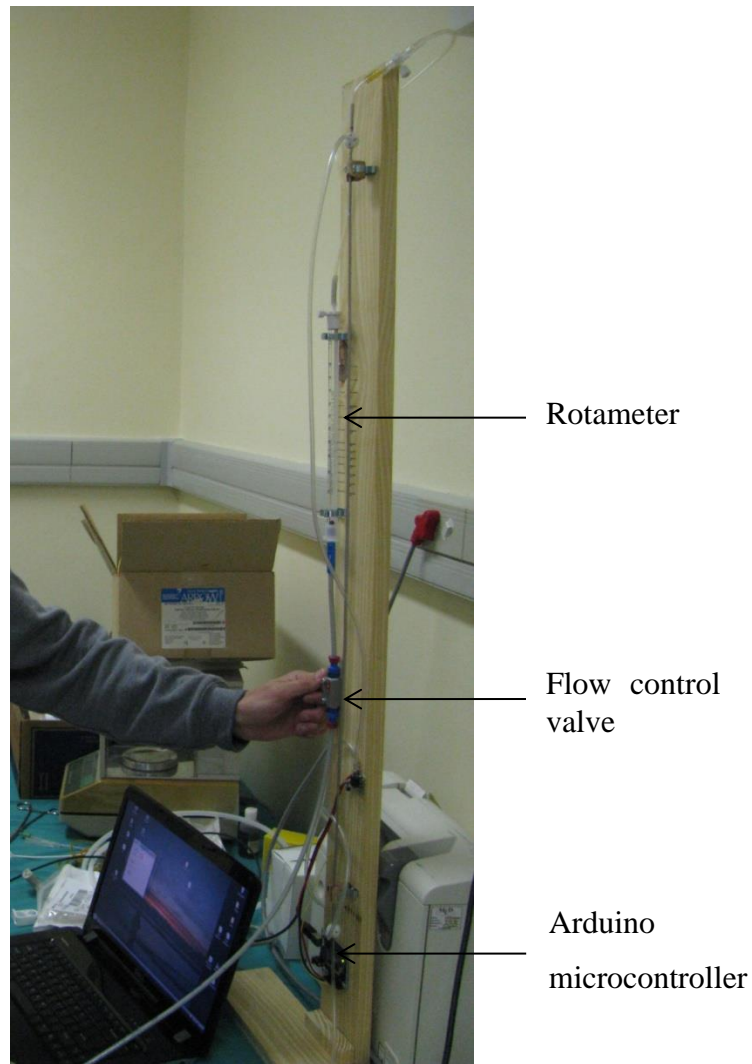


Figure 4-13: Flow meter being used during testing

4.6 Chapter Summary

It was found during testing that bubbles small enough to enable dissolution were difficult to produce. This is due to an insufficient amount of exposed surface area of the bubbles, but also due to the blood not mixing to ensure exposure to the new surfaces. In all the tests, there was room for error regarding the measurement of data and the determination of oxygen supply such that the concept could not be proven adequately. Firstly, in the in vivo tests the outer thrombus which formed on the device as seen in Figure 4-4, or large bubbles could have been the result of

the increased pulmonary pressure in the porcine model. It could be reasoned that the inability to completely oxygenate the animal sufficiently, and the inability to provide respiratory assistance results that the implementation of the device was unsuccessful.

Secondly, in the *ex vivo* test, a tear in the material resulted in very large bubbles being produced from this site. A leak in the circuit at one of the connector ports caused the blood to possibly become saturated with oxygen before reaching the device, reducing the oxygen uptake of the blood as supplied by the device to such an extent that no dissolution was seen. Large bubbles were formed and the consequent foam formed did not allow a sufficient surface area for oxygen transfer.

Thirdly, in the *in vitro* tests, the samples taken before and after the device showed that there was no oxygen uptake, but that the partial pressure of the oxygen (dissolved oxygen) was lower than before the device. This was unexpected considering that pure oxygen was introduced into the system. Bubble coalescence was seen due to limited dissolving of the oxygen in the saline solution, which minimised the exposed oxygen bubble surface and reduced dissolving of the oxygen.

5 Modelling Oxygen Diffusion

5.1 Introduction

Modelling of physiological process within the human body is often a difficult task due to the high complexity of the body as well as unknown factors that affect the different processes. Mathematical modelling of these processes does yield several advantages though; simulations can be changed with the change of a few parameters, whereas changing an experiment with a live model requires re-planning of the experiments. Experiments with live models are also time consuming and costly. Simulations generally cost less to perform (depending on the complexity of the process), and also allow for certain processes to be isolated and inspected independently, allowing a higher level of focus and control.

To inspect the performance of an intravenous oxygenator, and subsequently the feasibility thereof, the modelling of the diffusion of oxygen from a micro bubble into the surrounding blood can yield useful insight. The effect that parameters such as the starting radius and the distance between bubbles have on the diffusion rate can be inspected, factors that are very difficult to determine *in vivo*. Literature shows that bubbles in close proximity to each other can saturate the blood to such an amount that no more diffusion of oxygen takes place out of the bubble and hence the bubbles do not decrease in size (Fischer *et al.* 2009). In essence this indicates that even relatively small bubbles with diameter 200 μm introduced into the femoral artery could have adverse physiological effects in downstream capillaries and organs (Barak & Katz 2005). The modelling of diffusion from a gas bubble into an adjacent liquid within the body has similarities to many other processes and industries which

require such processes to be modelled (Tan *et al.* 2000), and hence such models can be used as reference for physiological diffusion.

5.2 Diffusion Model

5.2.1 Limitations and Focus

Bubble dissolution in blood occurs due to two factors – first is the dissolving of the bubble due to the gas partial pressure (PO_2), the second due to the chemical bonding of the oxygen to the haemoglobin (SO_2). The dissolving process is determined by the Hill saturation curve, whereas the bonding process can be described as a chemical reaction with kinetic constants for the forward and reverse reactions (Fischer *et al.* 2009). The amount of oxygen bound to the haemoglobin is dependent on the PO_2 of the blood plasma surrounding the red blood cells because the oxygen needs to diffuse through the plasma to reach the red blood cells. The case of modelling the dissolution of oxygen from a microbubble into surrounding blood is complicated by several factors. Firstly, the fact that mass transfer occurs due to diffusion as well as the chemical reaction of the dissolved gas and the haemoglobin within the red blood cells and the free haemoglobin within the boundary layer (Yang *et al.* 1971b). This reduces the dissolution rate of a bubble within the gas compared to a diffusion-only mass transfer, and causes a sharp decrease of bubble size immediately after introduction of the gas bubble in the blood. This sharp decrease is only observable for a very short time during which a ring of oxygenated blood forms around the bubble (Yang *et al.* 1971a), and is followed by steady shrinkage in the bubble size as the oxygen diffuses through the boundary layer and dissolves in the blood (Yang *et al.* 1971b), (Yang *et al.* 1971a). Near the moment of complete dissolution the rate of shrinkage of the gas bubble is seen to accelerate due to surface tension force (Yang 1971).

Secondly, the relative motion of the bubble within the blood, such as when the blood flows onto and around the bubble or when the bubble rises through a column of

blood due to buoyant forces, has an effect in increasing the dissolution rate of the bubble due to the thinning of the saturated boundary layer (Yang *et al.* 1971b). To model the thinning of the boundary layer it is required that convective mass transfer properties on the surface of the bubble are known, and calls into consideration the use of non-dimensional numbers to determine the ratio of convective mass transfer to diffusive mass transfer. For the sake of finding a baseline expression for the bubble dissolution rate the bubble will be considered to be in a quiescent blood environment.

Furthermore, mass transfer of oxygen gas from the bubble into the blood causes the bubble to decrease in size, and the bubble-blood interface translates with respect to the bubble centre. The moving boundary problem is known as the *Stefan problem* and is typically solved by numerical methods only due the non-linear nature of the moving boundary problem (Fazio 2000). To address this many numerical methods have been employed, which include isotherm migration, finite difference, finite element and variational inequalities, which all have purposes for different problems (Fazio 2000). One of the most widely used is the fixing-domain approach, where a Landau coordinate transformation allows the problem to be reduced to a computational domain (Illingworth & Golosnoy 2005), (Fazio 2000). A transformation of the moving boundary to Landau coordinates allows for computation in the constant Landau coordinate system even though the position to which this transformation corresponds actually varies (Illingworth & Golosnoy 2005). The classical solution to the diffusion problem, however, finds an analytical expression for the blood saturation levels at different spatial points within the calculation domain at different times. Although this does not allow the Stefan problem to be addressed via a Landau transformation, it does allow the solution to be derived from first principles and adapted to different modelling purposes. This approach will be followed, but to accurately track the bubble interface it will be required that spatial and time step sizes are small enough as to not have an effect on the movement of the bubble interface.

5.2.2 Proposed Solution

The classical approach to obtain the concentration at different points in the calculation domain requires that the solution to the diffusion equation be found. To obtain the solution to this partial differential equation it is required that the problem be well posed, i.e. consideration is given to the existing assumptions, initial conditions and boundary conditions. The feasibility of an intravenous oxygenator as implemented in the in vivo experiments could be supported by the solution to the diffusion model, if it is found that bubbles released into the bloodstream dissolve quickly enough. The dissolution rate of an oxygen bubble within arterial blood in the presence of nearby bubbles would increase due to the saturation of the blood around the bubble, inhibiting diffusion of oxygen out of the bubble. The conditions at the bubble interface can be modelled by a Dirichlet boundary condition and the conditions halfway between two adjacent bubbles can be modelled by a Neumann boundary condition. The Neumann boundary condition represents the fact that the rate of change of the concentration profile halfway between two adjacent bubbles is zero and takes on a range of values as time progresses, whereas the Dirichlet condition assumes that the blood saturation level (S) at the bubble interface is 100 %.

The mass fraction of dissolved oxygen at the two interfaces mentioned above, and the derivation of the solution can be found in Section 5.2.3. The Stefan problem will be addressed by mapping of the movement of the interface through a front-tracking method (Unverdi 1992), where the position of the interface will be calculated at each time interval and this mapped onto an already existing spatial point. The subsequent change in length of the calculation domain requires that the concentration profile be mapped onto the new discretised domain.

Taking into account the aforementioned limitations as well suggestions made by Dr. Kiran Dellimore (Dellimore 2012), certain assumptions can be made which aim to contain the focus of the model by simplification without removing the accuracy of the results obtained:

- The bubble is spherical and surrounded by blood at rest. Spherical symmetry exists for the mass fraction distribution of the dissolved oxygen.
- A clear boundary exists between the phases. No mist or vapour exists around the bubble. The only gas within the bubble is oxygen and it is modelled as an inviscid ideal gas.
- The pressure inside the bubble is atmospheric and spatially uniform at all times. At the gas-liquid interface diffusion is the only method of gas transfer.
- Inertial and temperature effects within the bubble and in the blood are neglected due to the relatively small size of the simulated bubbles. This implies that no temperature gradients exist and hence no convection.
- Surface tension is neglected.
- The model is limited to cases where dissolved gases other than oxygen do not significantly affect the dynamics of bubble dissolution.
- The erythrocytes are intact. Free haemoglobin has markedly larger oxygen uptake than intact erythrocytes (Coin & Olson 1979).
- Haemoglobin bound oxygen is assumed to be in equilibrium with the dissolved oxygen.
- Mass diffusion of the dissolved oxygen is governed by Fick's law with a diffusivity coefficient D .
- The concentration of the dissolved oxygen at the gas-blood interface is governed by Henry's law with a constant solubility α , i.e. the amount of dissolved oxygen is directly proportional to the partial pressure of oxygen.

5.2.3 Derivation of Solution

5.2.3.1 Boundary Conditions and Homogenisation

$$PO_2(r, 0) = 51 \text{ mmHg}$$

Prescribes the value of PO_2 at all spatial points (refer to Figure 5-1) at $t = 0$.

$$PO_2(0,t) = 760 \text{ mmHg}$$

Prescribes the value of PO_2 at the bubble interface, with the assumption that the partial pressure of oxygen in the blood at the surface of the bubble is as stated in the (Fischer *et al.* 2009)

$$\frac{dPO_2}{dr}(L,t) = 0 \text{ mmHg}$$

Prescribes the value of the rate of change of PO_2 at the boundary end.

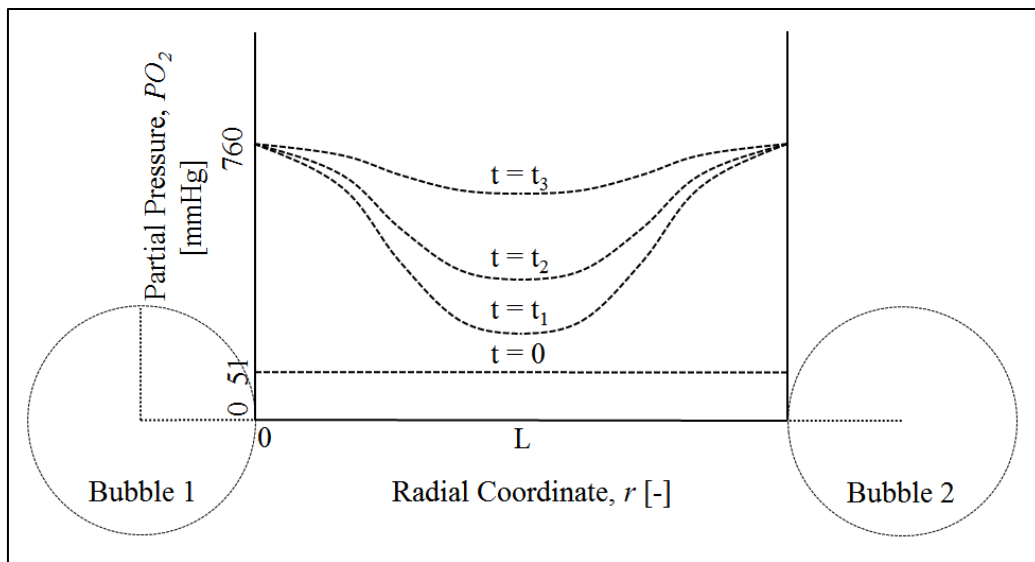


Figure 5-1: Partial Pressure curve vs. distance from the bubble interface

Now using

$$C_d = \frac{\rho_{STP}}{\rho_b} \alpha PO_2 \tag{8}$$

The following is found:

$$C_d(r,0) = 0.0206 \tag{IC1}$$

$$C_d(0,t) = 0.3074 \quad \text{BC1}$$

$$\frac{dC_d}{dr}(L,t) = 0 \quad \text{BC2}$$

Which can be homogenised by setting

$$C_d(r,t) = U(r,t) + V(r) \quad (9)$$

where $V = 0.3074$, which implies that

$$U(r,0) = -0.2868 \quad \text{IC2}$$

$$U(0,t) = 0 \quad \text{BC3}$$

$$\frac{dU}{dr}(L,t) = 0 \quad \text{BC4}$$

5.2.3.2 Partial Differential Equation

After noticing spherical symmetry, the diffusion equation can be simplified to the simplified spherical diffusion equation

$$\frac{\partial C_d}{\partial t} = D_f \left(\frac{2}{r} \frac{\partial C_d}{\partial r} + \frac{\partial^2 C_d}{\partial r^2} \right) \quad (10)$$

Which will first be adjusted for the non-homogeneous BC's by substituting (9) into (10). Since all derivations of $V = 0$, it is found that

$$U_t = D_f \left(\frac{2}{r} U_r + U_{rr} \right) \quad (11)$$

5.2.3.3 Separation of Variables

Equation (11) can now be analysed by setting $U(r,t) = R(r)T(t)$ and performing a separation of variables, where $R(r)$ is the spatial solution and $T(t)$ the temporal. This gives

$$T'(t) = -\lambda T D_f \quad (12)$$

With the solution

$$T(t) = e^{-\lambda t D_f} \quad (13)$$

Which can be seen to decay in time. The solution to the spatial component is

$$r^2 R'' + 2rR' + \lambda R r^2 = 0 \quad (14)$$

Which decays with an increase in the spatial coordinate.

5.2.3.4 Bessel Function

Now, the solution to Equation (14) is a Bessel function. Comparing this to the standard Bessel equation (Edwards & Penney 1992)

$$x^2 y'' + Axy' + (B + Cx^q)y = 0 \quad (15)$$

And letting $\lambda = K^2$, it can be seen that

$$A = 2; \quad B = 0; \quad C = K^2; \quad q = 2; \quad (16)$$

Which yields the following

$$\alpha = \frac{-1}{2}; \quad \beta = 1; \quad k = K; \quad p = \frac{1}{2}; \quad (17)$$

These can now be used to find a general solution of the form

$$R(r) = x^\alpha \left[C_1 J_p(kx^\beta) + C_2 J_{-p}(kx^\beta) \right] \quad (18)$$

$$R(r) = r^{-\frac{1}{2}} \left[C_1 J_{\frac{1}{2}}(Kr^1) + C_2 J_{-\frac{1}{2}}(Kr^1) \right] \quad (19)$$

Now, it is known that $J(x)$ is an elementary function if the order of p is half an odd integer:

$$J_{\frac{1}{2}}(x) = \sqrt{\frac{2}{\pi x}} \sin(x) \quad \text{and} \quad J_{-\frac{1}{2}}(x) = \sqrt{\frac{2}{\pi x}} \cos(x) \quad (20)$$

Which reduces the solution to

$$R(r) = r^{-\frac{1}{2}} \left[C_1 \sqrt{\frac{2}{\pi Kr}} \sin(Kr) + C_2 \sqrt{\frac{2}{\pi Kr}} \cos(Kr) \right] \quad (21)$$

And simplifying yields

$$R(r) = \frac{1}{r} \sqrt{\frac{2}{\pi K}} \left[C_1 \sin(Kr) + C_2 \cos(Kr) \right] \quad (22)$$

5.2.3.5 Applying Boundary and Initial Conditions

Using BC3 it can be seen that for the above equation to be physically limited it is required that $C_2 = 0$. Therefore,

$$R(r) = \frac{1}{r} \sqrt{\frac{2}{\pi K}} C_1 \sin(Kr) \quad (23)$$

Thus

$$\frac{dR}{dr}(r) = \frac{-1}{r^2} \sqrt{\frac{2}{\pi K}} C_1 \sin(Kr) + \frac{1}{r} \sqrt{\frac{2}{\pi K}} C_1 K \cos(Kr) \quad (24)$$

And simplifying yields

$$\frac{dR}{dr}(r) = \frac{1}{r} \sqrt{\frac{2}{\pi K}} C_1 \left[\frac{-1}{r} \sin(Kr) + K \cos(Kr) \right] \quad (25)$$

Applying BC4 the above can be further simplified to

$$\frac{dR}{dr}(L) = \frac{1}{L} \sqrt{\frac{2}{\pi K}} C_1 \left[\frac{-1}{L} \sin(KL) + K \cos(KL) \right] = 0 \quad (26)$$

And since $B \neq 0$, $K \neq 0$ and $L \neq 0$ can be simplified to

$$KL \cos(KL) - \sin(KL) = 0 \quad (27)$$

From which the eigenvalue can be found, but because the value of L changes with each time step, the eigenvalue will change also. Combining combine $R(r)$ and $T(t)$ to get

$$U(r, t) = \sum_{n=0}^{\infty} e^{-K_n^2 D_f t} \frac{1}{r} \sqrt{\frac{2}{\pi K_n}} C_n \sin(K_n r) \quad (28)$$

And using IC2 to determine C_n

$$U(r, 0) = 0.2868 = \sum_{n=0}^{\infty} \frac{1}{r} \sqrt{\frac{2}{\pi K_n}} C_n \sin(K_n r) \quad (29)$$

Now, to determine the constant C_n , the inner product in polar co-ordinates is used, which is known to be

$$\langle f(r), g(r) \rangle = \int_0^L f(r)g(r)rdr \quad (30)$$

Which gives

$$C_n = \frac{\left\langle 0.2868, \frac{1}{r} \sqrt{\frac{2}{\pi K_n}} \sin(K_n L) \right\rangle}{\langle \sin(K_n L), \sin(K_n L) \rangle} \quad (31)$$

Which after some simplification yields

$$C_n = \frac{0.2868 \sqrt{\frac{2}{\pi K_n}} \left[\frac{1}{K_n} - \frac{\cos(K_n L)}{K_n} \right]}{\frac{L}{2}} \quad (32)$$

The numerator and denominator must be calculated for each K and L . Now finally, combining everything and remembering that $C_d = U + V$, yields the final solution

$$C_d(r, t) = 0.2868 + \sum_{n=0}^{\infty} C_n e^{-\lambda D t} \frac{2}{r} \sin\left(\frac{\pi n r}{L}\right) \quad (34)$$

It is however noted that at the bubble interface

$$\lim_{r \rightarrow 0} e^{-\lambda D t} \frac{2}{r} \sin\left(\frac{\pi n r}{L}\right) = e^{-\lambda D t} \frac{2\pi n}{L} \quad (35)$$

5.2.3.6 Rate of Change of Bubble Diameter

Performing a mass balance of the gas bubble, it can be seen that the change of mass is a function of the flux (Fischer *et al.* 2009)

$$\rho_{STP} \frac{d}{dt} \left(\frac{4}{3} \pi R^3 \right) = -4\pi R^2 j \quad (36)$$

Which after some simplification yields the velocity of the interface (Fischer *et al.* 2009)

$$\frac{dR}{dt} = -\frac{j}{\rho_{STP}} \quad (37)$$

Now, considering the flux at the bubble-blood interface (Fischer *et al.* 2009)

$$j = -\rho_b D \left(\frac{\delta C_d}{\delta r} \right)_R \quad (38)$$

The partial derivative for the rate of change of the concentration can be found

$$\frac{\delta C_d}{\delta r} = e^{-K_n^2 D_f t} \frac{1}{r} \sqrt{\frac{2}{\pi K_n}} C_n \left\{ K_n \cos(K_n R) - \frac{1}{R} \sin(K_n R) \right\} \quad (39)$$

5.2.3.7 Step-wise Calculation Process

A step-wise procedure is followed in determining the blood oxygen saturation levels at different points for different times. Firstly, the total amount of time is broken down by a certain amount of time steps into discrete time intervals at which the calculations take place, and the calculation domain (including the bubble radius) is broken down into discrete points. Similarly, and taking into account the starting radius of the bubble, the domain of blood into which diffusion takes place is determined and discrete points at which the oxygen saturation can be calculated are created. Secondly, the blood properties, initial values and boundary conditions are calculated. Then within the main loop the following procedure is followed for each time step, which is implemented in the code (Appendix F):

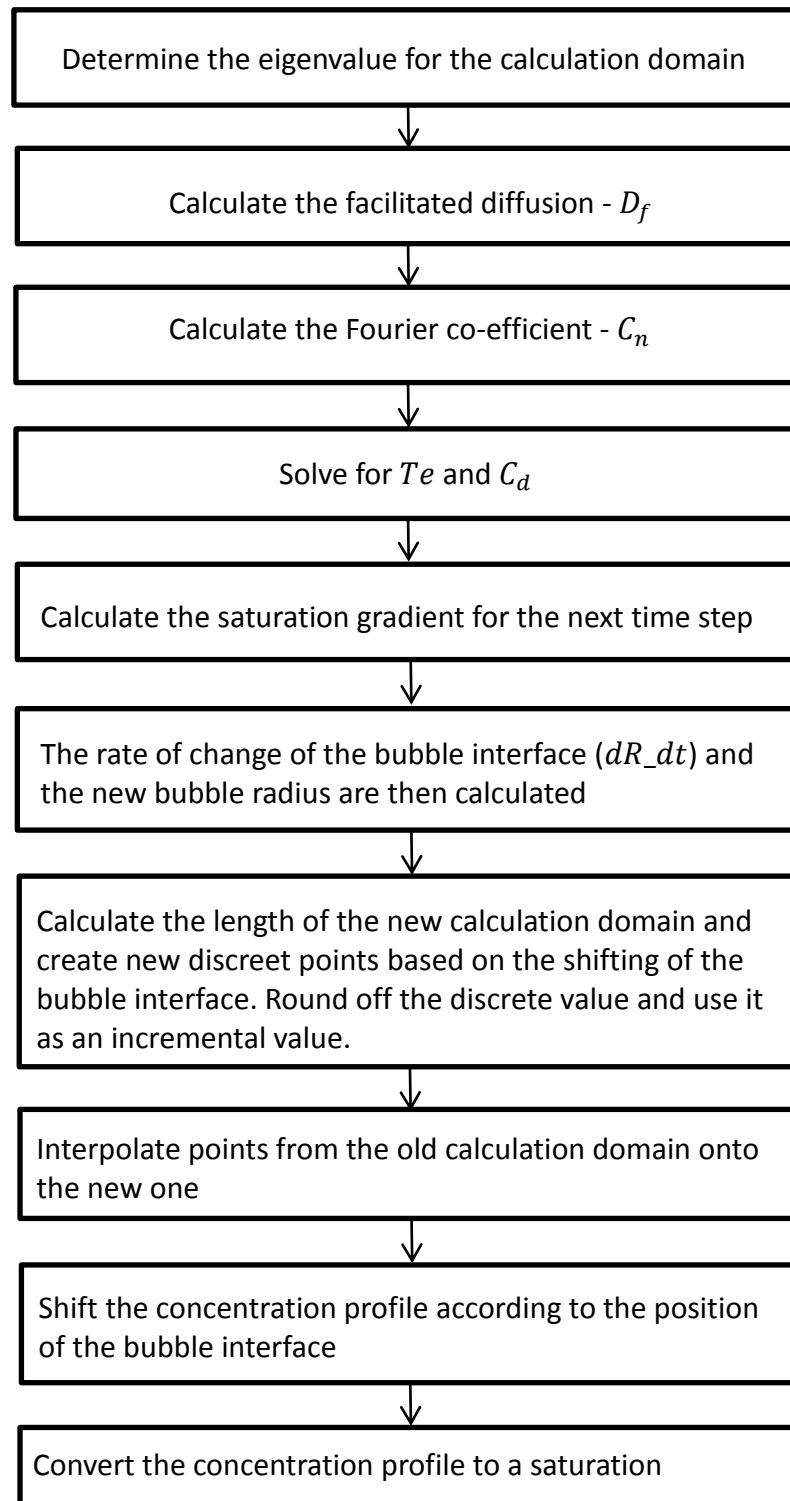


Figure 5-2: Flow diagram for implementation of code

5.3 Discussion

The aim of determining bubble dissolution times by use of the current model, and more specifically determining the accuracy of the model requires that a comparison be drawn up with existing models. The parameters as suggested in Fischer *et al.* (2009) are used as a guideline for input values when setting up the current model for a run of simulations, with the aim that the results would be compared with those mentioned in Fischer *et al.* (2009) Initially the model has systematically assembled from an analytical standpoint, but the difficulties with this approach were immediately seen. The input parameters used did not allow the model to run for more than one time step due to unrealistically large values for the rate of change of the bubble interface, among others. Constraining all these large values for the first few time steps in an attempt to stabilise the simulation did not yield the anticipated results, although it was identified that certain variables had a larger effect than others when constrained to a certain range. The two variables that were immediately identified were the Fourier Coefficient, C_n and the diffusion constant D . The value of D was constrained by analysing the differences between the results from this model with those found in Fischer *et al.* (2009), and the new values used in all the subsequent simulations for different values of Δ .

To compare the model to Fischer *et al.* (2009) a simulation was run of the dissolution rate of an oxygen bubble in the presence of another oxygen bubble, where the value of D adjusted by a factor of 10^{-5} and set equal to $1.8 \times 10^{-11} \text{ cm}^2/\text{s}$. The value of D is confirmed comprehensively in Heidelberger *et al.* as $8 \times 10^{-6} \text{ cm}^2/\text{s}$ (Heidelberger & Reeves 1990). The distance between the bubble interfaces is larger than the bubble radii; the distance between the bubble centres used was $\Delta = 500 \text{ }\mu\text{m}$. Drawing comparisons to the bubble dissolution times as suggested in Fischer *et al.* (2009) (Figure 5-3) it can be seen that for the case where $\Delta = 500 \text{ }\mu\text{m}$, dissolution times are not very similar, but that bubbles do not dissolve fast enough. It is therefore noted that bubbles with diameter of more than $200 \text{ }\mu\text{m}$ and in close proximity to each other (less than $300 \text{ }\mu\text{m}$ between surfaces) will not dissolve before reaching the heart or

other critical organs, and could cause irreparable tissue damage as mentioned in Chapter 2. It has been shown by other researchers that in a 20 % saline solution, 20 μm bubbles dissolve in 10-16 seconds whereas 10 μm bubbles dissolve in 8-14 seconds. These conditions were at body temperature and based on linear trends (Schubert *et al.* 2003). Taking into consideration the flow rate of blood in the vena cava it can be deduced that bubbles formed in the vena cava would reach the lungs within a few seconds, thus substantiating that bubbles smaller than 20 μm might be safest.

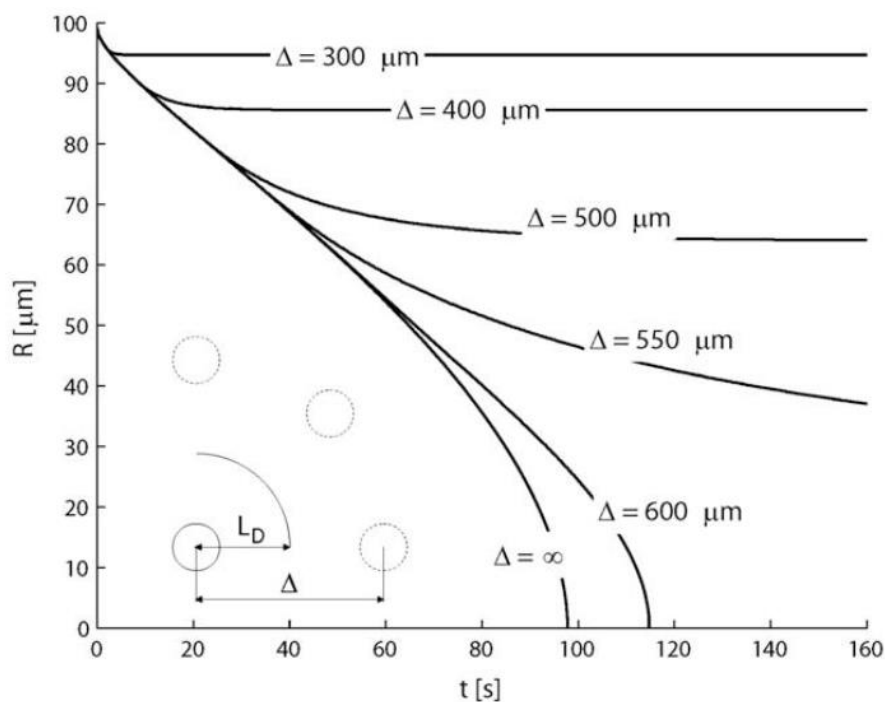


Figure 5-3: Radius-time relations for a bubble surrounded by multiple bubbles
(Fischer *et al.* 2009)

Figure 5-3 also indicates that an increase in distance of the centres of two adjacent bubbles would decrease the dissolution time, where the bubble will dissolve fastest (roughly 100 seconds) when the distance between the bubbles is appreciably large. For smaller distances between bubble centres the larger dissolution time is attributed to saturation of the blood with oxygen, which prevents mass transfer of oxygen from the bubble into the blood due to a decrease in the concentration gradient. Similar

values as seen in the above figure were used as input parameters for the current model for two reasons; to determine the bubble dissolution times, as well as determine the accuracy of the model.

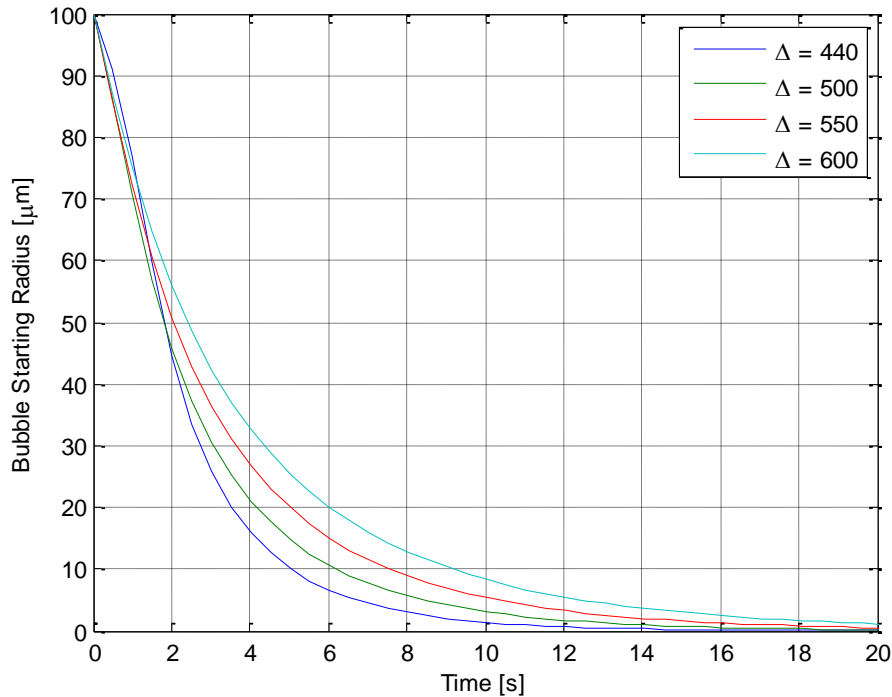


Figure 5-4: Bubble dissolution times ($R = 100 \mu\text{m}$, $D = 1.8 \times 10^{-11} \text{ m}^2/\text{s}$)

The resultant dissolution times as seen in Figure 5-4 do not correspond to bubble dissolution times in accordance with what was expected or when compared to literature; a larger dissolution space yields a larger dissolution time. Upon closer investigation of the model, and considering the intrinsic differences with numerical methods the reason for this difference can be found. The classic method of determining the concentration profile as implemented in the current model requires knowledge of the length of the calculation domain (i.e. the value of Δ) in order to determine the eigenvalue (equation (27)). The sinusoidal nature of the equation for the concentration profile (equation (28)) is immediately noted, and furthermore that the concentration profile is ‘stretched’ to fit onto the calculation domain. In other words, every spatial point is ‘aware’ of the value of Δ , although Fischer *et al.* (2009)

suggest that a saturation boundary layer of $3 \times R$ exists irrespective of the value of Δ . The shape of the concentration profile in the current model is a function of the eigenvalue, which in turn is a function of the distance between the two bubbles. The rate of change of the bubble radius with respect to time is a function of the rate of change of the concentration profile with respect to the spatial coordinate at the bubble interface (equation (39)). It was also noted that the size of the spatial steps of the radial coordinate would also have an effect on the rate of change of the concentration profile and was therefore kept constant. Considering the above, it can be seen that a larger calculation domain has the effect of a lower rate of change of concentration and hence a lower rate of change of bubble radius.

To illustrate the above phenomenon as well as highlight other differences in the model to suggested literature, a plot of the blood oxygen saturation vs. radial coordinate is shown in Figure 5-5.

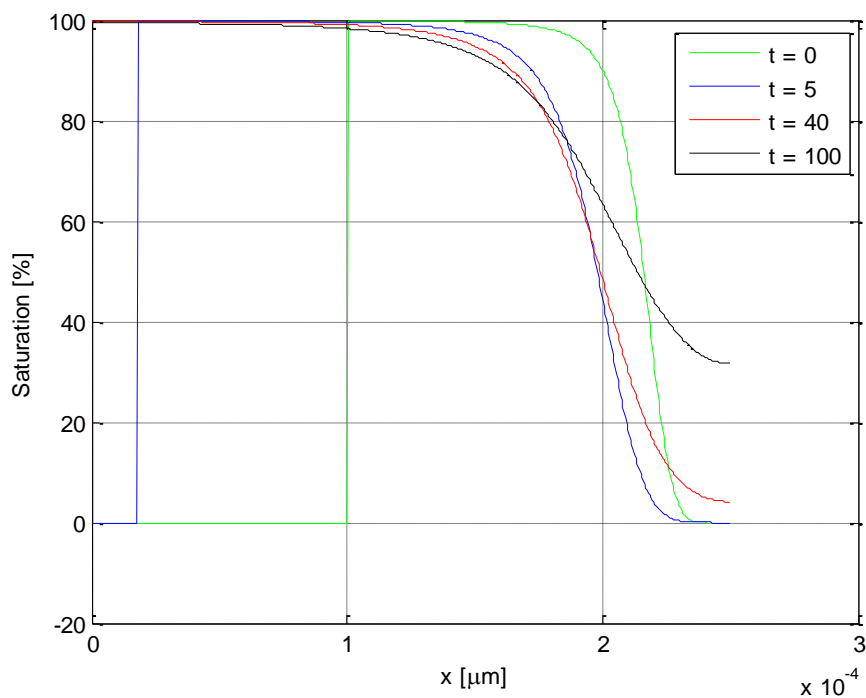


Figure 5-5: Saturation vs. radial coordinate for $\Delta = 500 \mu\text{m}$ ($R = 100 \mu\text{m}$, $D = 1.8 \times 10^{-11} \text{ m}^2/\text{s}$)

It can be seen that the boundary tracking and interpolation method as seen in Appendix F accurately tracks the movement of the interface, and should be noted that a significant reduction in the spatial step size did not have any effect in the bubble dissolution rate. What is also immediately obvious is the sinusoidal nature of the concentration profile as mentioned earlier, and that the right boundary (indicating half the distance between bubble centres) increases as dictated by the Neumann boundary condition.

5.4 Chapter Summary

As with most medical devices, the feasibility of an intravenous oxygenator is solely determined by two factors. Firstly, the oxygenator needs to achieve its purpose of sufficiently oxygenating the blood in order to meet the oxygen needs of a typical adult. Secondly, the oxygenator must not cause any serious or substantial harm which would negate its use on a patient. The determining factor would be whether or not oxygen bubbles of a size as typically introduced into venous blood by the suggested intravenous oxygenator would cause harm to the patient or not. As seen in Figure 5-4 and as discussed previously, bubbles which are in close proximity to each other and have a diameter equal to 200 μm do not dissolve within 100 seconds, and are considered to be potentially harmful to organs which are downstream of the oxygenator. Such long dissolution times imply that the bubbles could still be present when reaching the heart, lungs, or even the brain, and could potentially get lodged within capillaries or accumulate to create bubble clouds. This could cause the restriction of blood into tissue and cause necrosis. Based on this data it can be concluded that an oxygenator that produces bubbles is not feasible due to the overwhelming risk of the bubbles not dissolving quickly enough.

The mathematical model implemented above to determine the dissolution times has been compared to existing models and it has been found that certain limitations exist and that incorrect results are possible. It is noted that a numerical method as typically

used to solve more complex diffusion problems may be more suitable to address this problem and more specifically the Stefan problem.

6 Conclusion

The literature review (Chapter 2) indicated that oxygenation can be quantified, and that current methods of oxygenation do not address all critical care scenarios. There is thus space for an oxygenator that must be available for immediate use and does not place extra strain on the lungs of the patient. Considering the requirements of such a device (Table 3-1), conceptual designs were developed to investigate whether such a device could be developed, and if the blood could be oxygenated via microbubbles. Prototypes were developed to test the concept in animal models, although the requirements on biocompatibility and insertion methods were not applicable to these tests due to an aim in simplicity for the animal tests. It was however seen in the in vivo test that profuse clotting on the oxygenation section of the device occurred within 90 minutes, rendering the device useless for oxygenation purposes via microbubbles. Damage to the lungs of the animal was sustained, which was assumed to be due to gaseous emboli. This was indicated by an increase in pulmonary pressure and a decrease in SaO_2 while the animal was being ventilated. An ex vivo test performed subsequently provided more information regarding the formation of a bubble cloud, as well as coalescence of larger bubbles within the blood.

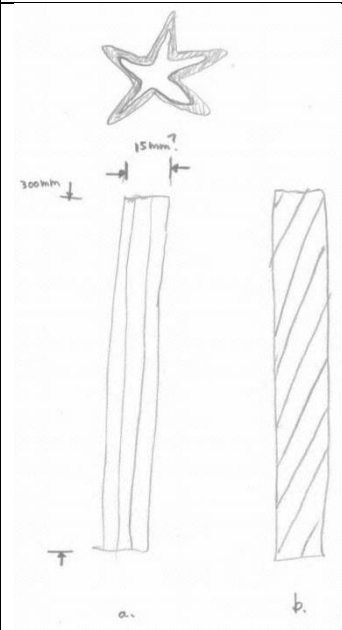
The in vivo test and the ex vivo test did not yield any conclusive information regarding the oxygenation of venous blood, nor could approximate dissolution times be assessed. The prototypes implemented in the tests were not assessed any further according to size requirements due to the lack of sufficient oxygenation, as the supply of oxygen was of main concern. Difficulty with the proof of concept to investigate the intravenous dissolution of microbubbles in blood can be attributed to two factors. Firstly, the testing methods could be improved to a degree that there is better control over bubble sizes and bubble separation. The determination of blood properties before and after the introduction of microbubbles, as well as the accurate control of oxygen flow could yield valuable information regarding oxygen dissolution within venous blood conditions.

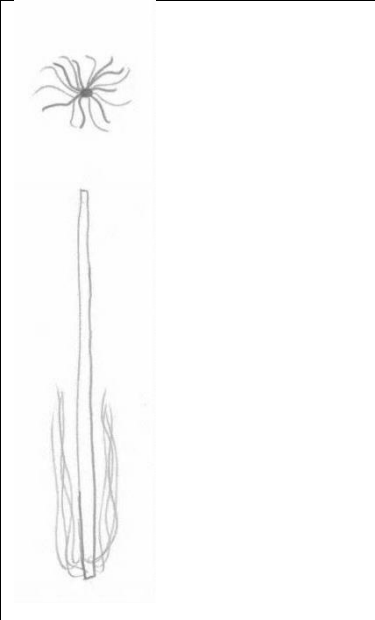
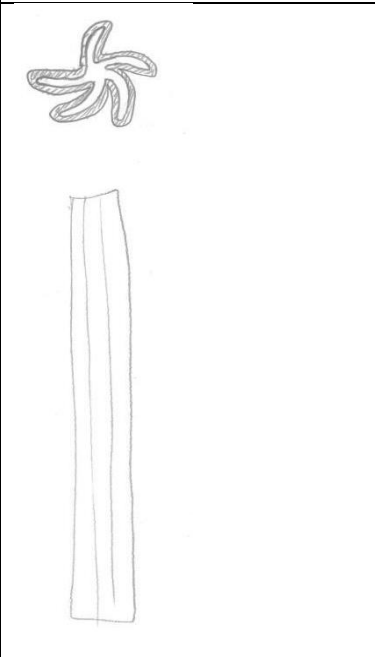
Secondly, the difficulty in proving the concept could be an indication that successful implementation of the concept is highly improbable. Considering however that the idea was very difficult to prove, even when attempting to perform oxygenation in a similar environment to how the device was expected to operate, it was shown that the concept may not be feasible. As simulation results show, bubble dissolution times are very large even for small bubbles, and that preventing the formation of clouds of oxygen bubbles is a very important factor for fast dissolution times, as the concentration boundary layer around the bubbles is the main reason for large dissolution times (Goerke *et al.* 2002). The separation of bubbles is however impossible with the veins and lobes as seen in Table 3-2, and is a highly idealised approach to microbubble dissolution within the blood.


Considering the large risk of introducing microbubbles into the blood, as well as the limited dissolution possible, different methods of introducing oxygen into the blood intravenously should be considered. According to Yasuda & Lin (2003), a tighter control on the free surface energy of the material used to produce bubbles, and hence the water contact angle, could lead to smaller bubbles being produced by the material. If a material could be produced that has a large water contact angle (hydrophilic) and with pores in the 0.1 – 1 μm range, bubbles could possibly be produced that are small enough to dissolve before reaching the lung capillaries. A suggestion for future work is to manufacture a device with pores of the size mentioned previously, that can be produced without compromising the structural integrity or biocompatibility of the device. A metal tube, such as stainless steel, could be used due to the known properties and large industry that exists for producing stainless steel parts and products. This would eliminate the concerns of excessively high pressures inside the device, and possibly simplify the manufacturing process. Literature shows that surface free energy of such materials can be altered by treatment by an atmospheric-pressure plasma jet such that very low contact angles can be achieved (Kim 2002).

Appendix A Conceptual Designs

Table A-1: Conceptual RAC designs

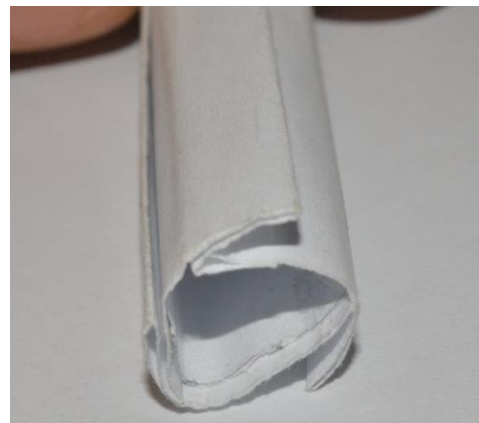
Concept Number	Description	Diagram	Comments
1	Star shaped profile, and twisted along the length of the oxygenation section		Increased surface area for increased oxygen transfer

<p>2</p>	<p>Fibres protrude from the device in a radial manner, and are soft enough to take the shape of the vein</p>	 <p>The diagram shows a top-down view of a device with several thin, hair-like fibers protruding radially from a central point. Below this is a side view of a long, thin, cylindrical shaft with a textured, fibrous appearance at the bottom end.</p>	<p>High increase in surface area, results in an increase in complexity and risk of fibres entangling</p>
<p>3</p>	<p>Folding, star shaped outer profile, determined by the preformed membrane. Oxygen is supplied through the centre.</p>	 <p>The diagram shows a top-down view of a device with a star-shaped outer profile, consisting of several rounded, overlapping lobes. Below this is a side view of a long, thin, cylindrical shaft with a textured surface.</p>	<p>Can be folded to reduce insertion size</p>

<p>4</p>	<p>Catheter balloon opens slightly in order to open the membrane. Balloon size determines opening of the lobes</p>		<p>Smaller size for ease of insertion, and easily adaptable from a catheter. May not provide enough surface area.</p>
----------	--	--	---

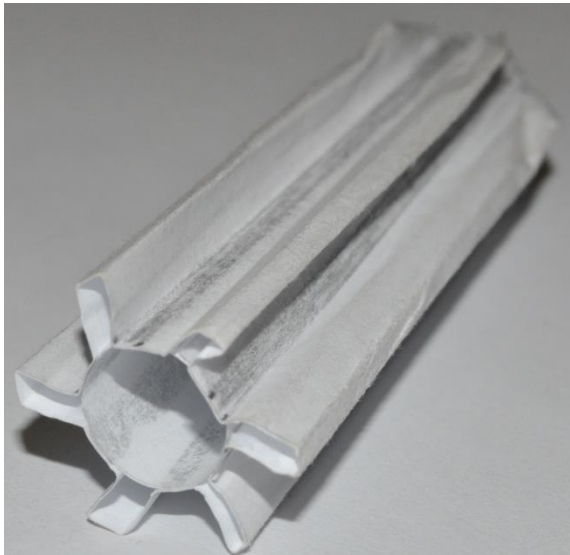


(a)

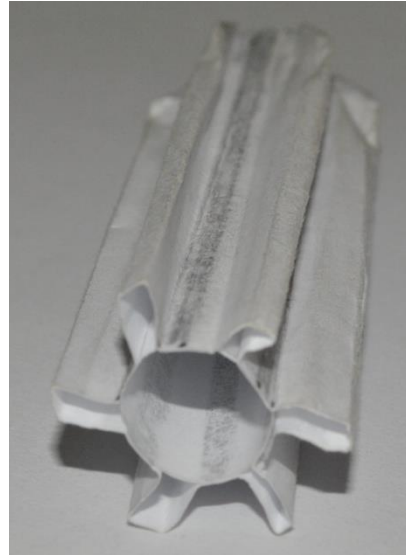


(b)

Figure A-1: (a) & (b) An example of open and closed implementations of cross-sectional concept 4



(a)



(b)

Figure A-2: (a) & (b) Another example of open and closed implementations of cross-sectional concept 4

Appendix B Material Screening

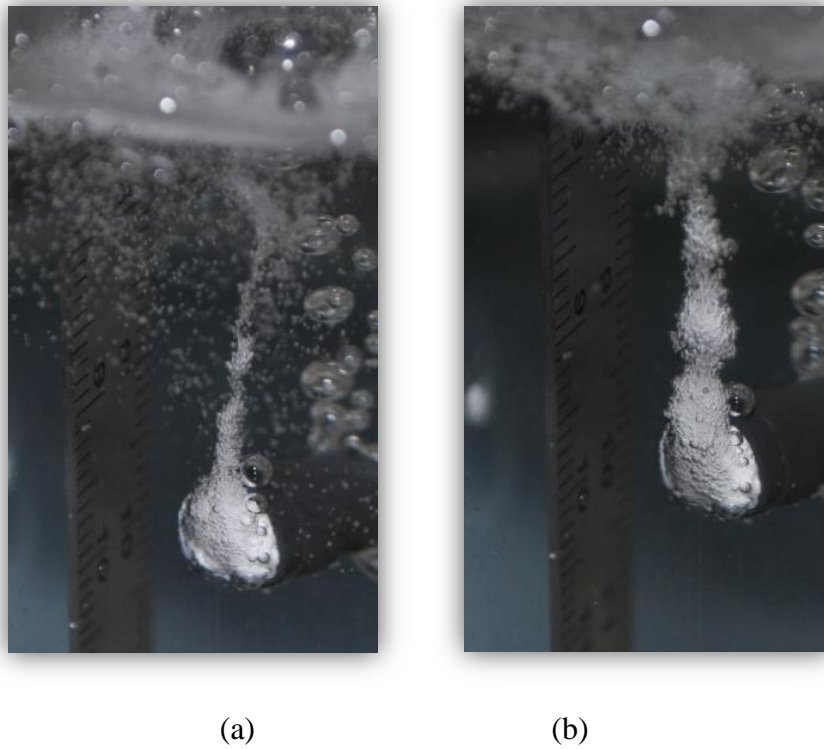


Figure B-1: Bubble formation from a submerged orifice

Table B-1: Sample material properties

Material	Description	Material	Hydrophilic/ Hydrophobic	Pore Size (μm)
M1	PALL LPS high efficiency leukocyte removal filter for plasma	Polyester	Hydrophilic	N/A

	Screen Filter for Rapid			
M2	Transfusion of blood products	N/A	N/A	40
M3	Purecell RC high efficiency leukocyte removal filter for blood transfusion	N/A	N/A	N/A
M4	Pall Purecell RN Neonatal high efficiency leukocyte removal filter for RBC	N/A	N/A	N/A
M5	Pall Lipipor TNA Filter	Nylon	Hydrophobic	1.2
M6	Pall Posidyne ELD Filter	Positively charged Nylon	N/A	0.2
M7	Pall Lipiguard SB Reinfusion filter for salvaged blood	Polyester	Hydrophobic	40
M7b	Pall Lipiguard SB Reinfusion filter for salvaged blood	Cover layer (N/A)	N/A	N/A
M8	Pall Ultipor Breathing system filter	Filter	Hydrophobic	N/A
Nylon	Ultipor, Biodyne A	Nylon	Hydrophilic	3
PES	Supor	Polyether-sulfone	Hydrophilic	5

Appendix C Fluid Properties

Table C-1: Fluid Properties

Fluid	Density kg/m ³ (at 1bar, 20deg C)	Viscosity Pa.s	Surface Tension mN/m
Water	998	1 mPa.s	72.8
Blood	1060	4 mPa.s	56
Glycerol	1261	1.2	64
Aqueous glycerol 48% (Anon n.d.)	1120	5.8 mPa.s	68
Aqueous glycerol/saline mixture	1125	N/A	N/A
Aqueous glycerol 50% v/v (Kazakis et al. 2008a)	1140	6.2	69
Aqueous glycerol 66.7% v/v (Kazakis et al. 2008a)	1180	16.6	67

Air	1.205	1.821×10^{-5}	N/A
Oxygen	1.331	1.92×10^{-5}	N/A
Nitrogen	1.165	1.755×10^{-5}	N/A

Appendix D Biocompatibility

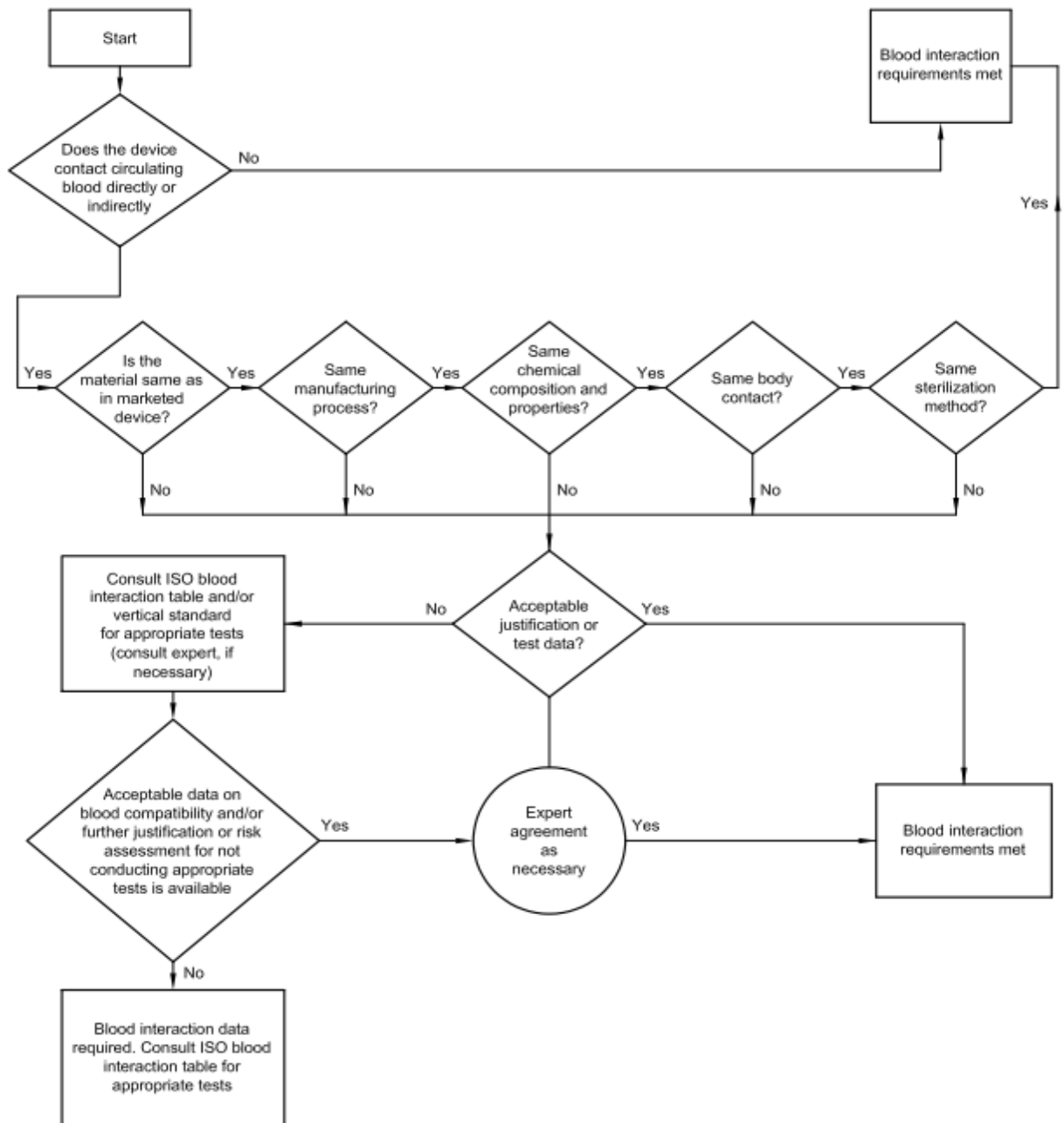


Figure D-1: ISO decision tree (ISO 2002)

Appendix E Flow Meter Calculations

Table E-1: Flow meter design calculations

<u>OXYGEN Properties</u>		<u>Colour indication:</u>	
Density (kg/m ³):	1.43	Values to be set:	Red
Viscosity (Pa.s):	2x10 ⁻⁵	Values that can alter:	Yellow
		Intermediate design values:	Green
Test Pressure Difference (Pa):	250	Tube length (m):	0.92
Flow rate measured (L/min):	0.397	Diameter (mm):	2.11
Q=P.diff x Kfactor		Area (m ²):	3.5x10 ⁻⁶
K relation	2.64x10 ⁻⁸	Velocity (m/s):	1.89
		Reynolds number:	285.18
		Friction factor:	0.22
		Entrance Length (cm):	3.61
		Introduce entrance length (cm):	4

Table E-2: Flow meter calibration readings and calculations

Batch/Sa mple	Distance: Start - end (mm)	Volume H2O	Time	Actual Flow	Meas. Flow	Actual/ Measured	Average	Tube Diameter mm	193.5
Units:	mm	ml	sec	ml/min	ml/min			Area m ²	0.02941
1.1	14.5	426.4	75.8	337.5	540	0.625			
1.2	7	205.9	61.5	200.83	320	0.628			
1.3	10	294.1	138	127.9	215	0.595		Current value of Calibrate = 1.9, multiply with Actual/measured to receive the actual reading	
1.4	9.5	279.4	220.5	76.0	130	0.585			
1.5	23	676.4	128.7	315.3	530	0.595			
1.6	31	911.6	82.6	662.2	1080	0.613			
1.7	9	264.7	121.6	130.6	210	0.622			
1.8	6	176.4	99.6	106.23	170	0.625			
1.9	4	117.6	260.5	27.1	50	0.542			
1.10	7.5	220.6	516.2	25.6	44	0.583	0.604		
2.1	13.5	397	84.7	281.2	280	1.004			
2.2	11	323.5	103.8	187.0	190	0.984			
2.3	27	794	72.4	658.0	645	1.020			
2.4	16.5	485.2	148	196.7	195	1.009			
2.5	6.2	182.3	161.2	67.9	70	0.969			
2.6	17.5	514.6	115	268.5	270	0.994	0.997		
3.1	13.5	397	380.7	62.6	62	1.009			
3.2	27.5	808.7	106.9	453.9	455	0.998			
3.3	19.2	564.6	74.7	453.5	455	0.997			
3.4	13.1	385.2	265	87.2	90	0.969			
3.5	13.3	391.1	547.2	42.9	45	0.953	0.985		

Appendix F Mathematical Model

```
%%%%%%%%%%%%%%%%%%%%%%%%%%%%%%%%%%%%%%%%%%%%%%%%%%%%%%%%%%%%%%%%%%%%%%%%
Bubble Dissolution Model
```

```
Purpose: To obtain the solution to a PDE; more specifically the
Diffusion Equation in spherical coordinates. Consists of a
homogeneous equation with Dirichlet LEFT boundary condition and a
Nuemann RIGHT boundary condition. There is also an Initial
Condition.
```

```
Author: Wesley Elson      Last modified: 28 January 2014
```

```
%%%%%%%%%%%%%%%%%%%%%%%%%%%%%%%%%%%%%%%%%%%%%%%%%%%%%%%%%%%%%%%%%%%%%%%%
```

```
clear
clc
format long
```

```
=====
% Model assumptions:
=====
% Some of the model implemented below is based on the model as
seen in Fischer et al. (2009), where the following assumptions are
valid:
% 1. The bubble is spherical and surrounded by blood at rest.
Spherical symmetry for the mass fraction distribution of the
dissolved oxygen.
% 2. A clear boundary exists between the phases. No mist or
vapour exists around the bubble. The only gas within the bubble is
oxygen and it is modelled as an inviscid ideal gas.
% 3. The pressure inside the bubble is atmospheric at all times
and spatially uniform at all times. At the gas-liquid interface
diffusion is the only method of gas transfer.
% 4. Inertial and temperature effects within the bubble and in
the blood are neglected due to the relatively small size of the
simulated bubbles. This implies that no temperature gradients
exist and hence no convection.
% 5. Surface tension is neglected.
% 6. The model is limited to cases where dissolved gases other
than oxygen do not significantly affect the dynamics of bubble
dissolution
% 7. The erythrocytes are intact. Free haemoglobin has markedly
larger oxygen uptake than intact erythrocytes.
% 8. Haemoglobin bound oxygen is assumed to be in equilibrium
with the dissolved oxygen.

% =====
% A. Prescribing the spatial and temporal properties
% =====
```

```

T = 100; % running time of model [s]
numtend = 200; % amount of discretised time steps
dt = T/(numtend-1); % size of time steps
t = 0:dt:T+dt; % initialising time array
n = 1; % 'mode' of the solution,
R0(1:numtend) = 0.1E-3; % starting radius of bubble [m]
dell = input('Distance between bubble centres in mm:'); % distance
between centres of adjacent bubbles
del = dell/(1000*2); % converting [mm] to [m], distance from
centre of bubble to end of comp. space
L(1) = del - R0(1) % end of spatial boundary [m]
dx = 5E-7; % spatial step size (total space) [m]

numxend = floor(del/dx) + 1; % amount of discretised spatial steps
(total space)
x = 0:dx:del; % initialising the radial array (total space)
numrend = floor((L(1)/del)*(numxend)); % amount of discretised
spatial steps (calc. domain)
dr = L(1)/(numrend-1); % spatial step size (calc. domain) [m]
r = 0:dr:L(1); % initialising the radial array (calc. domain)

% =====
% B. Prescribing the properties of the blood
% =====
alpha = 0.3; % physical solubility of oxygen [ml O2 / ml blood]
c = 0.166; % haemoglobin binding capacity [ml O2 / ml blood]
nn = 2.7; % constant parameter based on physiological condition of
blood (Fischer et al.)
rhostp = 1.429; % density of oxygen at STP [kg/m^3]
rhob = 1060; % density of blood [kg/m^3]
PO2b = 760; % partial pressure of oxygen at the bubble interface
[mmHg]
Cdb = PO2b*alpha*rhostp/rhob; % mass fraction of oxygen at the
bubble interface
PO2l = 51; % partial pressure of oxygen at the boundary end [mmHg]
V = PO2l*alpha*rhostp/rhob; % mass fraction of oxygen at t = 0,
homogenous solution, based on IC's
P50 = 28; % parameter of Hill's equation (Fischer et al.)
C50 = P50*alpha*rhostp/rhob; % parameter of Hill's equation
(Fischer et al.)
D = 1.8E-11 % diffusion constant of oxygen in blood [m^2/s]
lambda(numxend,numtend) = 0; % slope of saturation curve, Fischer
et al.
CdOFF(1:numxend,1:numtend) = 0; % initialising the offset matrix
and setting the value of non-calculated points
numRoff = numxend - numrend; % amount of discretised offset
spatial steps

% =====
% C. Main loop
% =====
for ti = 1:numtend
    f = inline('X*cos(X) - sin(X)'); % setting up the eigenvalue
solution
    KL = fzero(f,4); % the eigenvalue calculation
    K = KL/L(ti); % the eigenvalue calculation

```

```

%      Top = L(ti)*sqrt(pi*K/2); % numerator of the fourier
coefficient
%      Bot = (L(ti)/2 - sin(2*K*L(ti))/(4*K)); % denominator of the
fourier coefficient
      Top = 0.2868*sqrt(2/(pi*K))*(1/K - cos(K*L(ti))/K);
      Bot = L(ti)/2;
      Cn = Top/Bot; % Fourier co-efficient
% C.1 Determining the analytical solution
      for ri = 2:numrend
          Df = D/(1 + lambda(ri,ti)); % facilitated diffusion
constant, Fischer et al.
          Te = exp(-K^2*Df*t(ti)); % solution to temperature
equation
          sol = Cn*Te*(1/r(ri))*sqrt(2/(pi*K))*sin(K*r(ri)); %
general solution
          U = sol; % forming the summation of the solution
          Cd(ri,ti) = V + U; % combining homogeneous and non-
homogenous parts
          lambda(ri,ti+1) = (c*rhostp*nn/(rhob*C50))*...
(((Cd(ri,ti)/C50)^(nn-1))/((1 + (Cd(ri,ti)/C50)^nn)^2)); %
calculating saturation curve values, to be used in next iteration
step
          % C.2 Calculating the new bubble radius
          dCd_dr = 0.1*Te*(Cn/R0(ti))*sqrt(2/(pi*K))*
(K*cos(K*R0(ti)) - (sin(K*R0(ti))/R0(ti)));
          Cd(1,ti) = V + Cn*Te*sqrt(2*K/pi); % the value of Cd taken
as limit as r -> 0
          j = -rhob*D*dCd_dr; % mass flux
          dR_dt(ti) = -j/rhostp; % rate of change of bubble diameter
      end
      R0(ti+1) = R0(ti) + dR_dt(ti); % radius of bubble for the next
time step
      L(ti+1) = del - R0(ti+1); % diffusion space length for next
time step

% C.3 Preparing for interpolation
      numrnew = floor((L(ti+1)/del)*(numxend)); % new amount of
discretised spatial steps (calc. domain)
      drnew = L(ti+1)/(numrnew - 1); % new spatial step size (calc.
domain) [m]
      rnew = 0:drnew:L(ti+1); % initialising the new radial array
(calc. domain)
      Cdnew(1:numrnew,ti) = interp1(r,Cd(1:numrend,ti),rnew); %
interpolation procedure

% C.4 Shifting the concentration profile
      for ri = 1:numrend
          CdOFF(ri+numRoff,ti) = Cd(ri,ti); % shifting the
concentration profile according to the bubble radius
          CdOFF(1:numRoff,ti) = 0; % setting the value of Cd inside
the bubble = 0
      end
      numRoff = numxend - numrnew; % new amount of discretised
offset spatial steps
      numrend = numrnew; % equating the new amount of discretised
spatial steps to the previous amount

```

```

    r = rnew; % equating the new radial to the previous radial
array
end

clear Cd % clearing unused variables
clear Cdnew % clearing unused variables
clear lambda % clearing unused variables

% =====
% D. Converting Variables to be used in Plotting
% =====
for ti = 1:numtend
    for ri = 1:numxend
        PO2OFF(ri,ti) = CdOFF(ri,ti)*rhob/(alpha*rhostp);
% converting the mass fraction of oxygen to partial pressure
        SOFF(ri,ti) = (PO2OFF(ri,ti)/P50)^nn/(1 +
(PO2OFF(ri,ti)/P50)^nn); % converting the partial pressure to
saturation
    end
end
SOFF = 100*SOFF;
% converting the saturation to percentage
% =====
% E. Plotting
% =====
subplot(2,1,1)
h =
plot(x(:),SOFF(:,1),'k',x(:),SOFF(:,numtend/5),'r',x(:),SOFF(:,num
tend/2),'c',x(:),SOFF(:,numtend),'b');
set(h,'LineWidth',1);
set(h,'LineWidth',1);
h=xlabel('x');
set(h,'FontSize',8);
h=ylabel('S [%]');
set(h,'FontSize',8);
set(gca,'FontSize',10);
title('Oxygen Saturation vs Radial coordinate')
grid on

grid on
subplot(2,1,2)
plot(t,R0,'c',t,L,'r')
grid on

```

7 References

- Anon, 2010. Artificial Lungs. Available at: <http://artificial-lungs.blogspot.com/2010/09/drawing-of-novalung-made-in-germany.html> [Accessed November 28, 2011].
- Anon, Physical Properties of Glycerine and its Solutions. In *Society*. Available at: http://www.aciscience.org/docs/Physical_properties_of_glycerine_and_its_solutions.pdf.
- Author, U., Swan Ganz Picture. Available at: <http://drsantiagoherrero.files.wordpress.com/2012/10/swan-ganz.jpg> [Accessed October 29, 2013].
- Barak, M. & Katz, Y., 2005. Microbubbles: Pathophysiology and Clinical Implications. *Chest*, 128(4), pp.2918–32. Available at: <http://www.ncbi.nlm.nih.gov/pubmed/16236969> [Accessed April 8, 2011].
- Van Blankenstein, J.H. et al., 1997. Cardiac depression after experimental air embolism in pigs: role of addition of a surface-active agent. *Cardiovascular research*, 34(3), pp.473–82. Available at: <http://www.ncbi.nlm.nih.gov/pubmed/9231030>.
- Camboni, D. et al., 2009. First experience with a paracorporeal artificial lung in humans. *ASAIO journal (American Society for Artificial Internal Organs : 1992)*, 55(3), pp.304–6. Available at: <http://www.ncbi.nlm.nih.gov/pubmed/19282751> [Accessed August 18, 2010].
- Carey, W. a & Colby, C.E., 2009. Extracorporeal Membrane Oxygenation for the Treatment of Neonatal Respiratory Failure. *Seminars in cardiothoracic and vascular anesthesia*, 13(3), pp.192–7. Available at: <http://www.ncbi.nlm.nih.gov/pubmed/19713207> [Accessed July 27, 2010].
- Cassie, a B., Riddell, a G. & Yates, P.O., 1960. Hazard of antifoam emboli from a bubble oxygenator. *Thorax*, 15, pp.22–9. Available at: <http://www.pubmedcentral.nih.gov/articlerender.fcgi?artid=1018529&tool=pmcentrez&rendertype=abstract>.

- Coin, J.T. & Olson, J.S., 1979. The rate of oxygen uptake by human red blood cells. *The Journal of biological chemistry*, 254(4), pp.1178–90. Available at: <http://www.ncbi.nlm.nih.gov/pubmed/762123>.
- Conrad, S.A. et al., 1994. Major Findings from the Clinical Trials of the Intravascular Oxygenator. *International Society for Artificial Organs*, 18(11), pp.846–863.
- Corchero, G., Medina, a. & Higuera, F.J., 2006. Effect of wetting conditions and flow rate on bubble formation at orifices submerged in water. *Colloids and Surfaces A: Physicochemical and Engineering Aspects*, 290(1-3), pp.41–49. Available at: <http://linkinghub.elsevier.com/retrieve/pii/S0927775706003463> [Accessed September 15, 2010].
- Crow, S., Fischer, A.C. & Schears, R.M., 2009. Extracorporeal Life Support: Utilization, Cost, Controversy, and Ethics of Trying to Save Lives. *Seminars in Cardiothoracic and Vascular Anesthesia*, 13(3), pp.183–191.
- Dellimore, K., 2012. Spherical Diffusion of Oxygen in Blood.
- Department of Health Government Gazette, 2011. Medicines and Related Substances Act, 1965 (Act No. 101 of 1965). *Regulation*, (34463), p.6.
- Eash, H.J. et al., 2005. Evaluation of Local Gas Exchange in a Pulsating Respiratory Support Catheter. *American Society for Artificial Internal Organs*, 51(2), pp.152–157.
- Eash, H.J. et al., 2004. Evaluation of Plasma Resistant Hollow Fiber Membranes for Artificial Lungs. *ASAIO journal*, 50(1), pp.491–497. Available at: http://journals.lww.com/asaijournal/Abstract/2004/09000/Evaluation_of_Plasma_Resistant_Hollow_Fiber.15.aspx [Accessed April 7, 2011].
- Edwards, C.H. & Penney, D.E., 1992. *Elementary Differential Equations with Boundary Problems*, Prentice-Hall.
- Edwards Life Sciences, 2002. *Understanding Continuous Mixed Venous Oxygen Saturation (SvO₂) Monitoring with the Swan-Ganz Oximetry TD System*, Available at: <http://ht.edwards.com/resourcegallery/products/swanganz/pdfs/svo2edbook.pdf>.
- Encyclopaedia Britannica, O., 2011. pulmonary alveolus: alveoli and capillaries in the lungs. Available at: <http://www.britannica.com/EBchecked/media/107200/The-alveoli-and-capillaries-in-the-lungs-exchange-oxygen-for> [Accessed October 2, 2011].

- Fazio, R., 2000. The Iterative Transformation Method: Numerical Solution of One-Dimensional Parabolic Moving Boundary Problems. *International Journal of Computer Mathematics*, 00, pp.1–11.
- Fischer, M., Zinovik, I. & Poulikakos, D., 2009. Diffusion and reaction controlled dissolution of oxygen microbubbles in blood. *International Journal of Heat and Mass Transfer*, 52(21-22), pp.5013–5019. Available at: <http://linkinghub.elsevier.com/retrieve/pii/S0017931009003366> [Accessed August 17, 2010].
- Fourie, P.R., 2010. Re: Vergadering, e-mail to W. Elson [online], 4 August. , (i).
- Frenckner, B. & Radell, P., 2008. Respiratory failure and extracorporeal membrane oxygenation. *Seminars in Pediatric Surgery*, 17(1), pp.34–41.
- Gnyloskurenko, S. V et al., 2003. Influence of wetting conditions on bubble formation at orifice in an inviscid liquid. Transformation of bubble shape and size. *Colloids and Surfaces A: Physicochemical and Engineering Aspects*, 218(1-3), pp.73–87. Available at: <http://linkinghub.elsevier.com/retrieve/pii/S0927775702005927> [Accessed June 9, 2011].
- Hakoshima, A. et al., 1989. Alteration of Red Cell Deformability During Extracorporeal Bypass: Membrane v Bubble Oxygenator. *Journal of cardiothoracic anesthesia*, 3(2), pp.189–92. Available at: <http://www.ncbi.nlm.nih.gov/pubmed/2519944>.
- Hattler, B.G. et al., 2002. A respiratory gas exchange catheter : In vitro and in vivo tests in large animals. *The Journal of Thorac and Cardiovascular Surgery*, 124(3), pp.520–530.
- Haworth, W.S., 2003. The Development of the Modern Oxygenator. *The Annals of Thoracic Surgery*, 76(6), pp.2216–2219. Available at: <http://linkinghub.elsevier.com/retrieve/pii/S0003497503018253> [Accessed February 23, 2011].
- Heidelberger, E. & Reeves, R.B., 1990. O₂ transfer kinetics in a whole blood unicellular thin layer. *Journal of applied physiology (Bethesda, Md. : 1985)*, 68(5), pp.1854–64. Available at: <http://www.ncbi.nlm.nih.gov/pubmed/2361888>.
- Illingworth, T.C. & Golosnoy, I.O., 2005. Numerical solutions of diffusion-controlled moving boundary problems which conserve solute. *Journal of Computational Physics*, 209(1), pp.207–225. Available at: <http://linkinghub.elsevier.com/retrieve/pii/S0021999105000859> [Accessed October 30, 2011].

- ISO, 2002. *ISO 10993-4 Biological Evaluation of Medical Devices - Part 4: Selection of tests for interactions with blood*, International Standards Organisation.
- Iwahashi, H., Yuri, K. & Nosé, Y., 2004. Development of the oxygenator: past, present, and future. *Journal of artificial organs : the official journal of the Japanese Society for Artificial Organs*, 7(3), pp.111–20. Available at: <http://www.ncbi.nlm.nih.gov/pubmed/15558331> [Accessed August 4, 2010].
- Kaar, J.L. et al., 2007. Towards improved artificial lungs through biocatalysis. *Biomaterials*, 28(20), pp.3131–3139. Available at: <http://www.ncbi.nlm.nih.gov/pubmed/17433433> [Accessed March 17, 2011].
- Kazakis, N.A., Mouza, A.A. & Paras, S. V, 2008a. Coalescence during bubble formation at two neighbouring pores: An experimental study in microscopic scale. *Chemical Engineering Science*, 63(21), pp.5160–5178. Available at: <http://linkinghub.elsevier.com/retrieve/pii/S0009250908003655> [Accessed August 3, 2010].
- Kazakis, N.A., Mouza, A.A. & Paras, S. V, 2008b. Experimental study of bubble formation at metal porous spargers: Effect of liquid properties and sparger characteristics on the initial bubble size distribution. *Chemical Engineering Journal*, 137(2), pp.265–281. Available at: <http://linkinghub.elsevier.com/retrieve/pii/S1385894707003117>.
- Kim, G., Kwon, T. & Hung, C., 2006. Design of an intravenous oxygenator. *The Japanese Society for Artificial Organs*, 9, pp.34–41.
- Kim, M., 2002. Surface modification for hydrophilic property of stainless steel treated by atmospheric-pressure plasma jet. *Surface and Coatings Technology*, 171(1-3), pp.312–316. Available at: <http://linkinghub.elsevier.com/retrieve/pii/S0257897203002925> [Accessed October 5, 2011].
- Kim, S.S. & Schubert, R., 2007. Generation and Usage of Microbubbles as a Blood Oxygenator.
- Krishnan, A., 1994. *Intravascular Microbubble Blood Oxygenator: Principles and Limitations*. Available at: <http://microbubble.com/>.
- Leonard, R.J., 2003. The transition from the bubble oxygenator to the microporous membrane oxygenator. *Perfusion*, 18(3), pp.179–83. Available at: <http://www.ncbi.nlm.nih.gov/pubmed/12952125>.
- Leverett, L. et al., 1972. Red Blood Cell Damage by Shear Stress. *Biophysical Journal*, 12(3), pp.257–273. Available at:

- <http://linkinghub.elsevier.com/retrieve/pii/S0006349572860855> [Accessed January 10, 2011].
- Liddicoat, J.E. et al., 1974. Membrane vs Bubble Oxygenator: Clinical Comparison. In J. E. Liddicoat, ed. *Annual Meeting of the Southern Surgical Association*. Boca Raton, pp. 747–752.
- Litwak, R.S., 2002. Leland C. Clark and Frank Gollan: Bubble Oxygenators and Perfusion Hypothermia. *The Annals of thoracic surgery*, 74(2), pp.612–614. Available at: <http://www.ncbi.nlm.nih.gov/pubmed/12173868>.
- Mao, C. et al., 2004. Various approaches to modify biomaterial surfaces for improving hemocompatibility. *Advances in Colloid and Interface Science*, 110, pp.5–17. Available at: <http://www.ncbi.nlm.nih.gov/pubmed/15142821> [Accessed August 4, 2011].
- Martin, M., Montes, F. & Galan, M., 2006. Numerical calculation of shapes and detachment times of bubbles generated from a sieve plate. *Chemical Engineering Science*, 61(2), pp.363–369. Available at: <http://linkinghub.elsevier.com/retrieve/pii/S0009250905005592> [Accessed August 18, 2010].
- Masters, R.G., 1989. Pro: The Superiority of the Membrane Oxygenator. *Journal of Cardiothoracic Anesthesia*, 3(2), pp.235–237.
- Misra, S. & Gadhinglajkar, S., 2009. Unexpected Air in the Left Ventricle after Aortic Cannulation in Two Patients with Severe Aortic Insufficiency: Possible Mechanisms and Clinical Implications. *Journal of cardiothoracic and vascular anesthesia*, xx(x), pp.1–4. Available at: <http://www.ncbi.nlm.nih.gov/pubmed/20006523> [Accessed August 17, 2010].
- Mortensen, J.D., 1992. Intravascular Oxygenator: A New Alternative Method for Augmenting Blood Gas Transfer in Patients With Acute Respiratory Failure. *Artificial Organs*, 16(1), pp.75–82.
- Nahra, H.K. & Kamotani, Y., 1998. Bubble Formation and Detachment and in Liquid Flow Under Reduced Gravity Normal. In *36th Aerospace Meeting & Exhibit*.
- O'Rourke, P.P. et al., 1989. Extracorporeal Membrane Oxygenation and Conventional Medical Therapy in Neonates with Persistent Pulmonary Hypertension of the Newborn - A Prospective Randomized Study. *Pediatrics*, 84(6), pp.957–963.

- Patel, D.N. et al., 2003. Oxygen Toxicity. *Journal, Indian Academy of Clinical Medicine*, 4(3), pp.234–237.
- Petrou, S. et al., 2006. Cost-effectiveness of neonatal extracorporeal membrane oxygenation based on 7-year results from the United Kingdom Collaborative ECMO Trial. *Pediatrics*, 117(5), pp.1640–1649. Available at: <http://www.ncbi.nlm.nih.gov/pubmed/16651318>.
- Rodriguez, R., 2011. Re; Mixture ratios, e-mail to W. Elson [online], 7 March.
- Schmid, C. et al., 2008. Bridge to lung transplantation through a pulmonary artery to left atrial oxygenator circuit. *The Society of Thoracic Surgeons*, 85(4), pp.1202–5. Available at: <http://www.ncbi.nlm.nih.gov/pubmed/18355495> [Accessed August 17, 2010].
- Schubert, R.W., A, C.S. & Kim, S.S., 2003. Using MicroBubbles to Oxygenate Blood: Possible? In *25th Annual International Conference of the IEEE EMBS*. Cancun, pp. 16–19.
- Snyder, T.A. et al., 2006. Blood Biocompatibility Assessment of an Intravenous Gas Exchange Device. *Artificial Organs*, 30(9), pp.657–664.
- Stamatialis, D.F. et al., 2008. Medical applications of membranes: Drug delivery, artificial organs and tissue engineering. *Journal of Membrane Science*, 308, pp.1–34.
- Steinhorn, R.H., 2011. Persistent Newborn Pulmonary Hypertension. Available at: <http://emedicine.medscape.com/article/898437-overview> [Accessed June 1, 2011].
- Tan, R.B.H., Chen, W.B. & Tan, K.H., 2000. A non-spherical model for bubble formation with liquid cross-flow. *Chemical Engineering Science*, 55(24), pp.6259–6267. Available at: <http://linkinghub.elsevier.com/retrieve/pii/S0009250900002116>.
- Thakkar, D.R., Sinha, A.C. & Wenker, O.C., 2001. Concepts of Neonatal ECMO. *The Internet Journal of Perfusionists*, 1(2).
- Thomson, M., 2011. Personal Interview. 15 September, Tygerberg. , (September).
- Tse, K. et al., 1998. Visualisation of bubble coalescence in a coalescence cell, a stirred tank and a bubble column. *Chemical Engineering Science*, 53(23), pp.4031–4036. Available at: <http://linkinghub.elsevier.com/retrieve/pii/S0009250998001821>.

- Unverdi, S.O., 1992. A Front-Tracking Method for Viscous , Incompressible , Multi-fluid Flows. , 2537.
- Villavicencio, J.L. & Warren, R., 1962. Experiences with a Low Prime Bubble Oxygenator for Cardiopulmonary Bypass. *American Journal of Surgery*, 103(January).
- Wickramasinghe, S.R. & Han, B., 2005. Designing Microporous Hollow Fibre Blood Oxygenators. *Chemical Engineering Research and Design*, 83(A3), pp.256–267.
- Yang, W.J., 1971. Dynamics of gas bubbles in whole blood and plasma. *Journal of biomechanics*, 4(2), pp.119–25. Available at: <http://www.ncbi.nlm.nih.gov/pubmed/5119407>.
- Yang, W.J. et al., 1971a. Experimental Studies of the Dissolution of Gas Bubbles in Whole Blood and Plasma - I Stationary Bubbles. *Journal of Biomechanics*, 4(I 970), pp.275–281.
- Yang, W.J. et al., 1971b. Experimental studies of the dissolution of gas bubbles in whole blood and plasma - II. Moving bubbles or liquids. *Journal of Biomechanics*, 4(4), pp.283–288. Available at: <http://www.ncbi.nlm.nih.gov/pubmed/5122821>.
- Yasuda, H.K. & Lin, J.N., 2003. Small Bubbles Oxygenation Membrane. *Journal of Applied Polymer Science*, 90(2), pp.387–398. Available at: <http://doi.wiley.com/10.1002/app.12616> [Accessed August 25, 2010].